CMM 11
International conference on the mechanical behavior of Materials
COMO LAKE ITALY
JUNE 5 - 9 2011

Simulation of debonding in Al/epoxy T-peel joints using a potential based cohesive zone model

(Session: Fundamentals of Cohesive Zone Models, paper no. 3732)

M. Alfano and G. Lubineau
[a]Composite and Heterogeneous Materials Analysis and Simulations,
King Abdullah University of Science & Technology (KAUST)
Kingdom of Saudi Arabia

F. Furgiuele
[b]Department of Mechanical Engineering, University of Calabria, Italy

G. H. Paulino
[c]Department of Civil and Environmental Engineering,
University of Illinois at Urbana-Champaign, USA

Como Lake, Italy, June 7th 2011

Introduction and motivation

Adhesive bonding and surface preparation

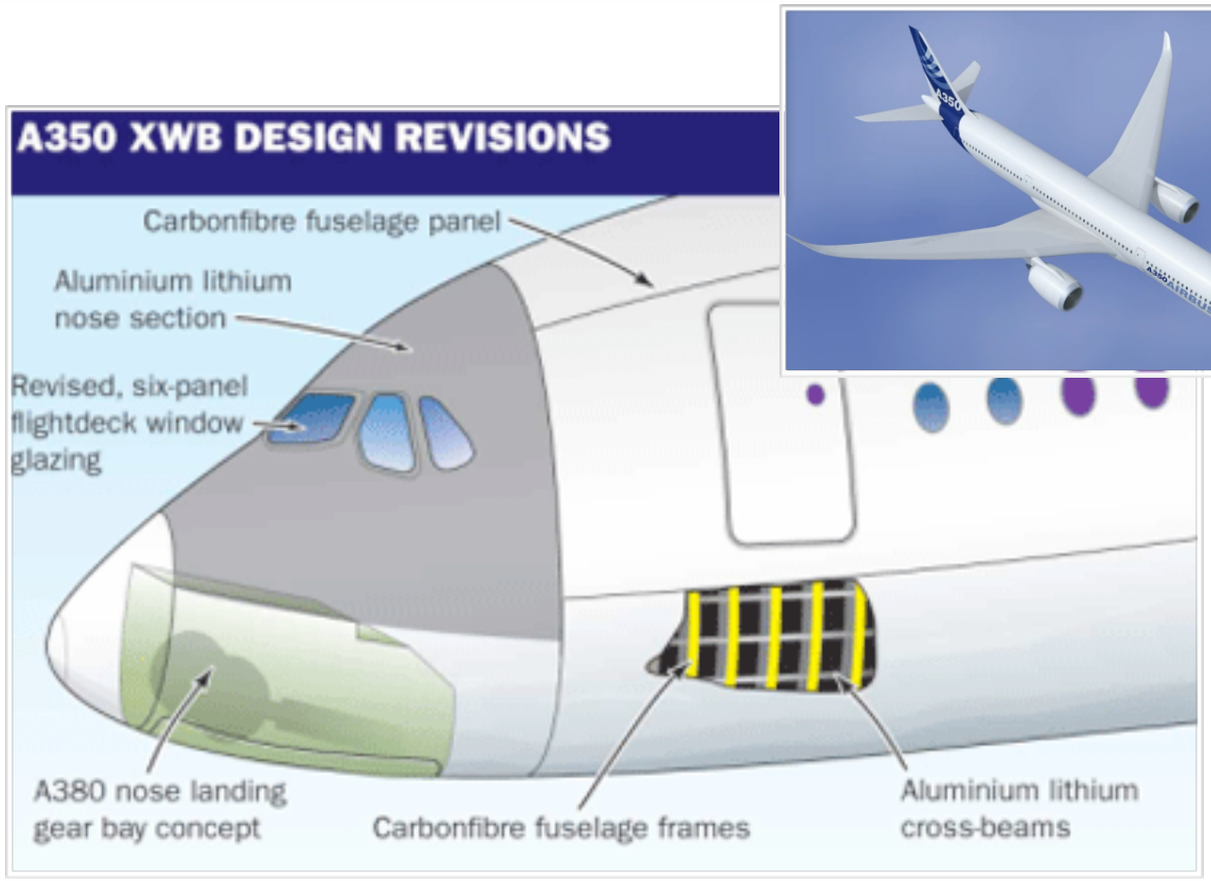

Introduction and motivation

Adhesive bonding and surface preparation

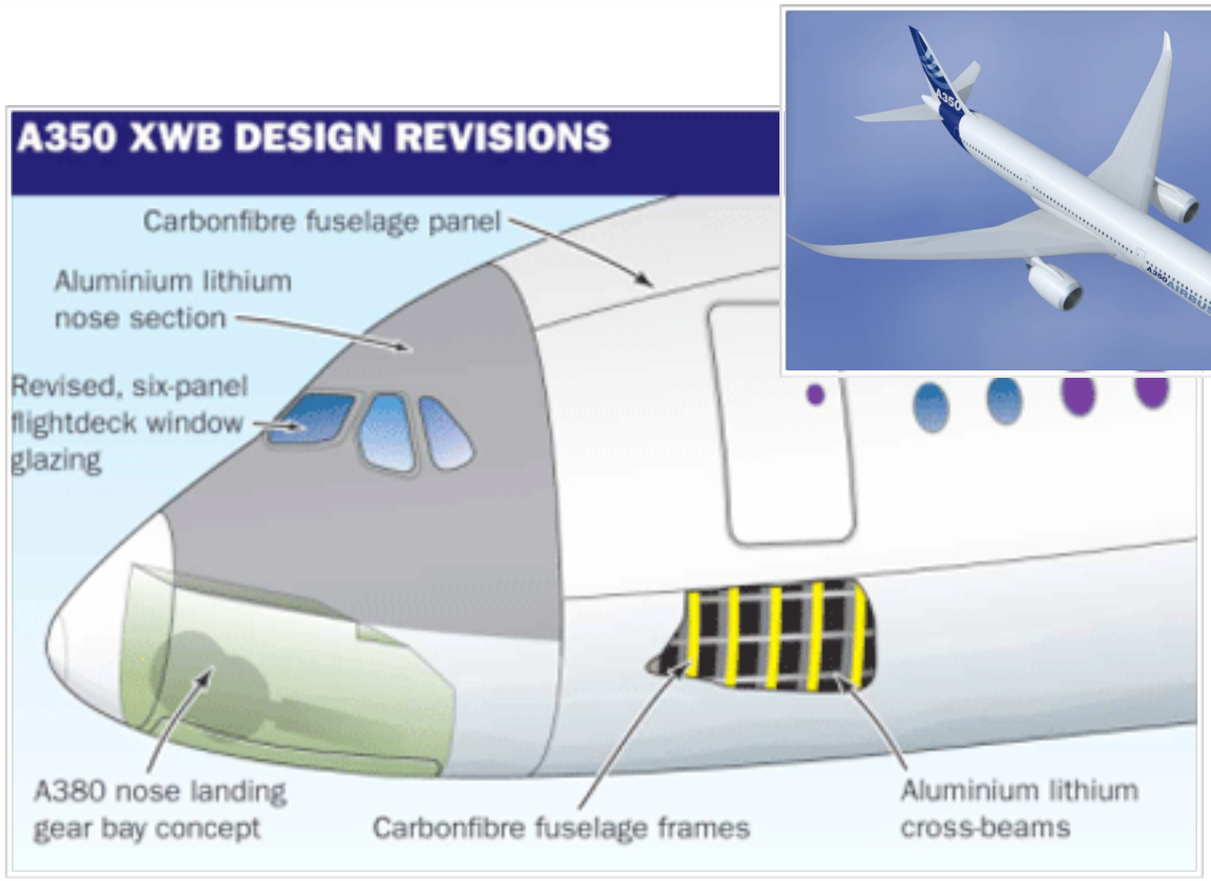

- Multi-material adhesive bonding

Introduction and motivation

Adhesive bonding and surface preparation

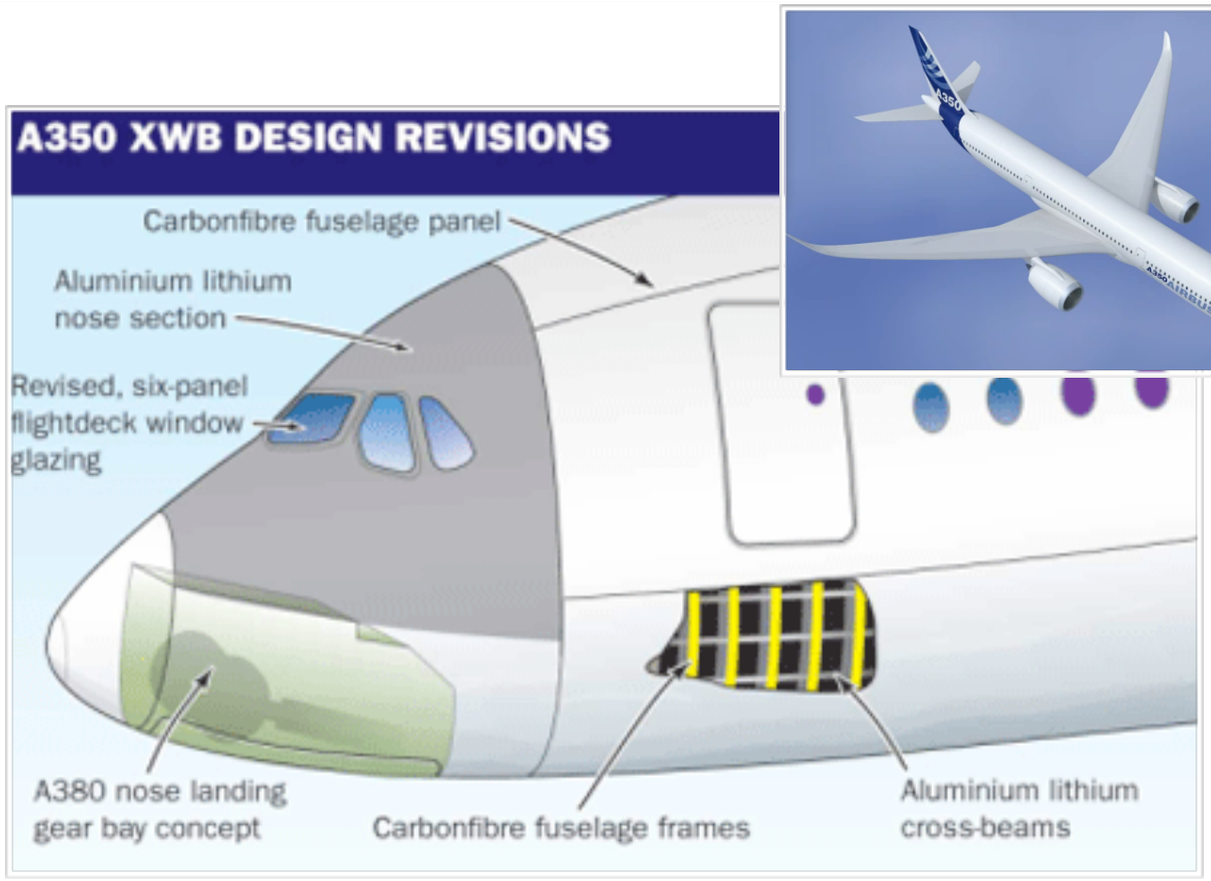

- Multi-material adhesive bonding
- Laser surface irradiation represents a suitable ecological alternative to “wet” chemical treatments

Introduction and motivation

Adhesive bonding and surface preparation

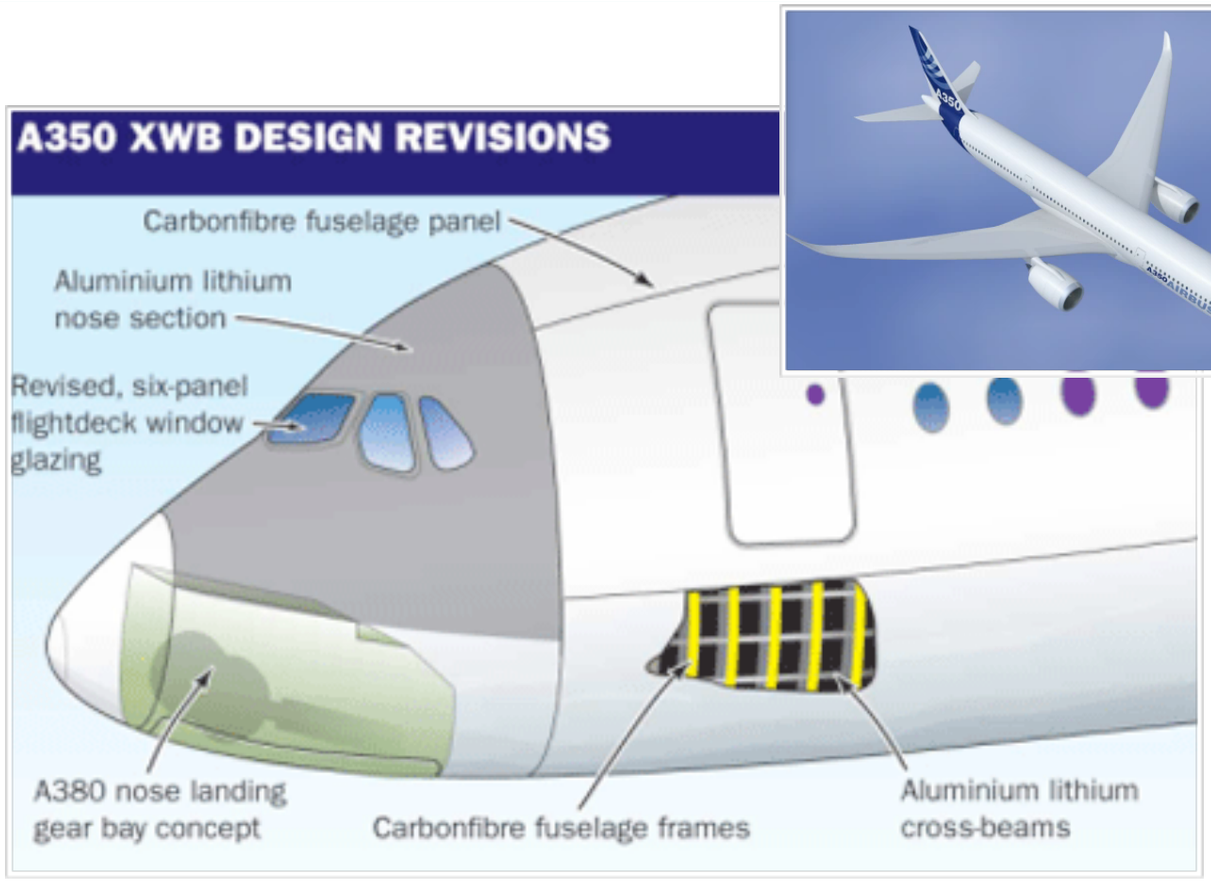

- Multi-material adhesive bonding
- Laser surface irradiation represents a suitable ecological alternative to “wet” chemical treatments
- Previous work focused on Al/Mg adhesive joints

M. Alfano et al., Influence of laser surface irradiation on bonding strength of Al/Mg adhesive joints. JAST, 25, 2011, p. 1261

Introduction and motivation

Adhesive bonding and surface preparation

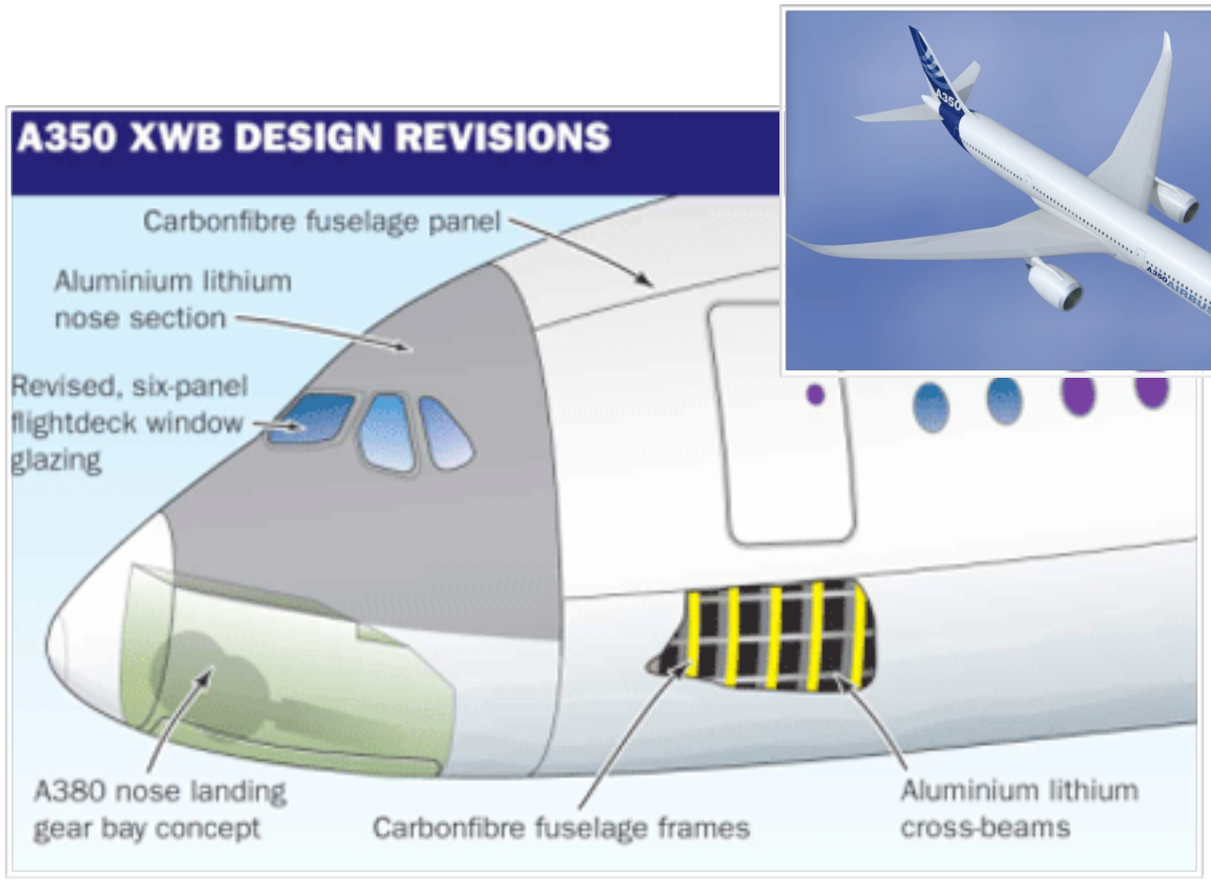

- Multi-material adhesive bonding
- Laser surface irradiation represents a suitable ecological alternative to “wet” chemical treatments
- Previous work focused on Al/Mg adhesive joints
- Limitations: SLJ nominal shear strength and lack of quantitative information on bond toughness, no systematic analysis on the interaction between laser process parameters and surface morphology/wetting

M. Alfano et al., Influence of laser surface irradiation on bonding strength of Al/Mg adhesive joints. JAST, 25, 2011, p. 1261

Substrates pre-treatment

Laser surface irradiation of AA6082T6 substrates

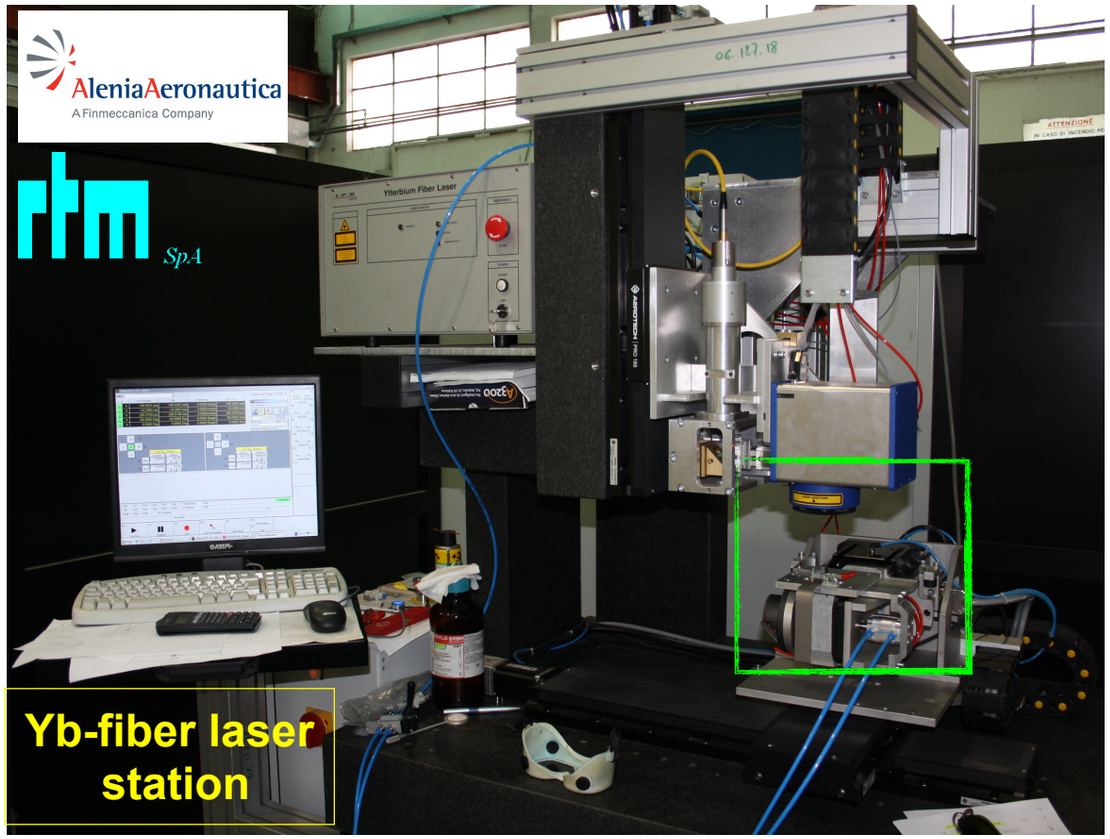

Substrates pre-treatment

Laser surface irradiation of AA6082T6 substrates

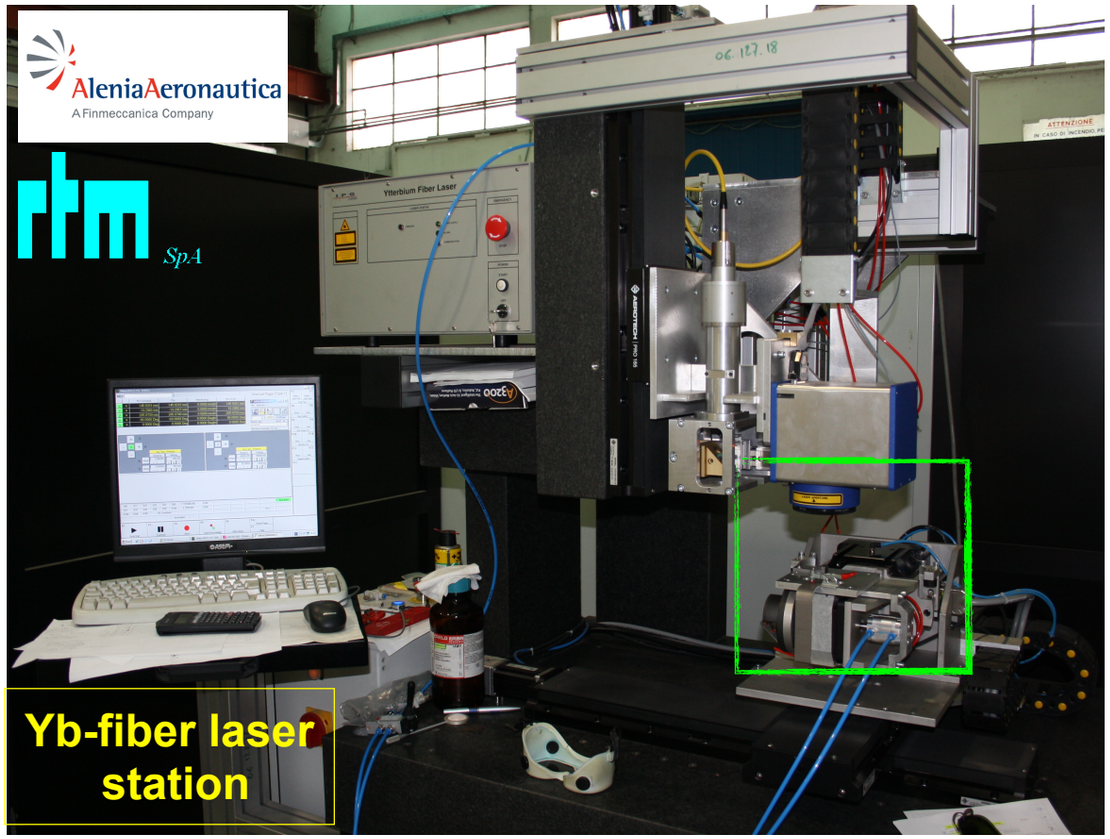

Laser process parameters	
Laser wavelength, nm	1064
Pulse repetition rate, kHz	100
Pulse width, ns	150
Pulse energy, mJ	1
Average Power, W	**40/100**
Laser velocity, mm/s	**500/750/1000**
Line spacing, μm	**50/100/150**

Substrates pre-treatment

Laser surface irradiation of AA6082T6 substrates

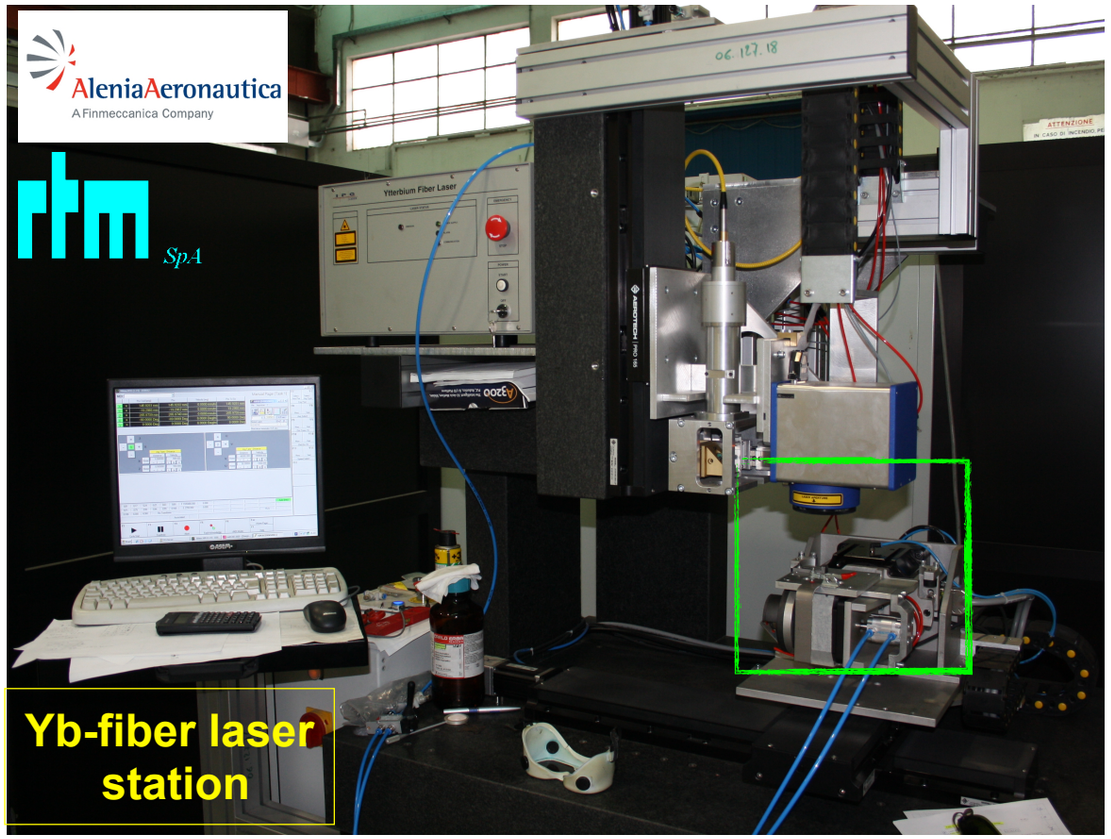

Laser process parameters	
Laser wavelength, nm	1064
Pulse repetition rate, kHz	100
Pulse width, ns	150
Pulse energy, mJ	1
Average Power, W	**40/100**
Laser velocity, mm/s	**500/750/1000**
Line spacing, μm	**50/100/150**

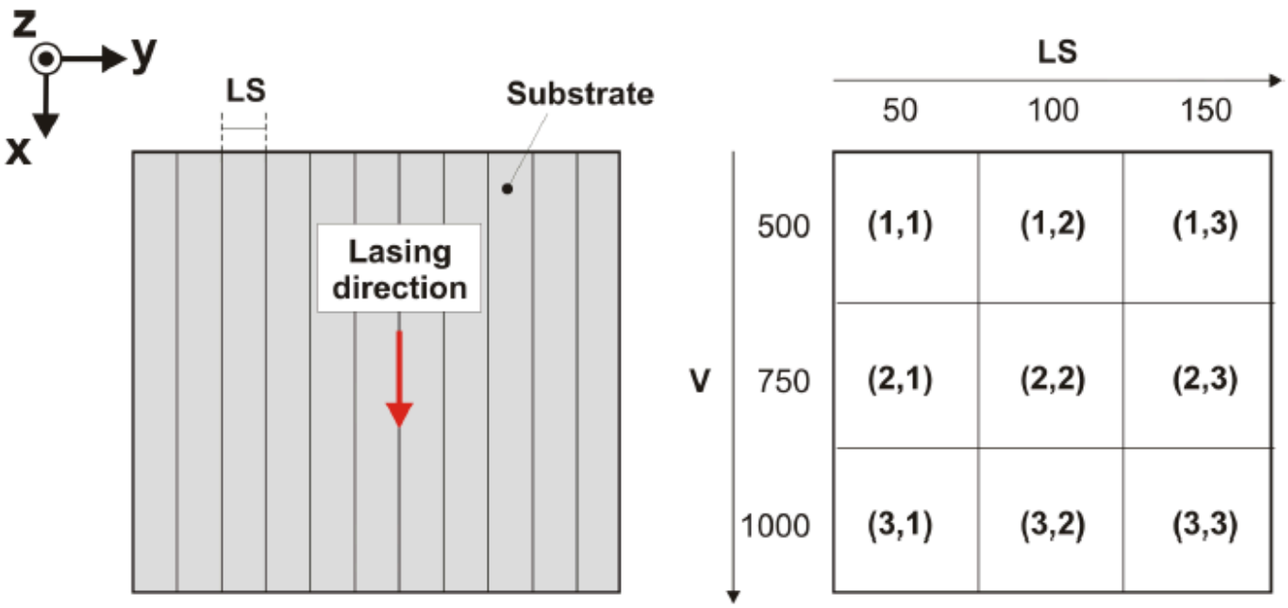

Substrates pre-treatment

Laser surface irradiation of AA6082T6 substrates

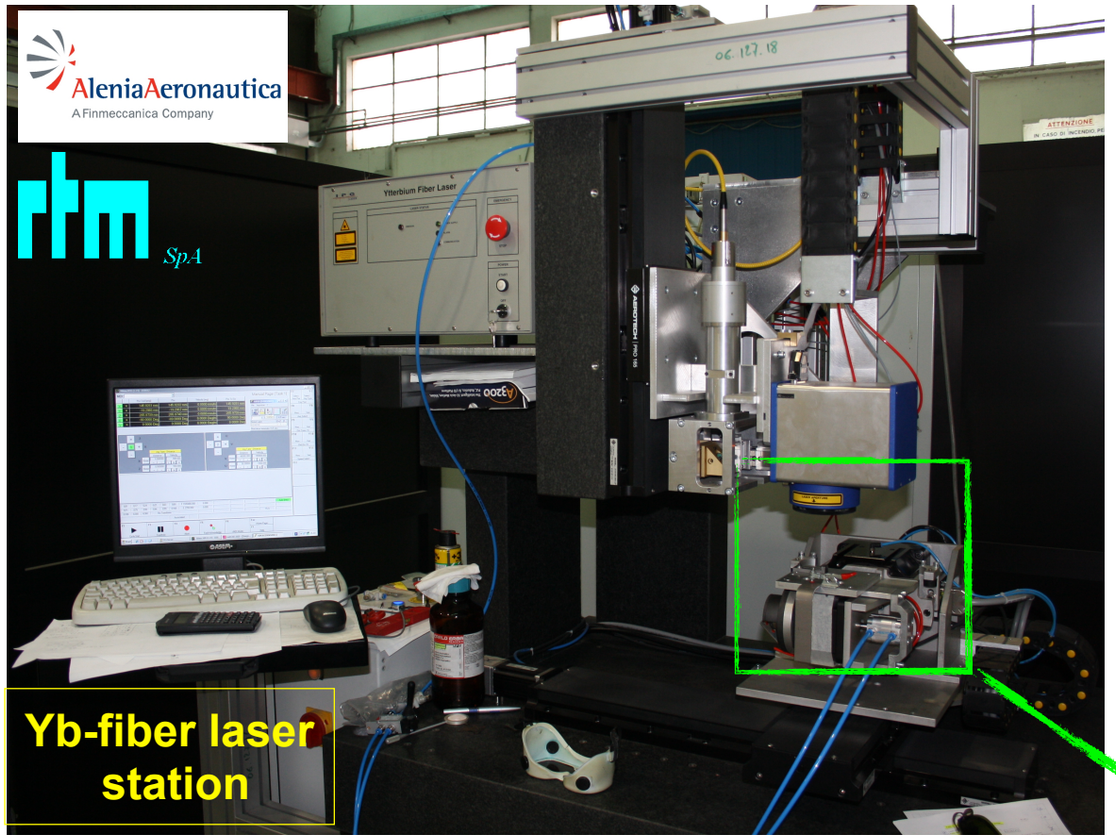

Laser process parameters	
Laser wavelength, nm	1064
Pulse repetition rate, kHz	100
Pulse width, ns	150
Pulse energy, mJ	1
Average Power, W	**40/100**
Laser velocity, mm/s	**500/750/1000**
Line spacing, µm	**50/100/150**

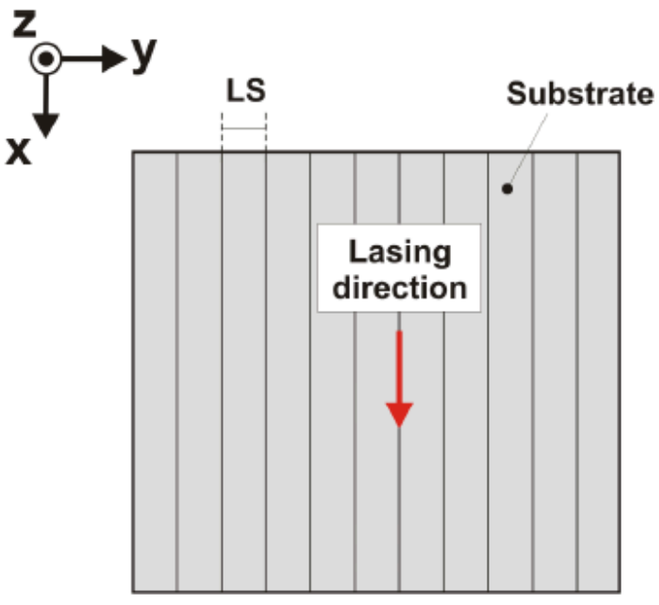

V \ LS	50	100	150
500	(1,1)	(1,2)	(1,3)
750	(2,1)	(2,2)	(2,3)
1000	(3,1)	(3,2)	(3,3)

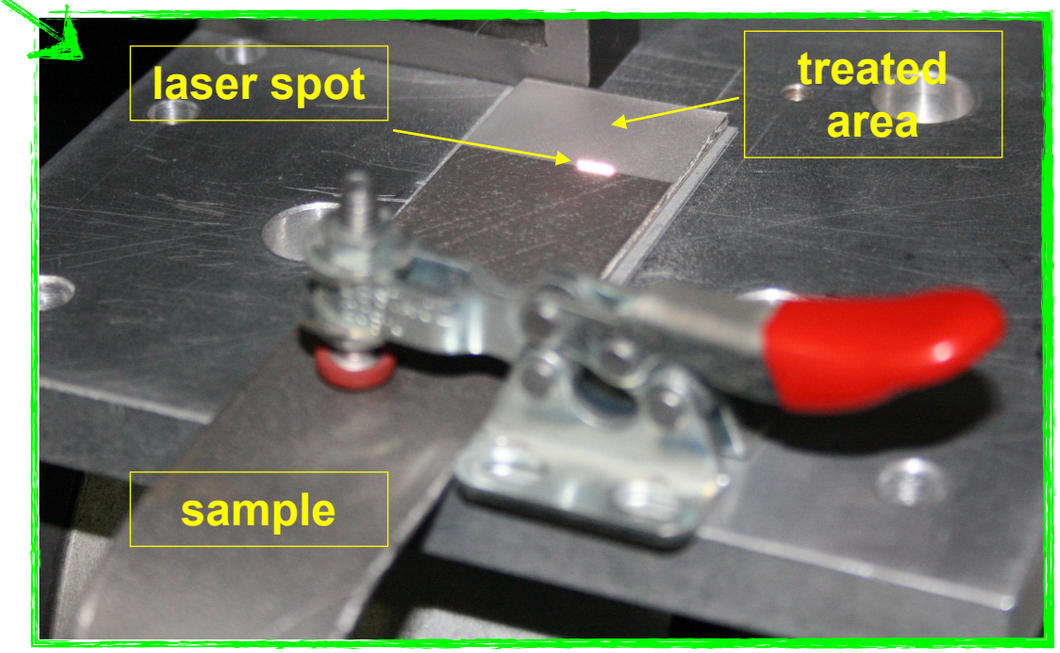

Substrates pre-treatment

SEM analyses

V \ LS	50	100	150
500	(1,1)	(1,2)	(1,3)
750	(2,1)	(2,2)	(2,3)
1000	(3,1)	(3,2)	(3,3)

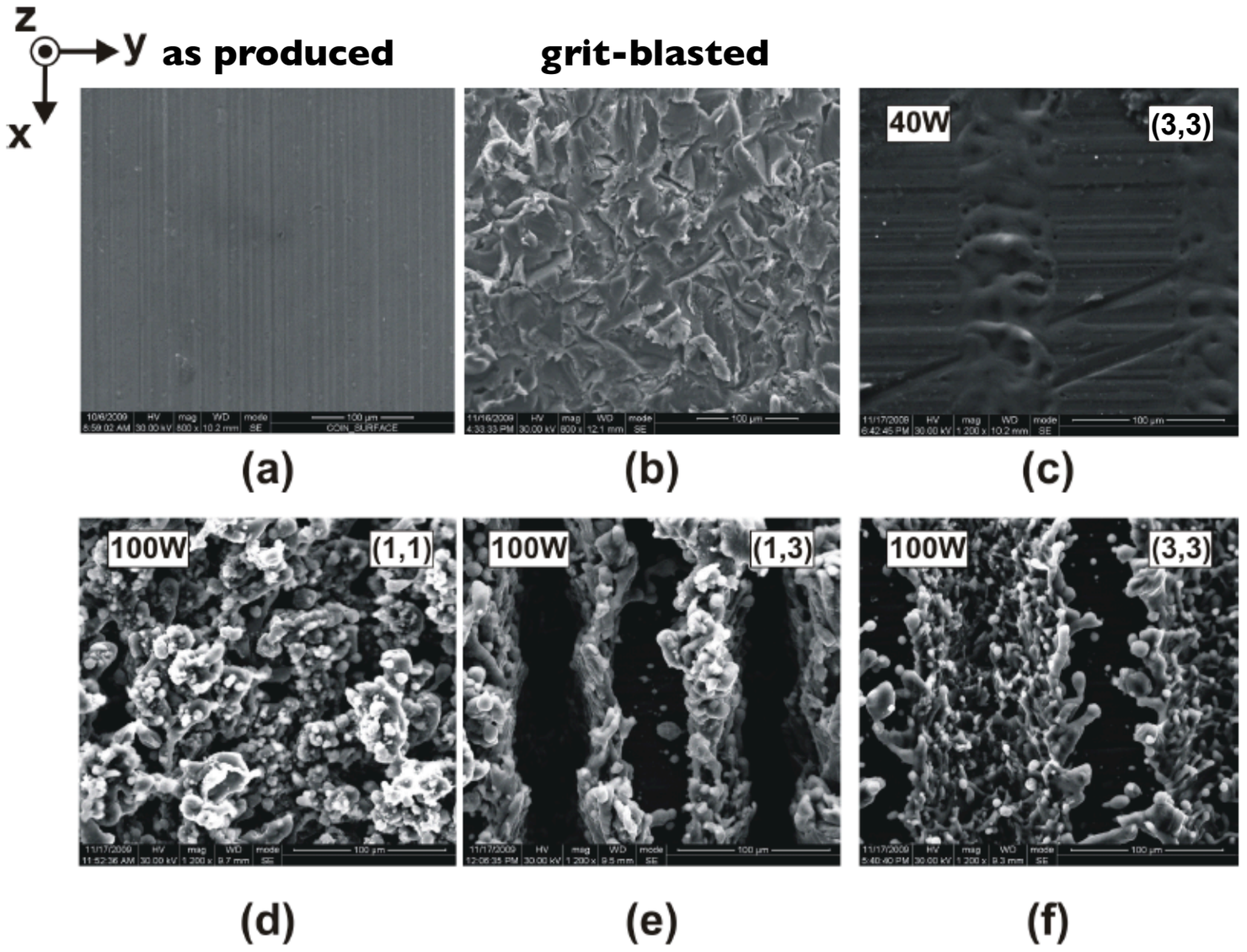

Figure 2: SEM observations of (a) as-produced surface; (b) grit blasted surface and laser treated surface with (c) P=40W, LS=150μm, V=1000 mm/s, (d) P=100W, LS=50μm, V=500 mm/s, (e) P=100W, LS=150μm, V=500 mm/s, (f) P=100W, LS=150μm, V=1000 mm/s

M. Alfano, F. Furgiuele, G. Lubineau, G. H. Paulino, Role of laser surface preparation on damage and decohesion of Al/epoxy joints. Submitted for publication.

Substrates pre-treatment

SEM analyses

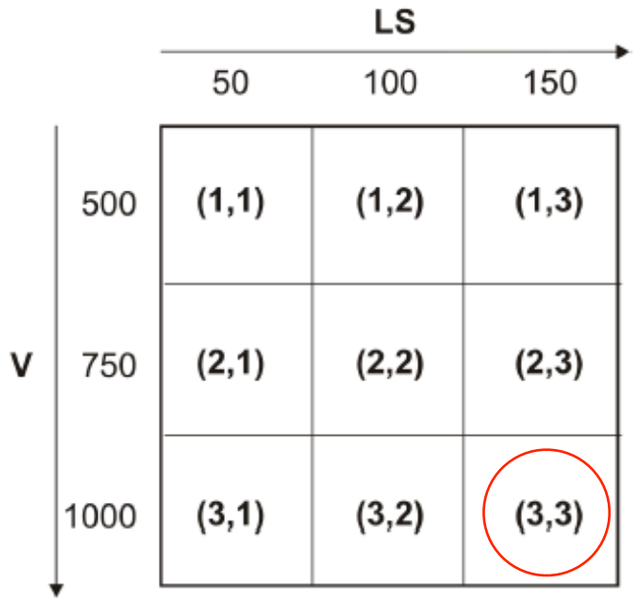

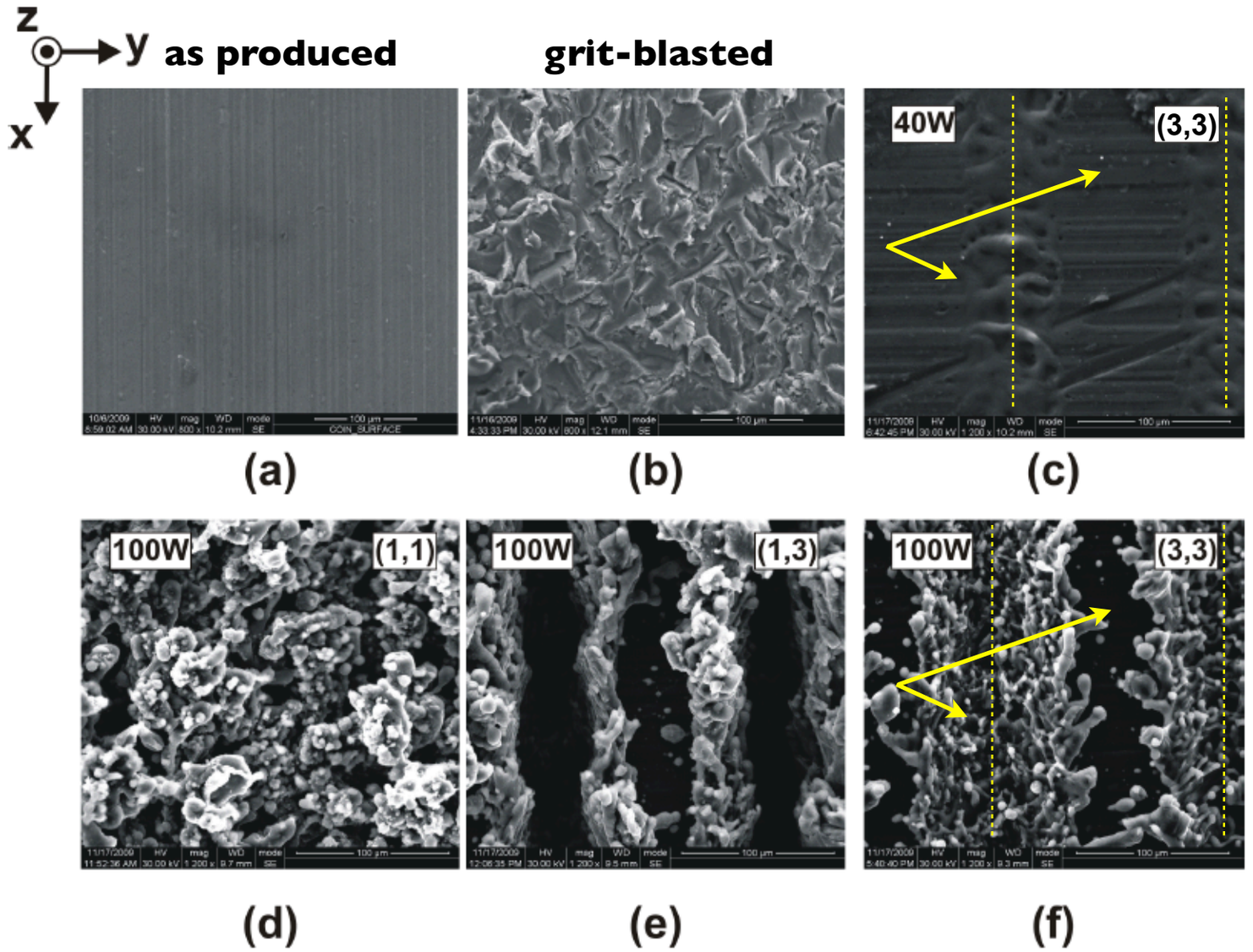

Figure 2: SEM observations of (a) as-produced surface; (b) grit blasted surface and laser treated surface with (c) P=40W, LS=150μm, V=1000 mm/s, (d) P=100W, LS=50μm, V=500 mm/s, (e) P=100W, LS=150μm, V=500 mm/s, (f) P=100W, LS=150μm, V=1000 mm/s

M. Alfano, F. Furgiuele, G. Lubineau, G. H. Paulino, Role of laser surface preparation on damage and decohesion of Al/epoxy joints. Submitted for publication.

Substrates pre-treatment

SEM analyses

V \ LS	50	100	150
500	(1,1)	(1,2)	(1,3)
750	(2,1)	(2,2)	(2,3)
1000	(3,1)	(3,2)	(3,3)

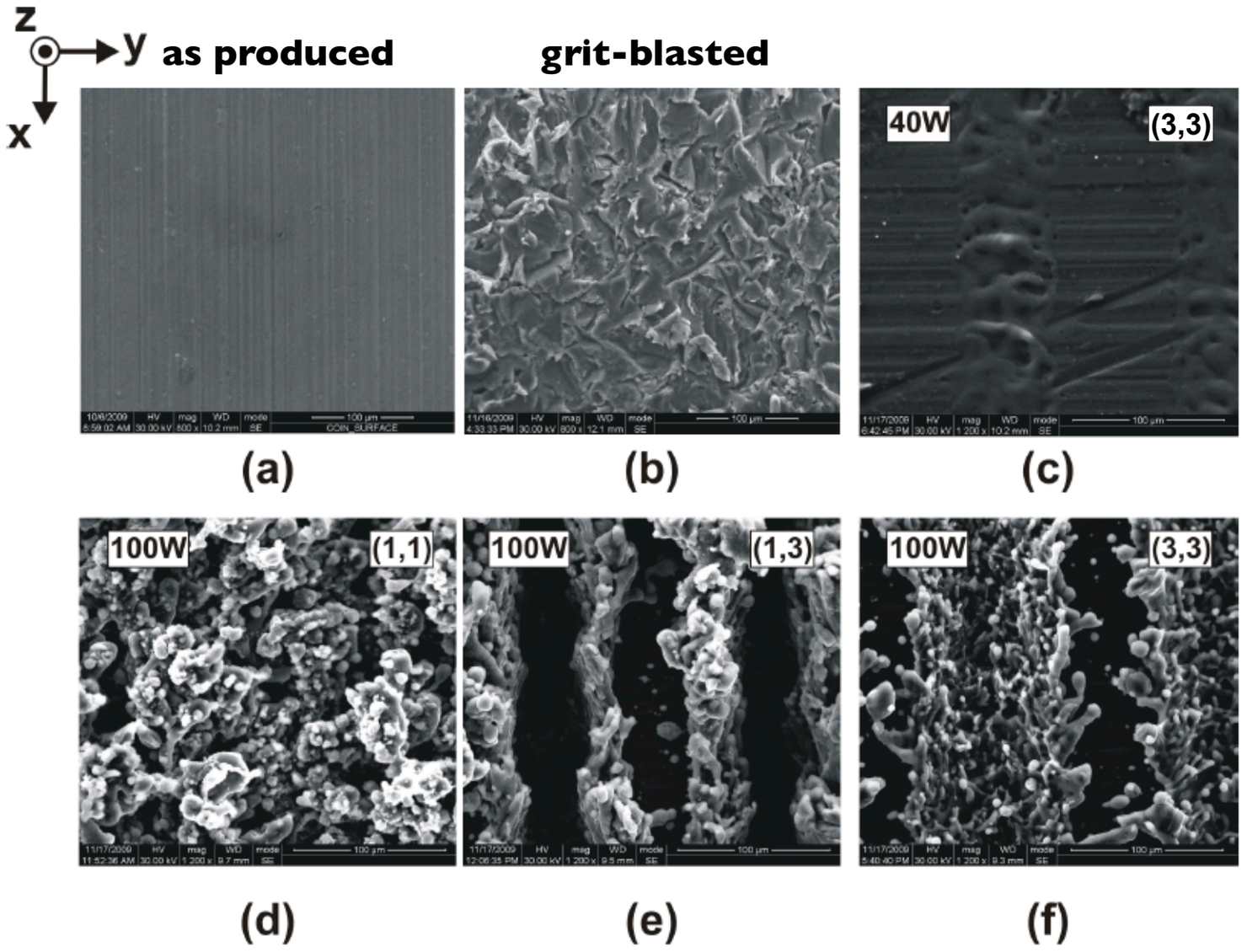

Figure 2: SEM observations of (a) as-produced surface; (b) grit blasted surface and laser treated surface with (c) P=40W, LS=150μm, V=1000 mm/s, (d) P=100W, LS=50μm, V=500 mm/s, (e) P=100W, LS=150μm, V=500 mm/s, (f) P=100W, LS=150μm, V=1000 mm/s

M. Alfano, F. Furgiuele, G. Lubineau, G. H. Paulino, Role of laser surface preparation on damage and decohesion of Al/epoxy joints. Submitted for publication.

Substrates pre-treatment

SEM analyses

V \ LS	50	100	150
500	(1,1)	(1,2)	(1,3)
750	(2,1)	(2,2)	(2,3)
1000	(3,1)	(3,2)	(3,3)

Spacing

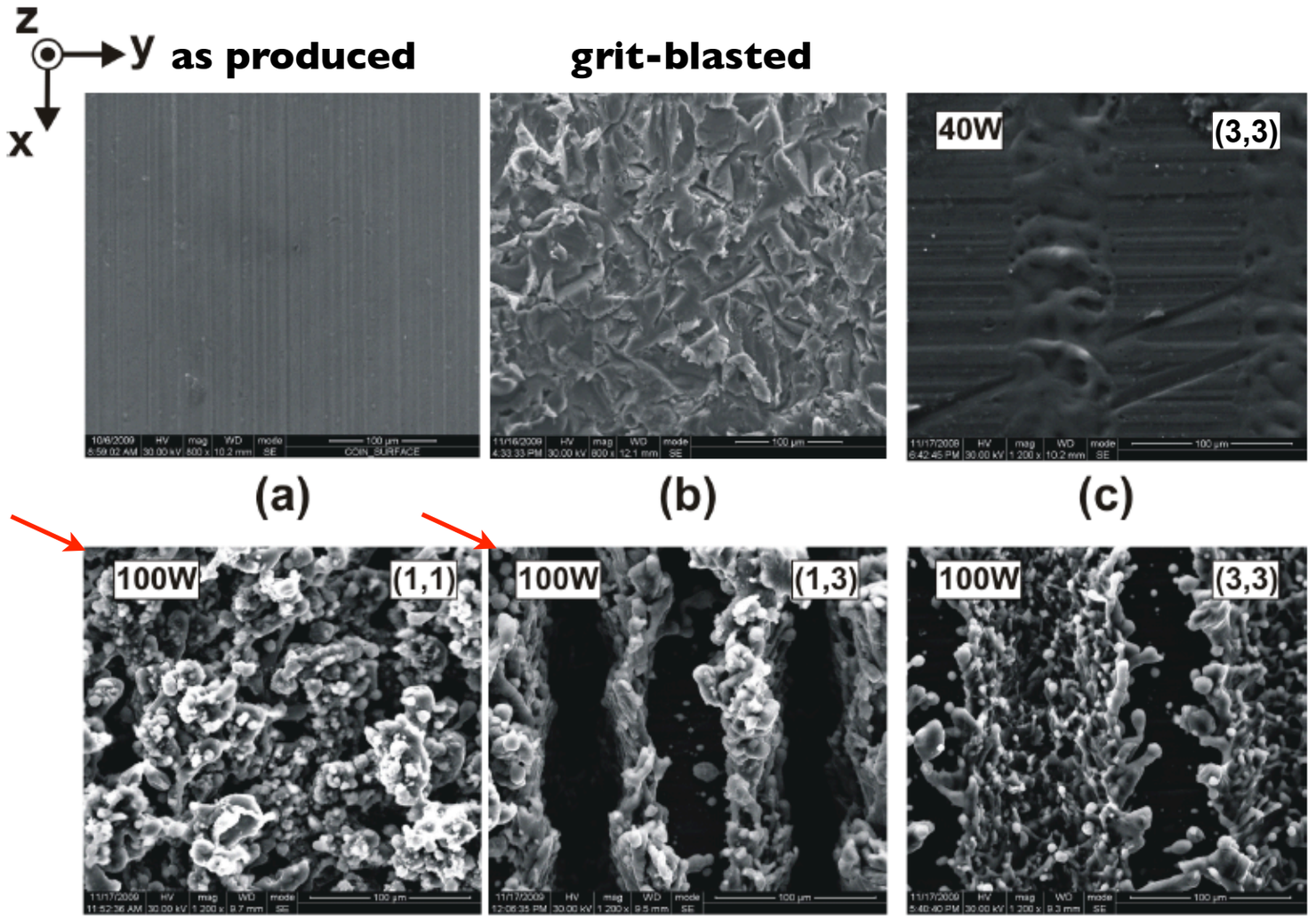

Figure 2: SEM observations of (a) as-produced surface; (b) grit blasted surface and laser treated surface with (c) P=40W, LS=150μm, V=1000 mm/s, (d) P=100W, LS=50μm, V=500 mm/s, (e) P=100W, LS=150μm, V=500 mm/s, (f) P=100W, LS=150μm, V=1000 mm/s

M. Alfano, F. Furgiuele, G. Lubineau, G. H. Paulino, Role of laser surface preparation on damage and decohesion of Al/epoxy joints. Submitted for publication.

Substrates pre-treatment

SEM analyses

V \ LS	50	100	150
500	(1,1)	(1,2)	(1,3)
750	(2,1)	(2,2)	(2,3)
1000	(3,1)	(3,2)	(3,3)

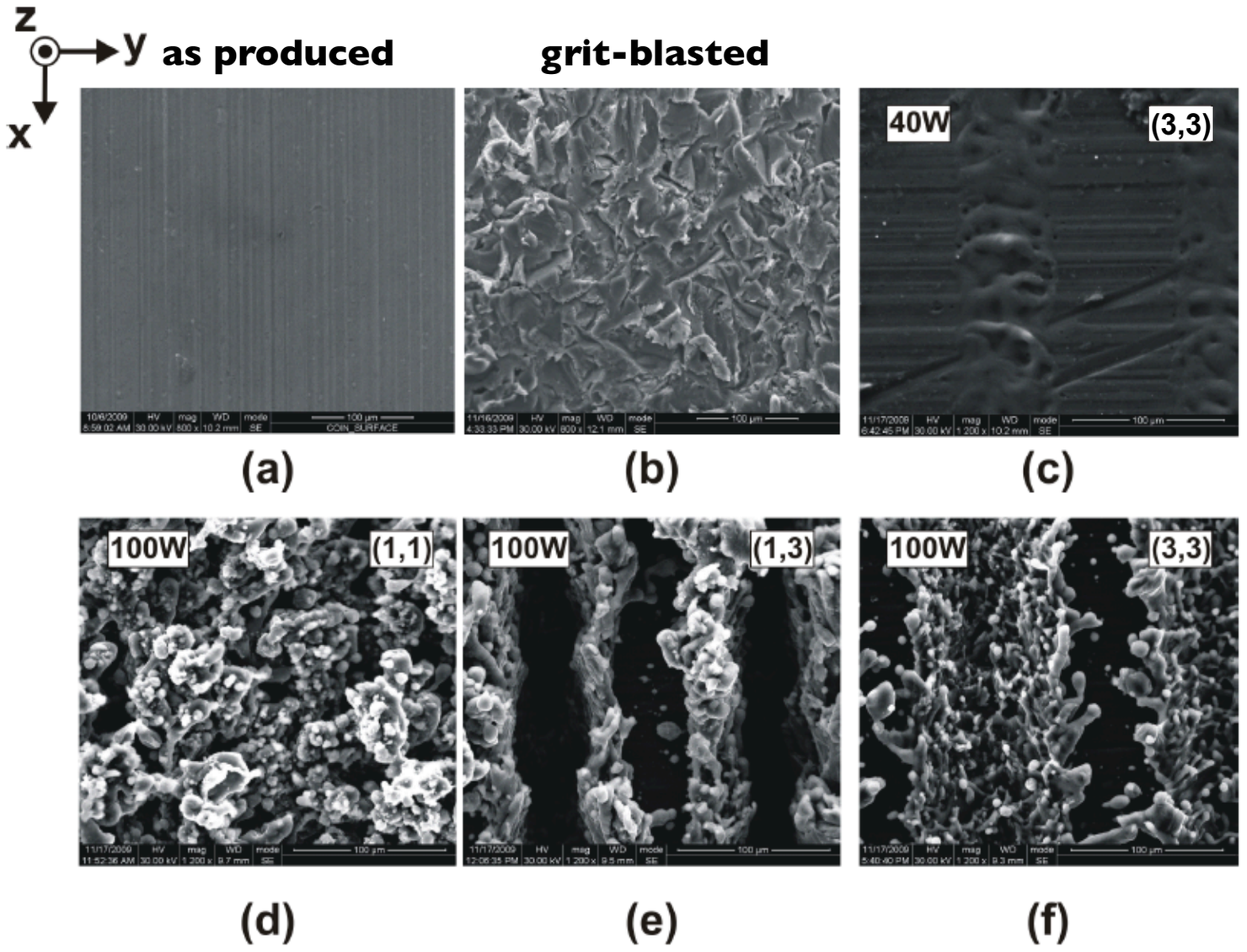

Figure 2: SEM observations of (a) as-produced surface; (b) grit blasted surface and laser treated surface with (c) P=40W, LS=150μm, V=1000 mm/s, (d) P=100W, LS=50μm, V=500 mm/s, (e) P=100W, LS=150μm, V=500 mm/s, (f) P=100W, LS=150μm, V=1000 mm/s

M. Alfano, F. Furgiuele, G. Lubineau, G. H. Paulino, Role of laser surface preparation on damage and decohesion of Al/epoxy joints. Submitted for publication.

Substrates pre-treatment

SEM analyses

V \ LS	50	100	150
500	(1,1)	(1,2)	(1,3)
750	(2,1)	(2,2)	(2,3)
1000	(3,1)	(3,2)	(3,3)

Speed

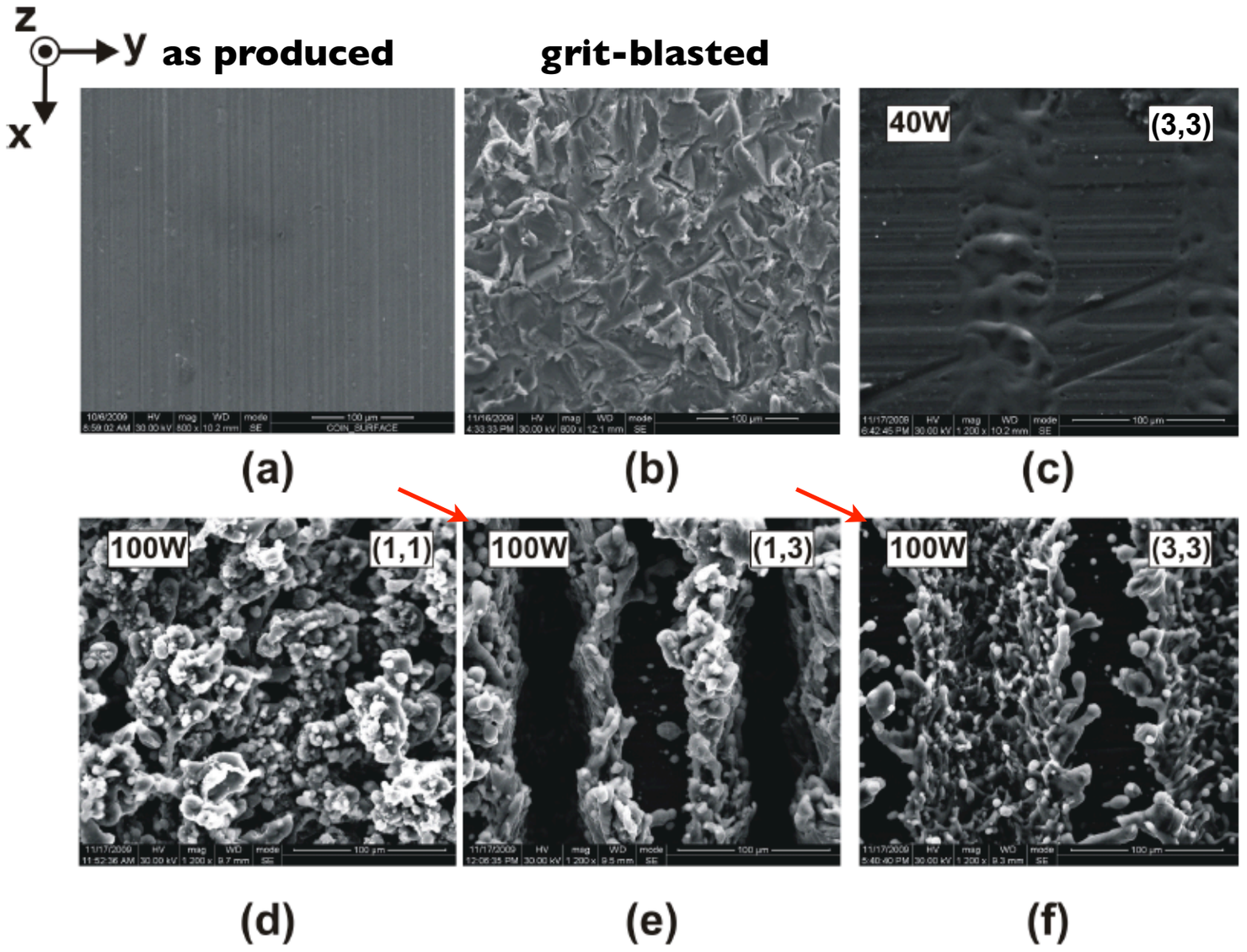

Figure 2: SEM observations of (a) as-produced surface; (b) grit blasted surface and laser treated surface with (c) P=40W, LS=150μm, V=1000 mm/s, (d) P=100W, LS=50μm, V=500 mm/s, (e) P=100W, LS=150μm, V=500 mm/s, (f) P=100W, LS=150μm, V=1000 mm/s

M. Alfano, F. Furgiuele, G. Lubineau, G. H. Paulino, Role of laser surface preparation on damage and decohesion of Al/epoxy joints. Submitted for publication.

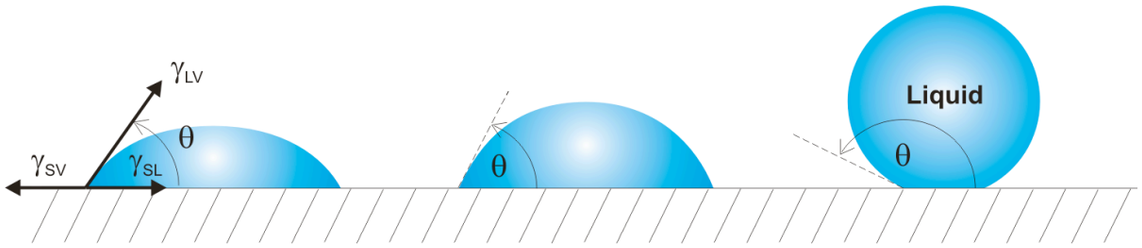

R.D. Adams et al, Structural Adhesives Joints in Engineering, Chapman&Hall, 1997.

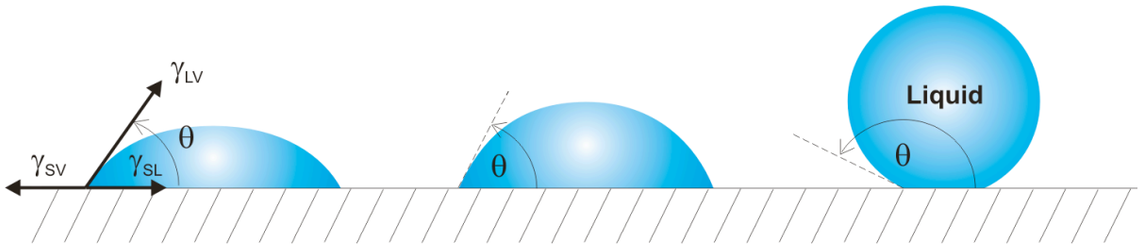

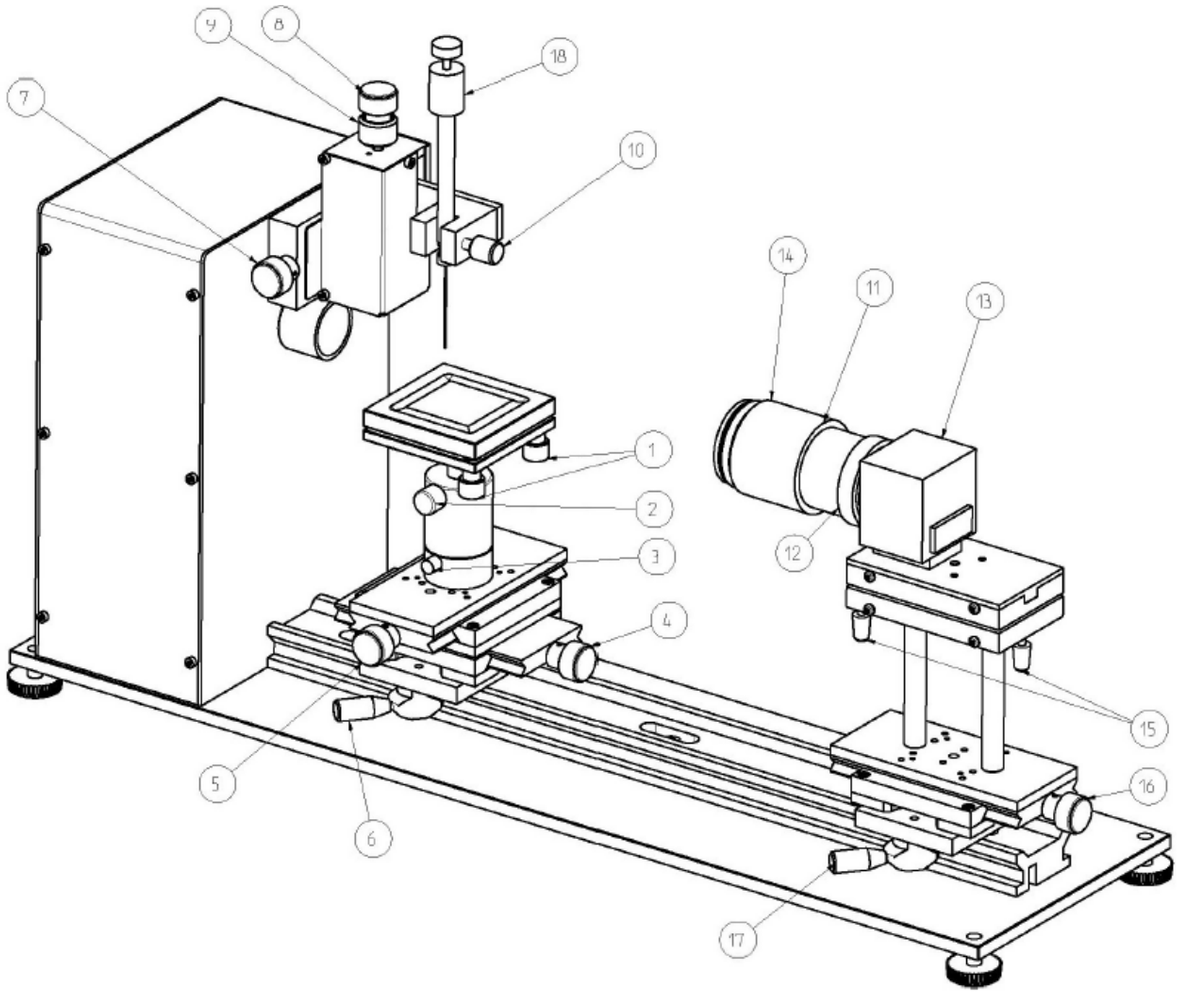

CAM200, KSV Instruments Ltd

R.D. Adams et al, Structural Adhesives Joints in Engineering, Chapman&Hall, 1997.

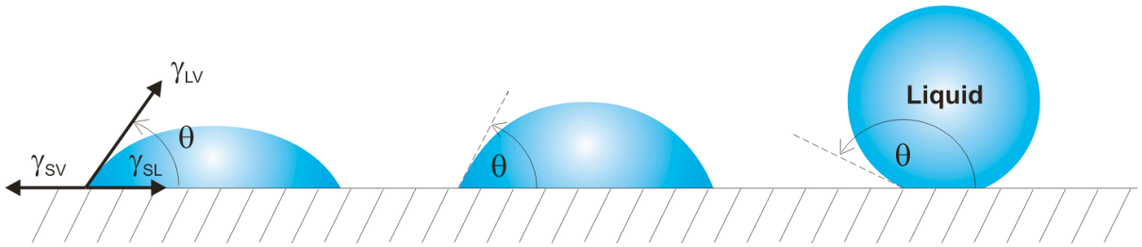

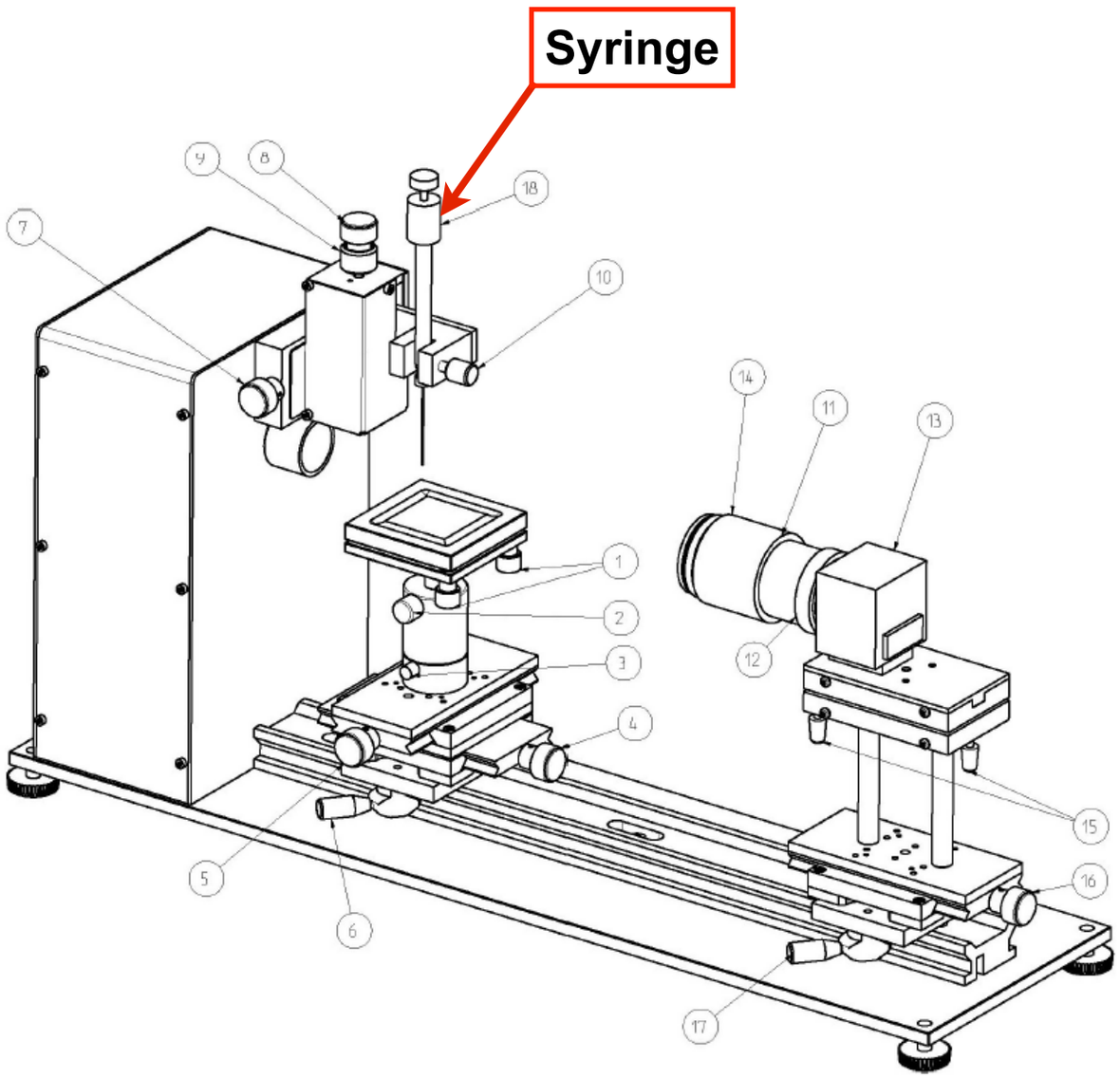

CAM200, KSV Instruments Ltd

R.D. Adams et al, Structural Adhesives Joints in Engineering, Chapman&Hall, 1997.

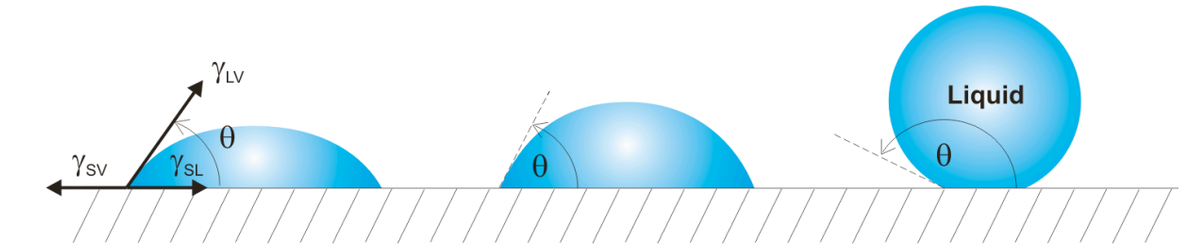

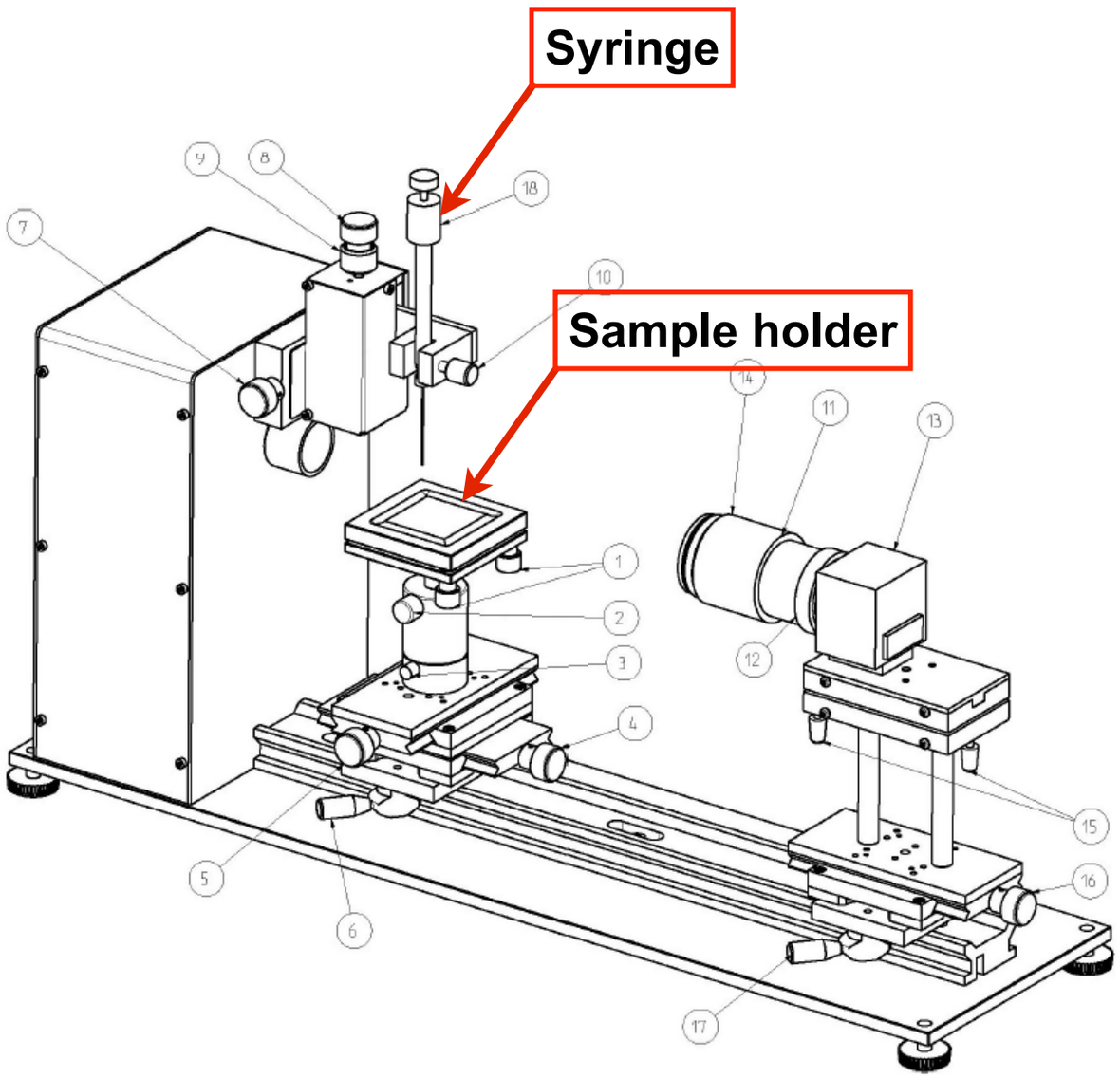

CAM200, KSV Instruments Ltd

R.D. Adams et al, Structural Adhesives Joints in Engineering, Chapman&Hall, 1997.

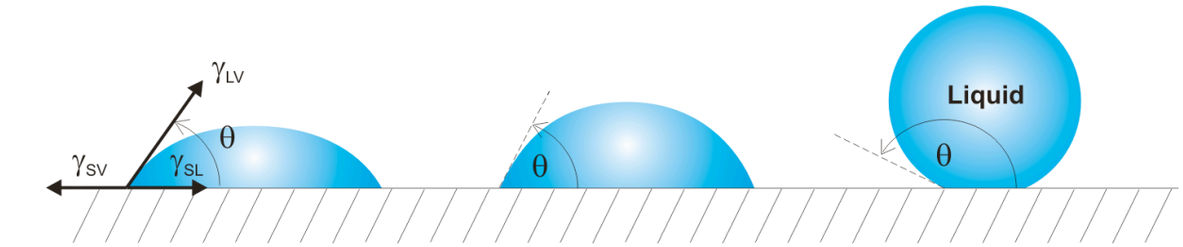

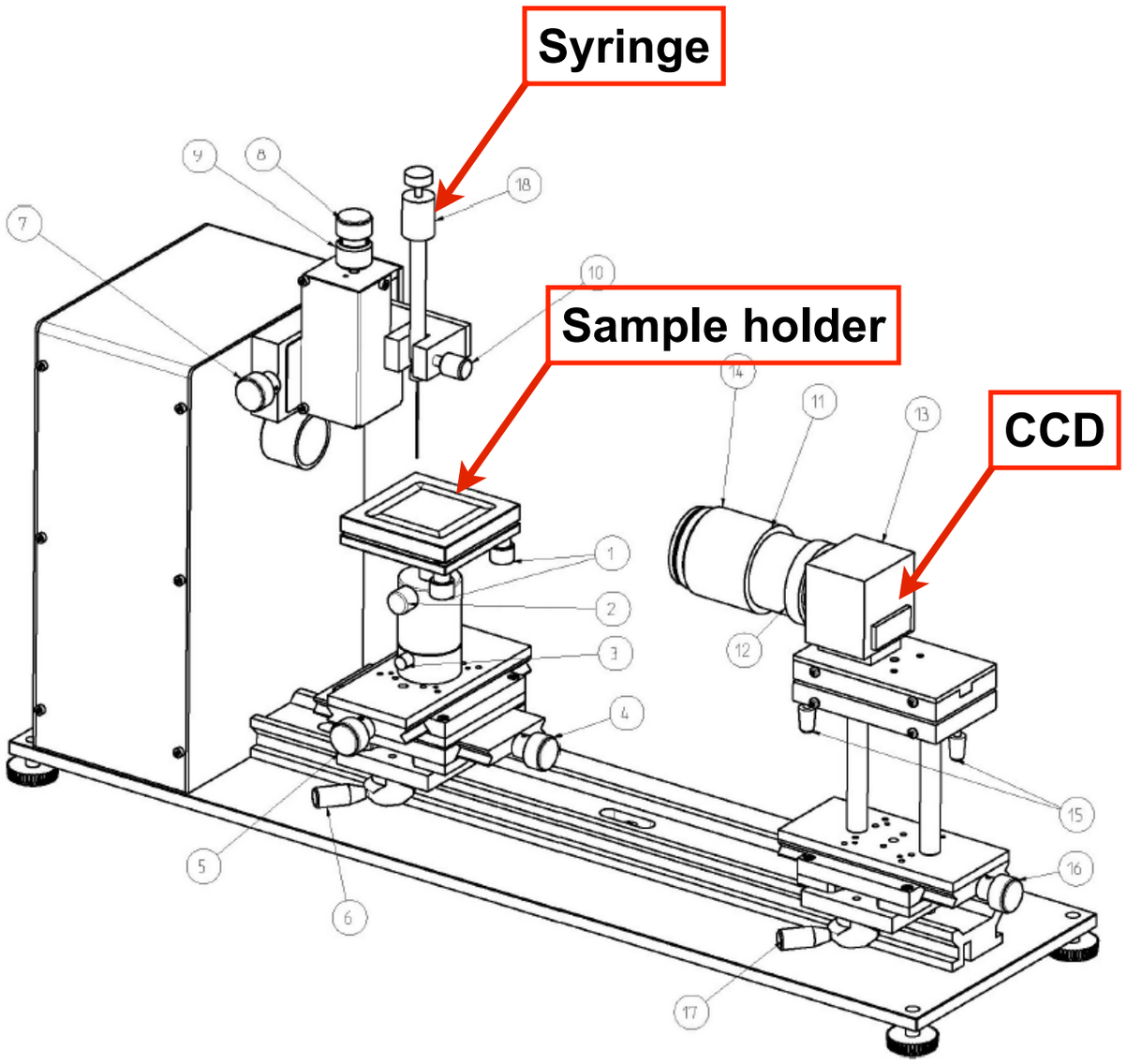

CAM200, KSV Instruments Ltd

R.D. Adams et al, Structural Adhesives Joints in Engineering, Chapman&Hall, 1997.

Substrates pre-treatment

Determination of contact angle

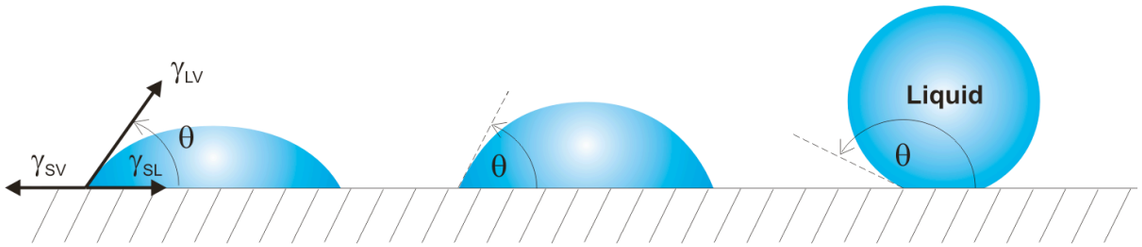

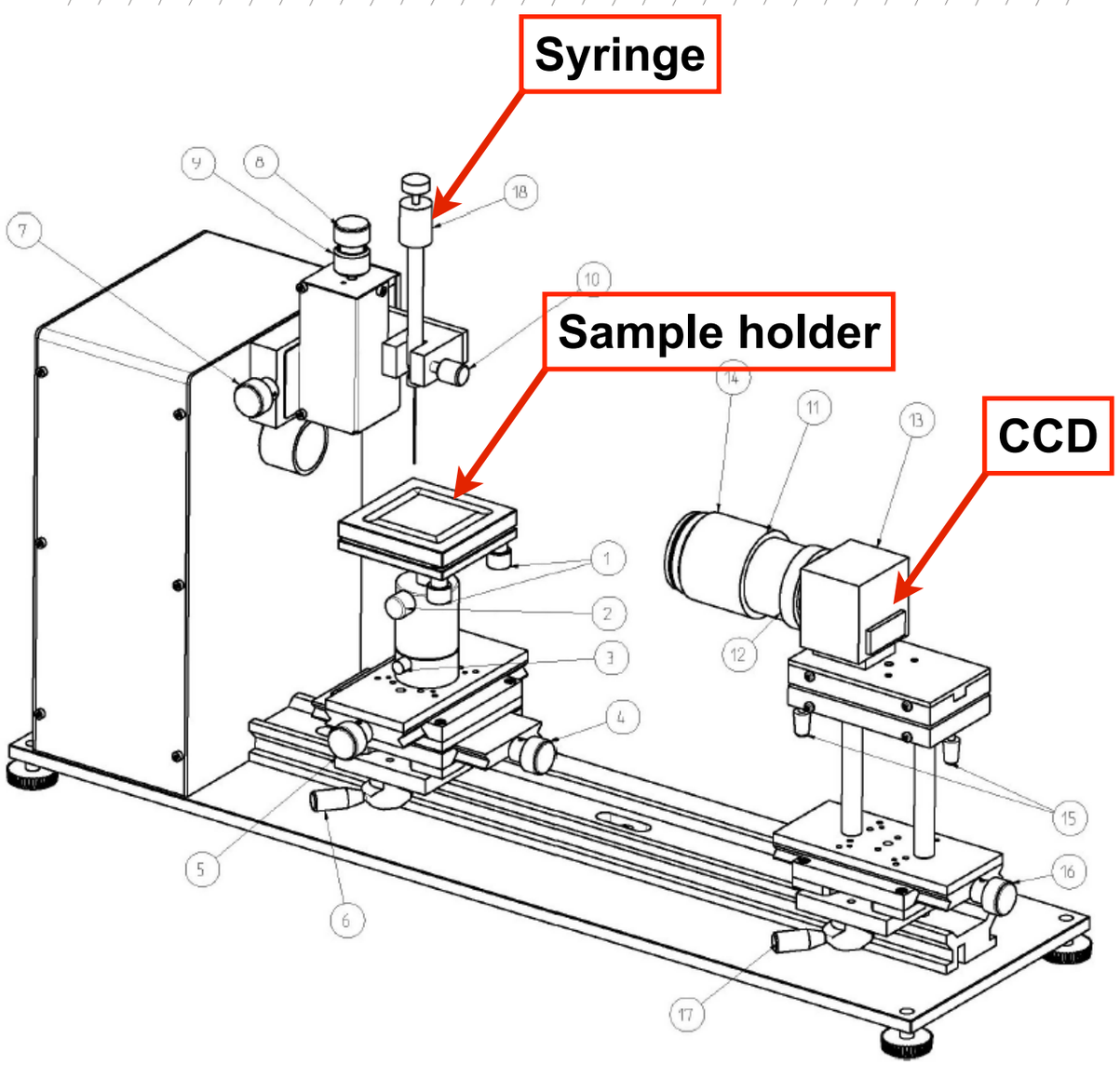

CAM200, KSV Instruments Ltd

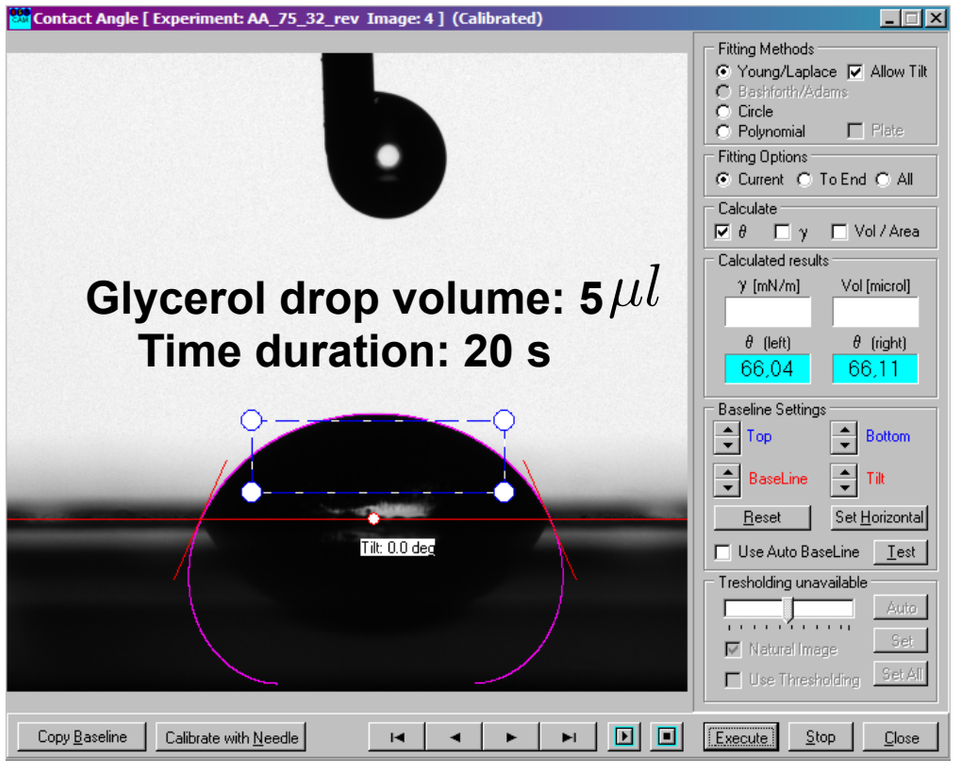

R.D. Adams et al, Structural Adhesives Joints in Engineering, Chapman&Hall, 1997.

Substrates pre-treatment

Determination of contact angle

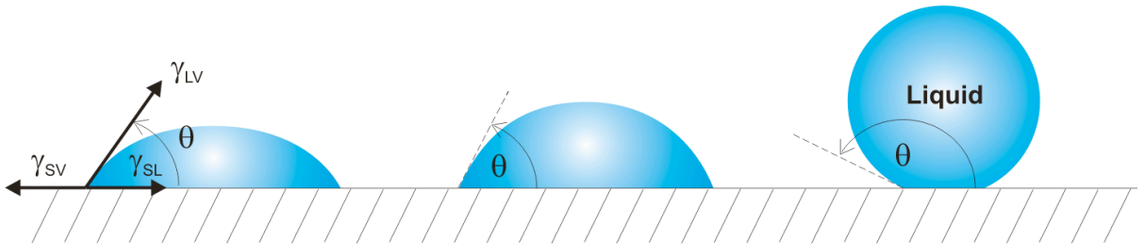

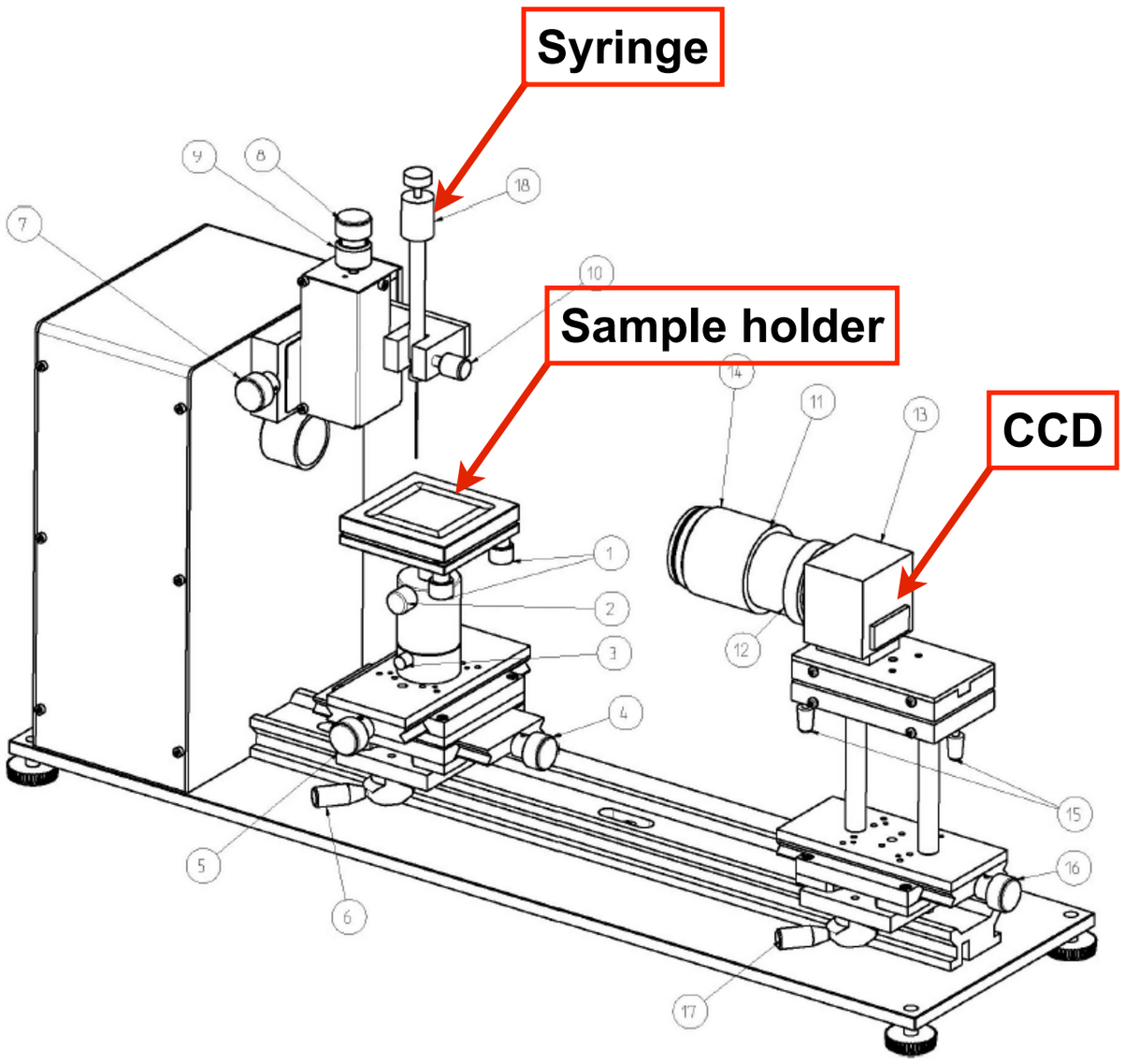

CAM200, KSV Instruments Ltd

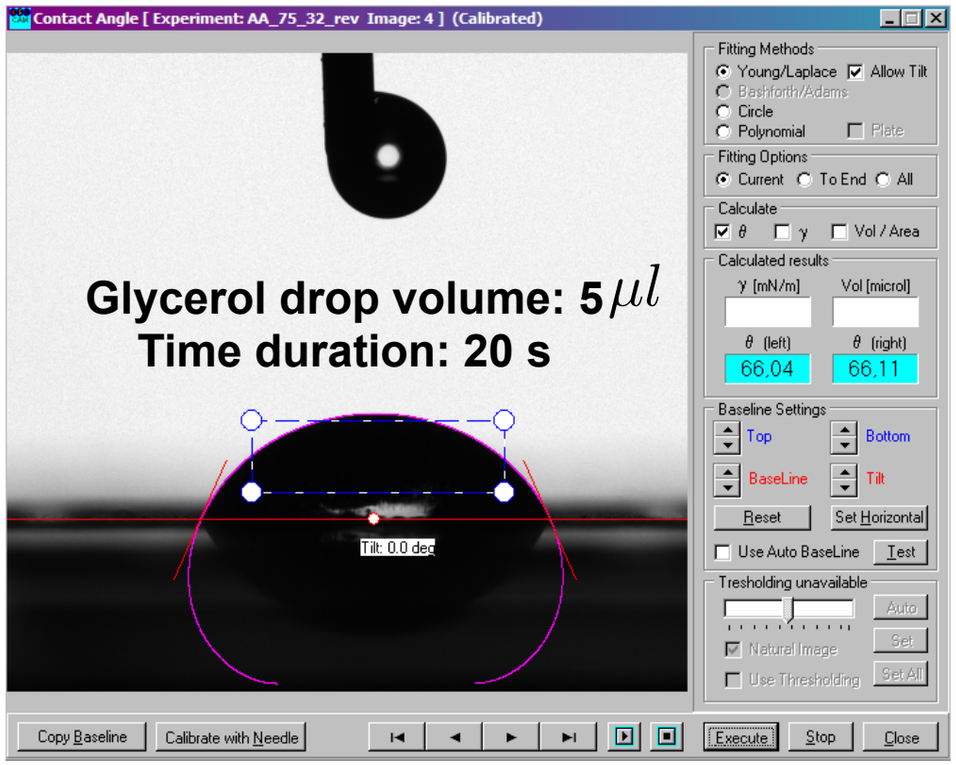

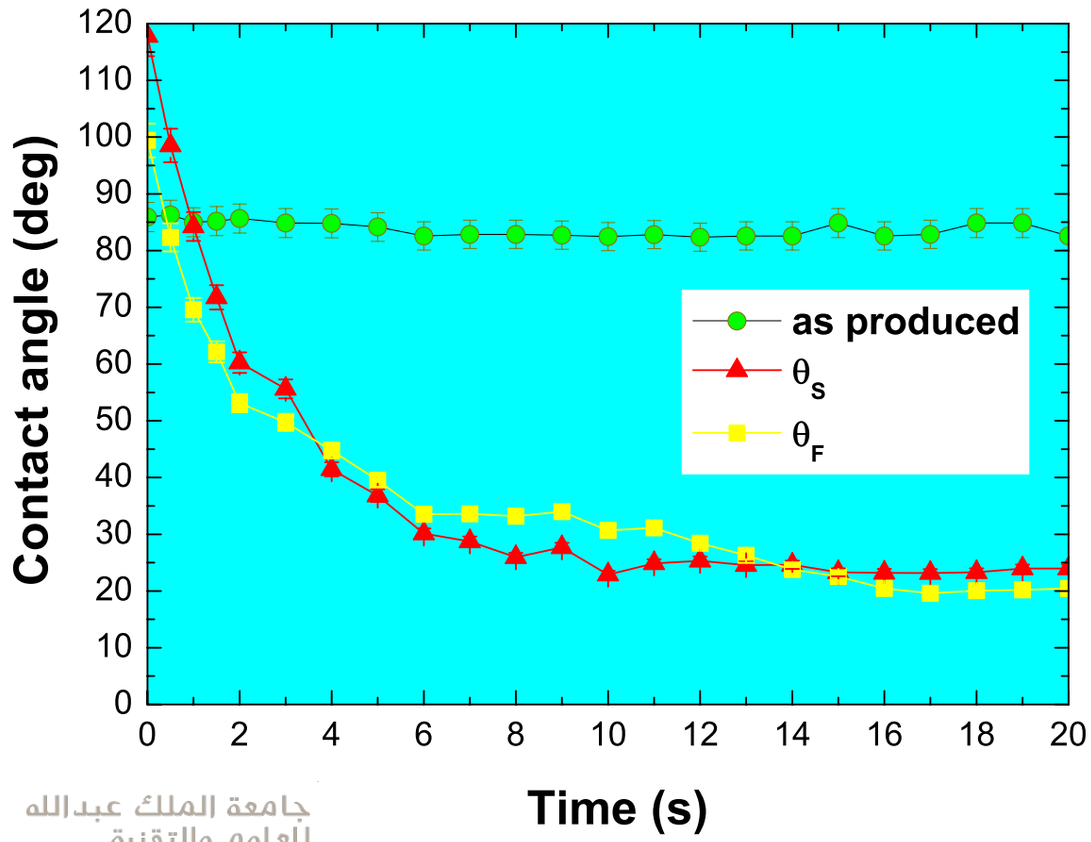

R.D. Adams et al, Structural Adhesives Joints in Engineering, Chapman&Hall, 1997.

Substrates pre-treatment

Determination of contact angle

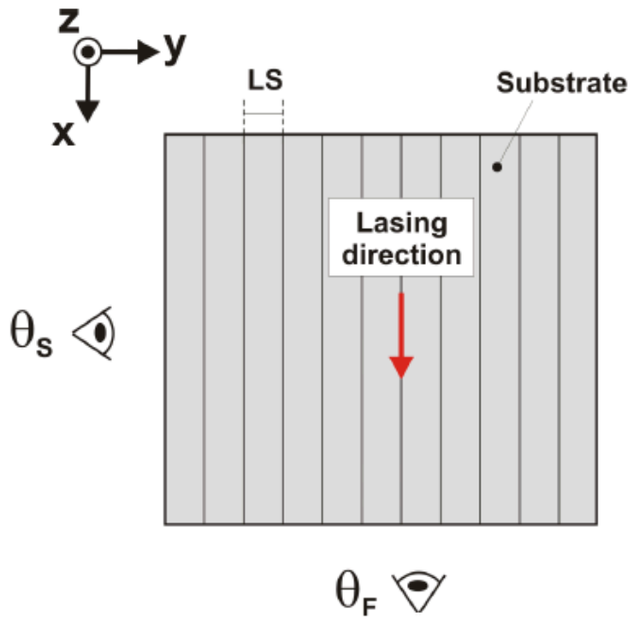

M. Alfano, F. Furgiuele, G. Lubineau, G. H. Paulino, Role of laser surface preparation on damage and decohesion of Al/epoxy joints. Submitted for publication.

Substrates pre-treatment

Determination of contact angle

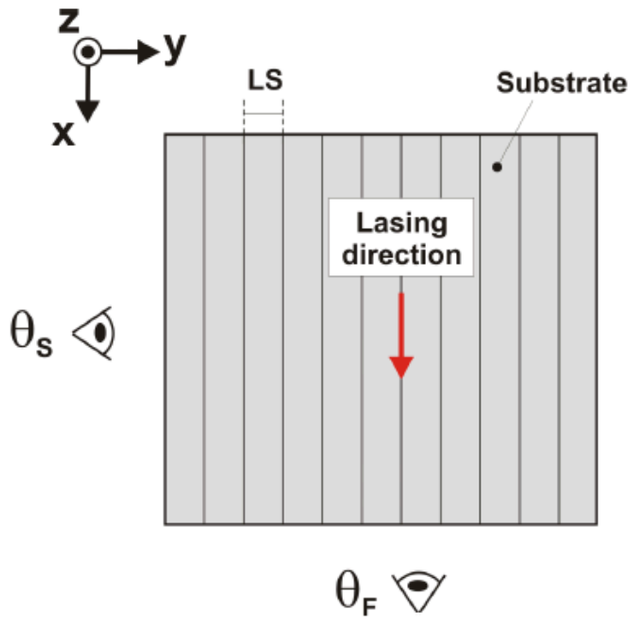

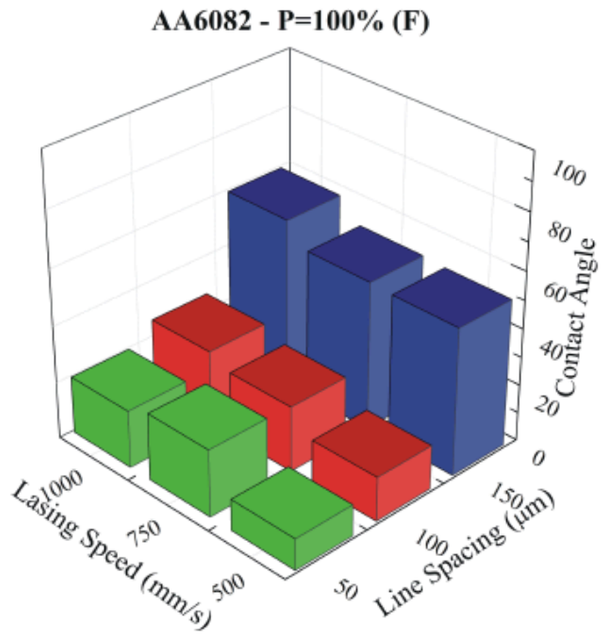

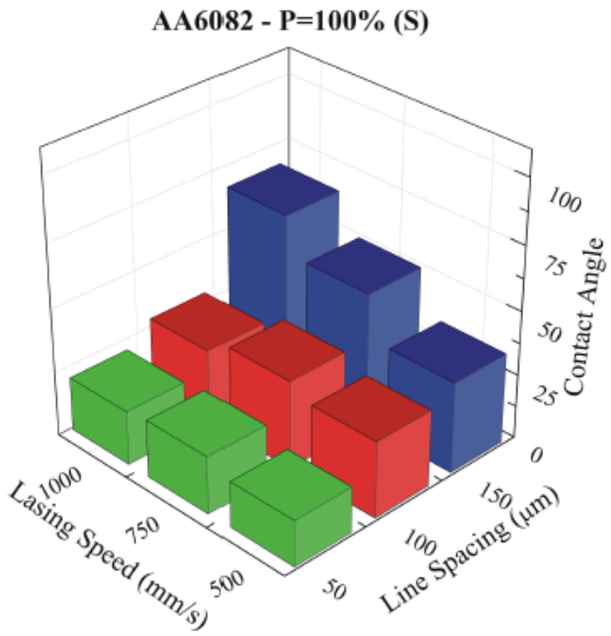

M. Alfano, F. Furgiuele, G. Lubineau, G. H. Paulino, Role of laser surface preparation on damage and decohesion of Al/epoxy joints. Submitted for publication.

Substrates pre-treatment

Determination of contact angle

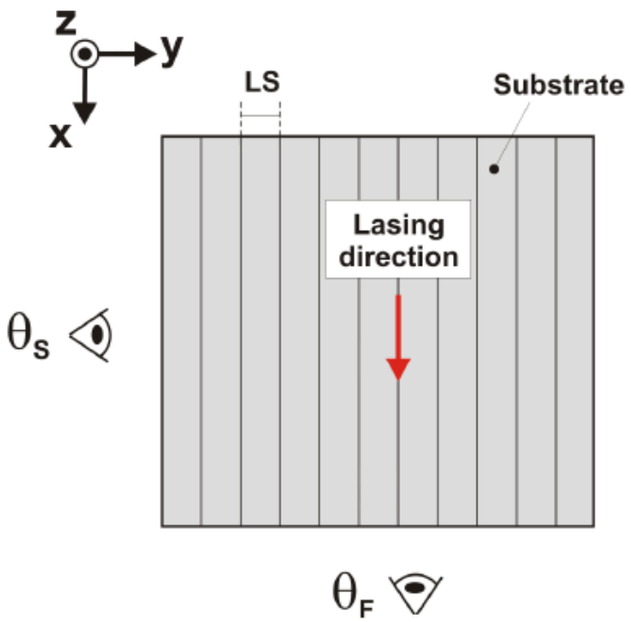

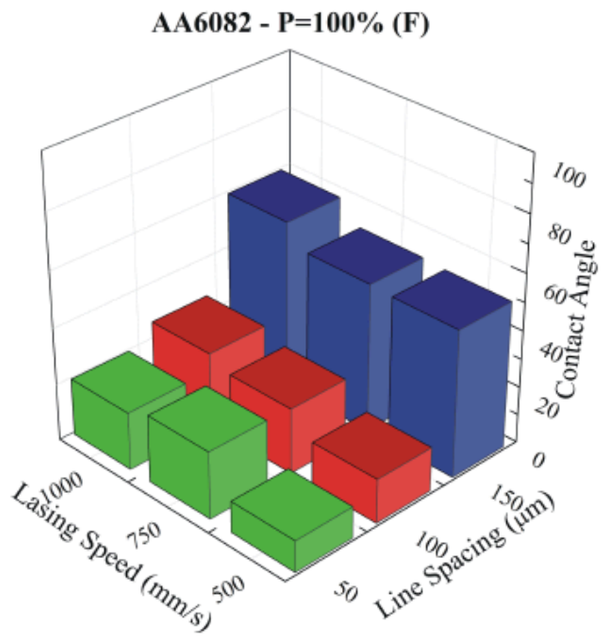

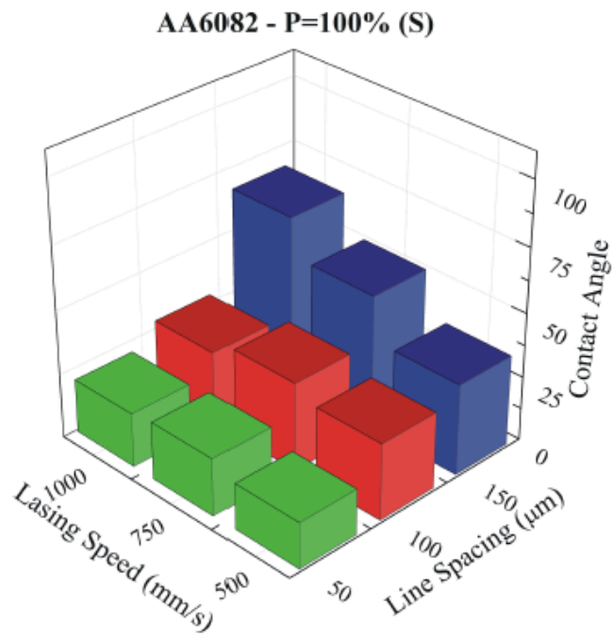

- θ_F and θ_S increase with line LS,
- in addition, for higher LS: $\theta_F \neq \theta_S$,
- for lower LS: $\theta_F \approx \theta_S$ - slight dependence on V

M. Alfano, F. Furgiuele, G. Lubineau, G. H. Paulino, Role of laser surface preparation on damage and decohesion of Al/epoxy joints. Submitted for publication.

Substrates pre-treatment

Determination of contact angle

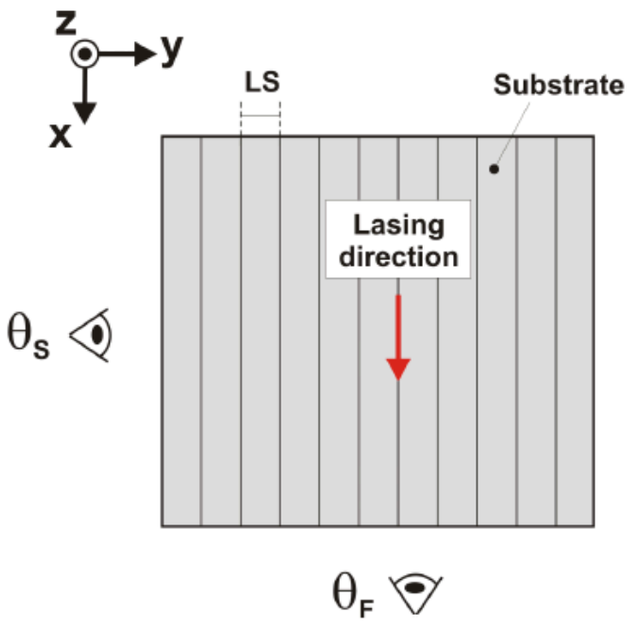

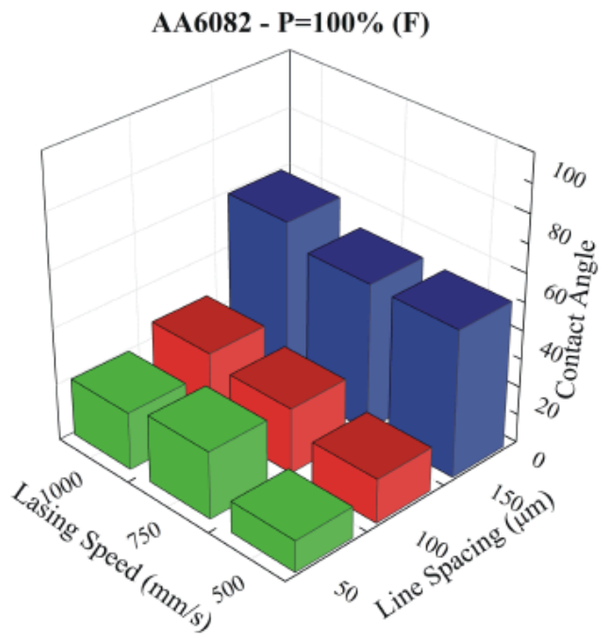

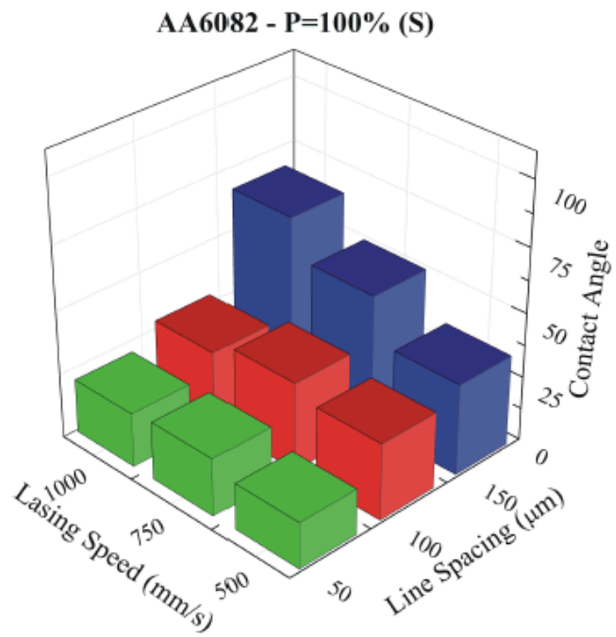

- θ_F and θ_S increase with line LS,
- in addition, for higher LS: $\theta_F \neq \theta_S$,
- for lower LS: $\theta_F \approx \theta_S$ - slight dependence on V

$$\theta \approx 83^o$$

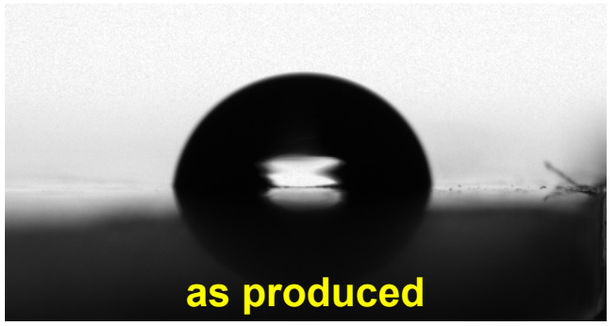

M. Alfano, F. Furgiuele, G. Lubineau, G. H. Paulino, Role of laser surface preparation on damage and decohesion of Al/epoxy joints. Submitted for publication.

Substrates pre-treatment

Determination of contact angle

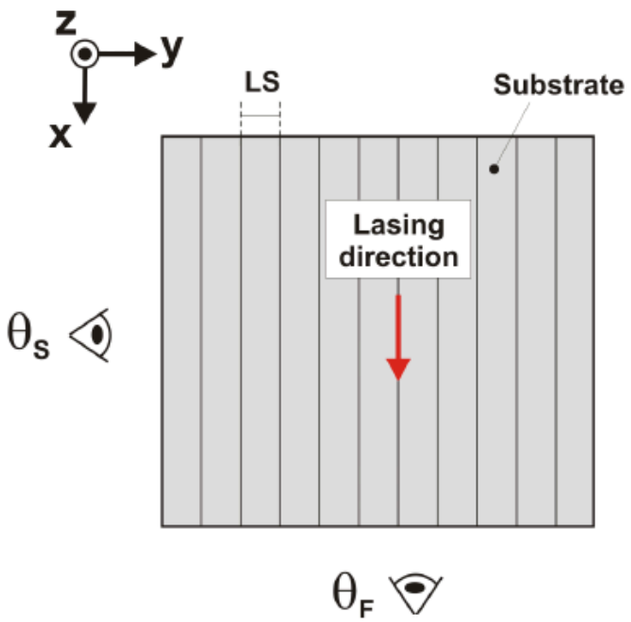

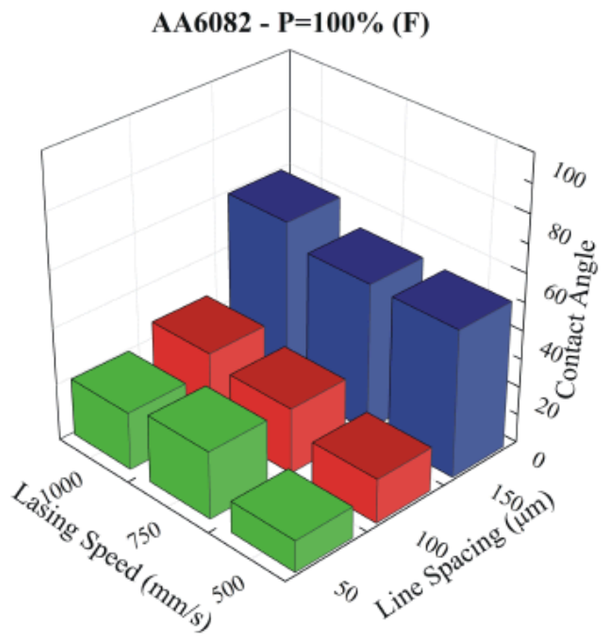

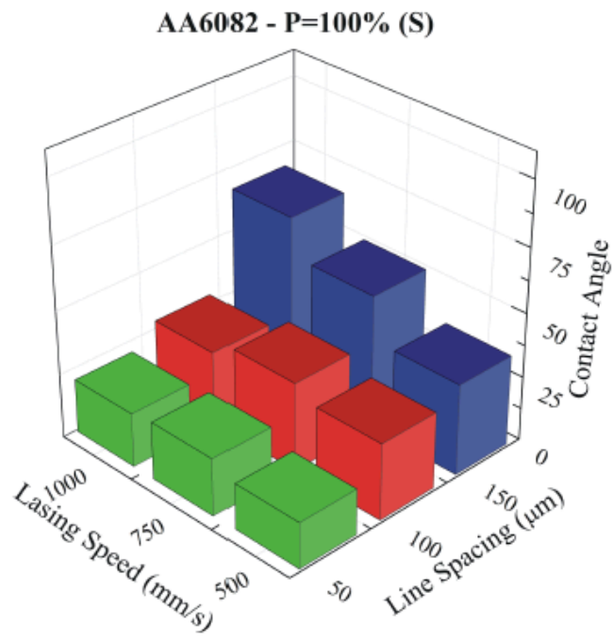

- θ_F and θ_S increase with line LS,
- in addition, for higher LS: $\theta_F \neq \theta_S$,
- for lower LS: $\theta_F \approx \theta_S$ - slight dependence on V

$\theta \approx 83^o$

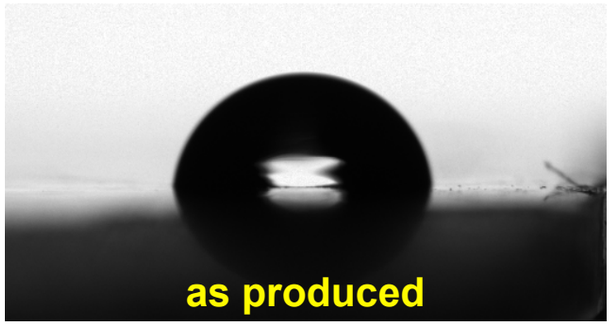

20^o

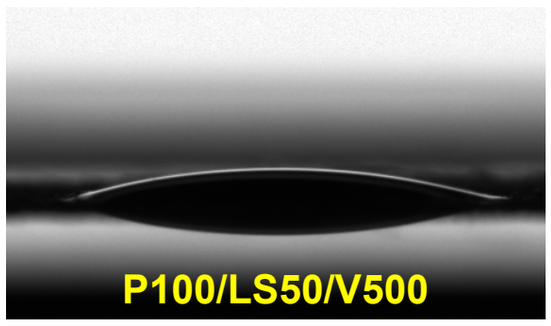

M. Alfano, F. Furgiuele, G. Lubineau, G. H. Paulino, Role of laser surface preparation on damage and decohesion of Al/epoxy joints. Submitted for publication.

Substrates pre-treatment

Determination of contact angle

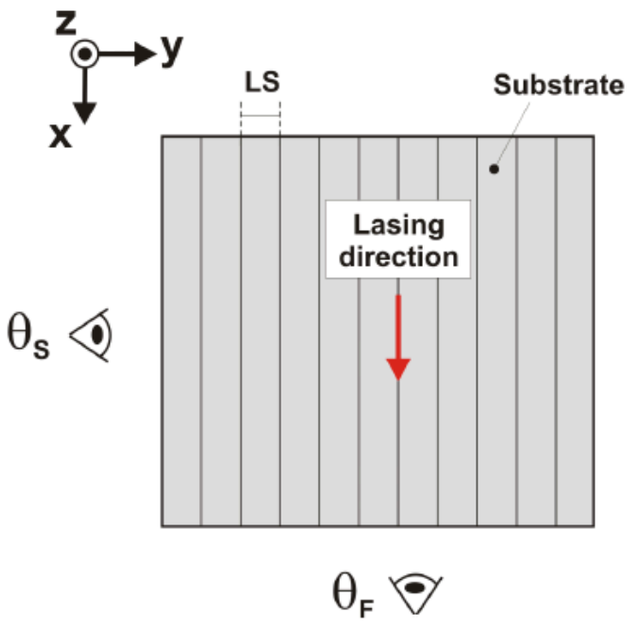

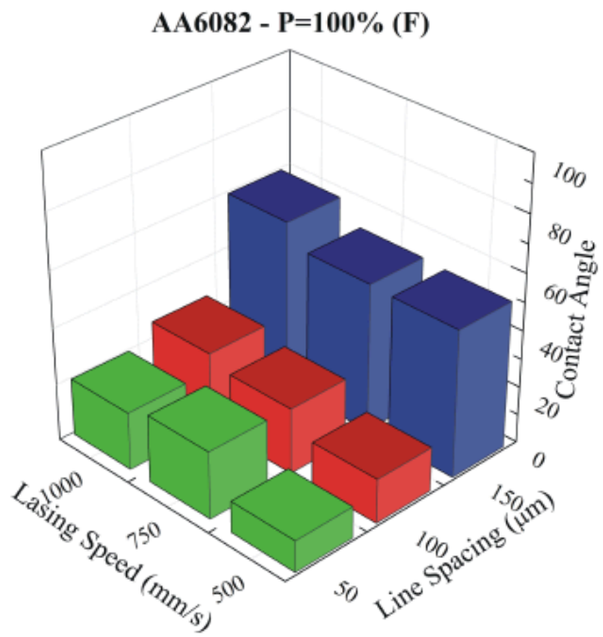

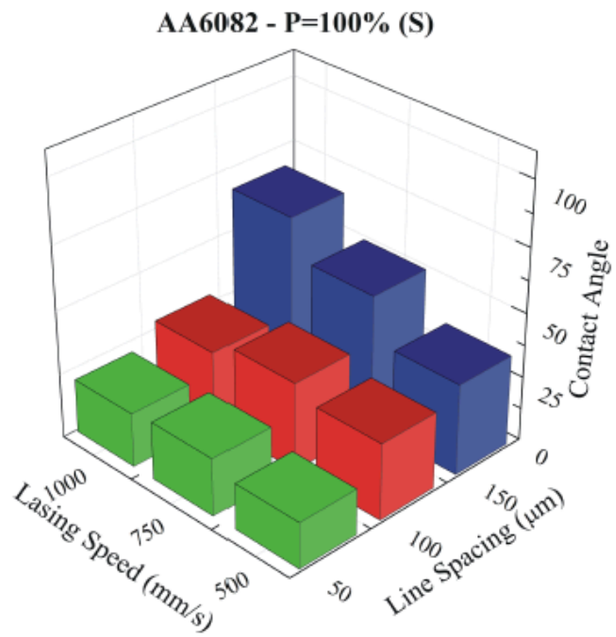

- θ_F and θ_S increase with line LS,
- in addition, for higher LS: $\theta_F \neq \theta_S$,
- for lower LS: $\theta_F \approx \theta_S$ - slight dependence on V

$\theta \approx 83^o$ 20^o

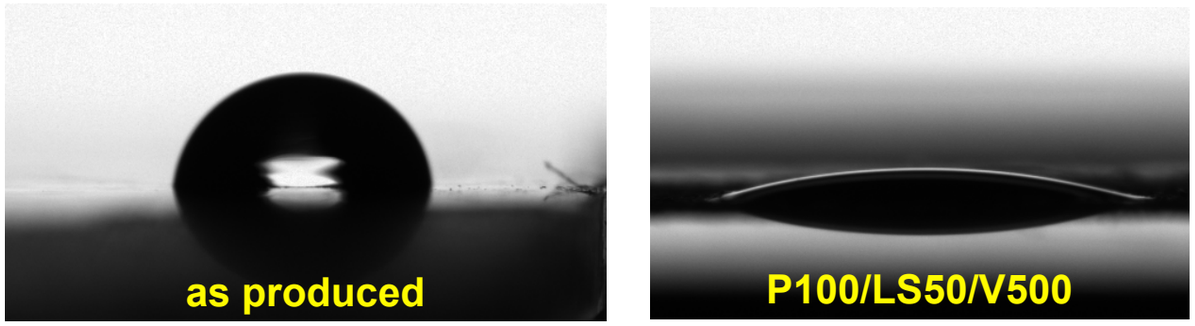

M. Alfano, F. Furgiuele, G. Lubineau, G. H. Paulino, Role of laser surface preparation on damage and decohesion of Al/epoxy joints. Submitted for publication.

Laser velocity increases →

Substrates pre-treatment

Determination of contact angle

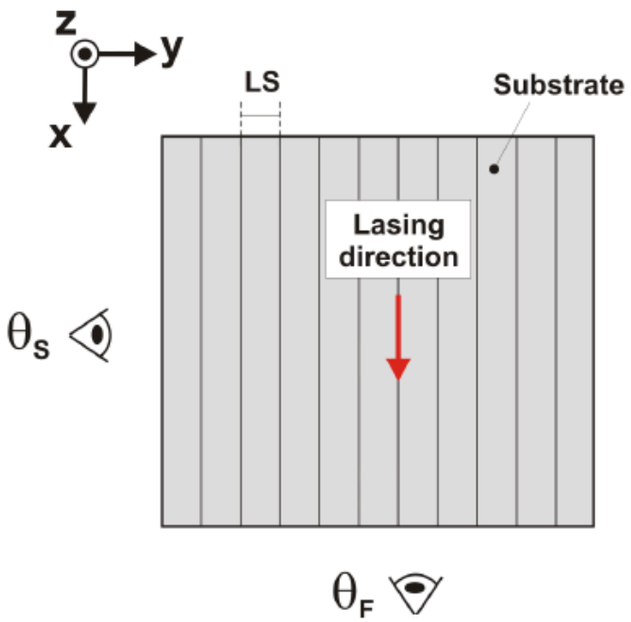

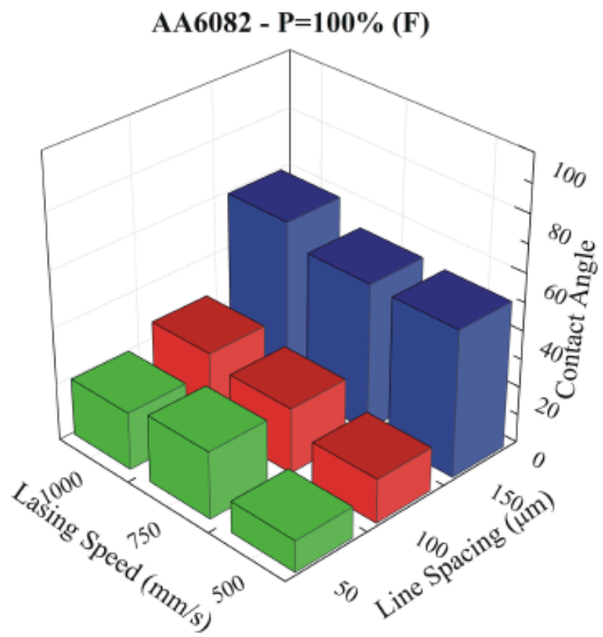

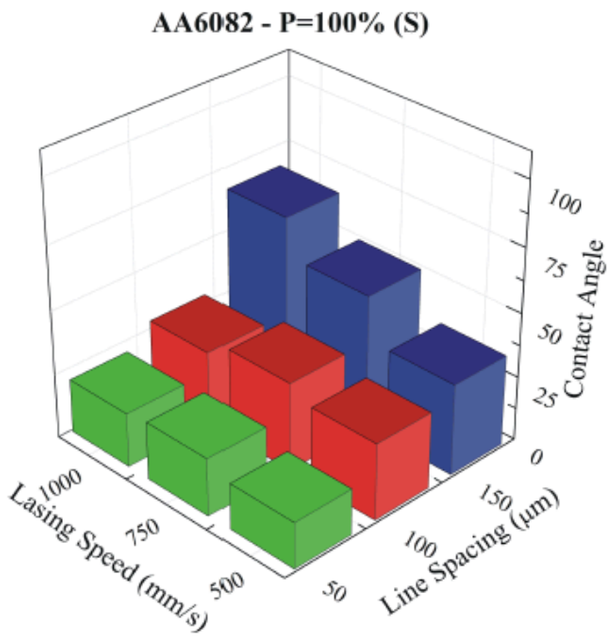

- θ_F and θ_S increase with line LS,
- in addition, for higher LS: $\theta_F \neq \theta_S$,
- for lower LS: $\theta_F \approx \theta_S$ - slight dependence on V

$\theta \approx 83^o$ 20^o 25^o

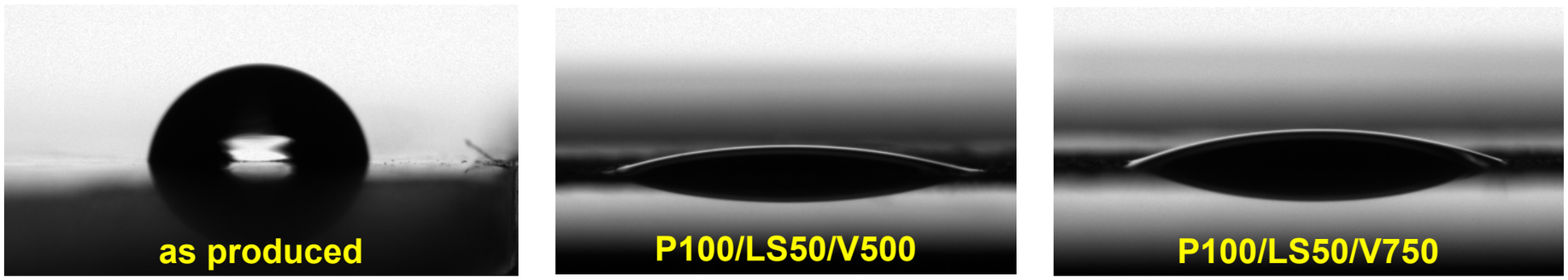

Laser velocity increases →

M. Alfano, F. Furgiuele, G. Lubineau, G. H. Paulino, Role of laser surface preparation on damage and decohesion of Al/epoxy joints. Submitted for publication.

Substrates pre-treatment

Determination of contact angle

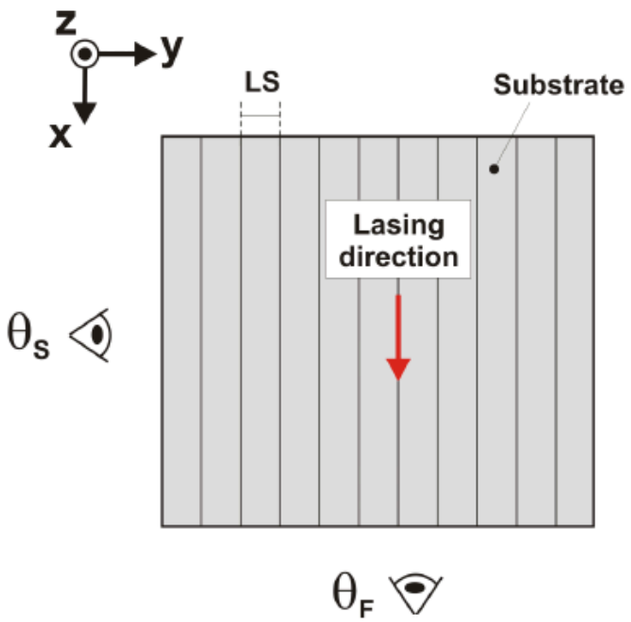

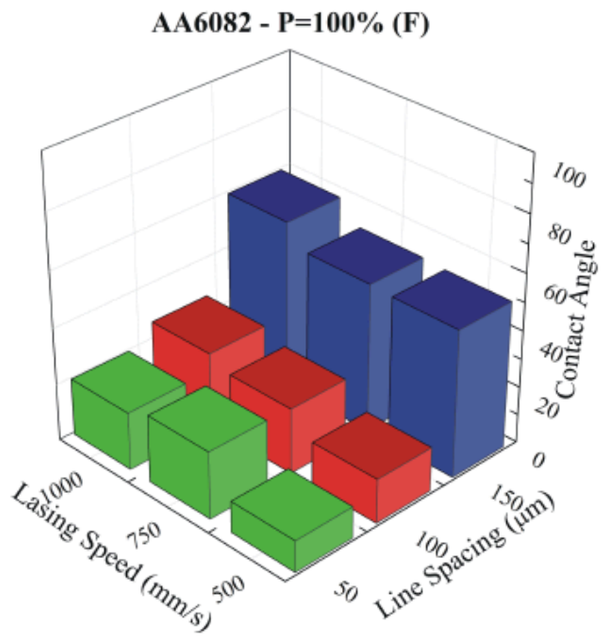

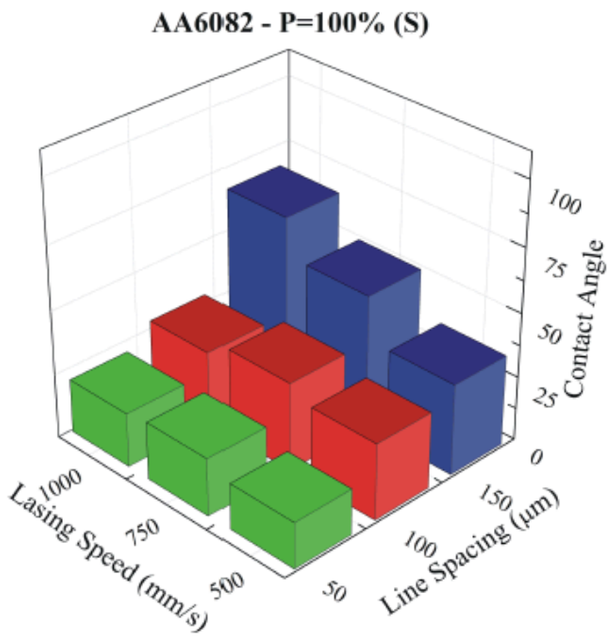

- θ_F and θ_S increase with line LS,
- in addition, for higher LS: $\theta_F \neq \theta_S$,
- for lower LS: $\theta_F \approx \theta_S$ - slight dependence on V

$\theta \approx 83^o$	20^o	25^o	23^o
as produced	P100/LS50/V500	P100/LS50/V750	P100/LS50/V1000

Laser velocity increases →

M. Alfano, F. Furgiuele, G. Lubineau, G. H. Paulino, Role of laser surface preparation on damage and decohesion of Al/epoxy joints. Submitted for publication.

Substrates pre-treatment

Determination of contact angle

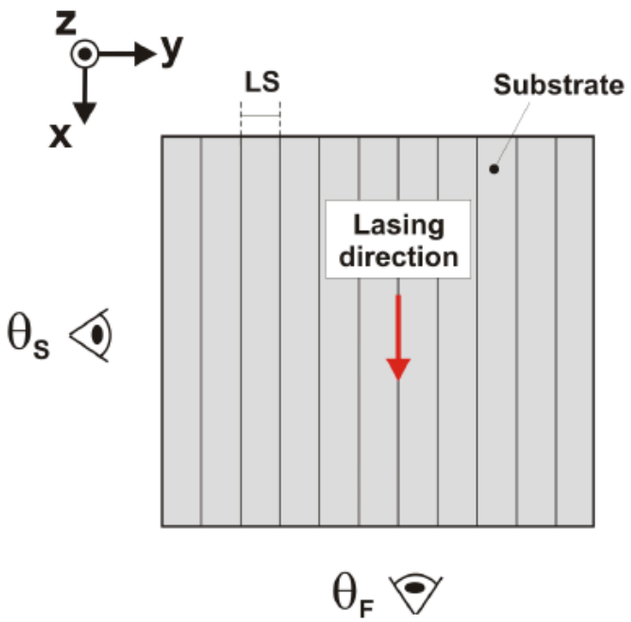

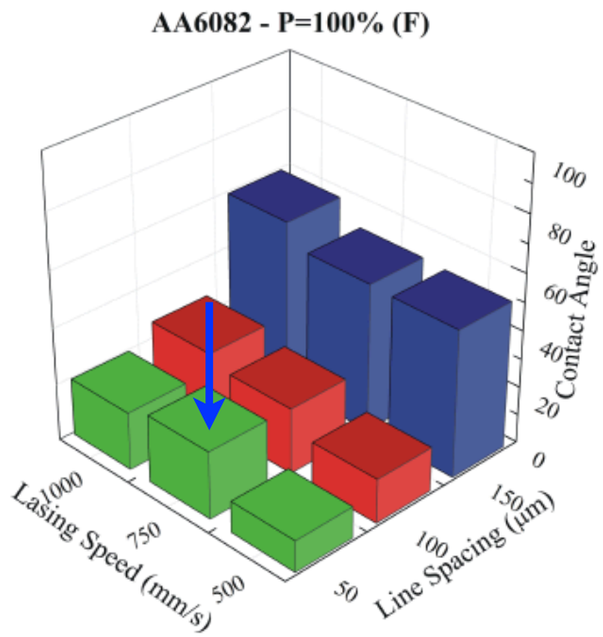

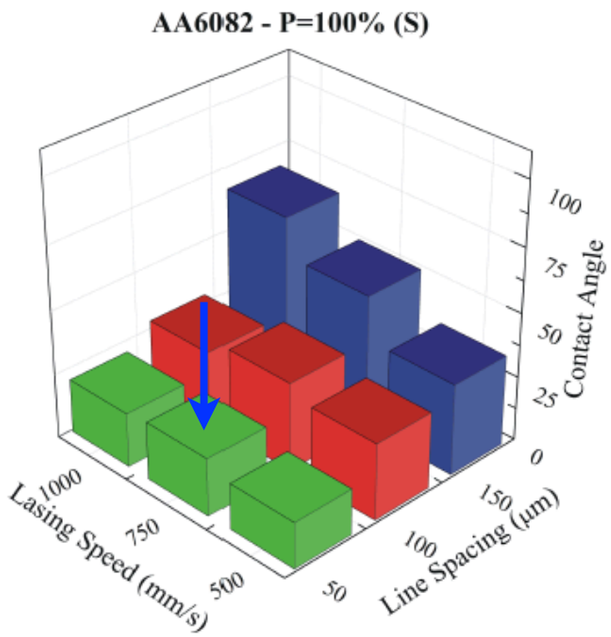

- θ_F and θ_S increase with line LS,
- in addition, for higher LS: $\theta_F \neq \theta_S$,
- for lower LS: $\theta_F \approx \theta_S$ - slight dependence on V

$\theta \approx 83^o$	20^o	25^o	23^o
as produced	P100/LS50/V500	P100/LS50/V750	P100/LS50/V1000

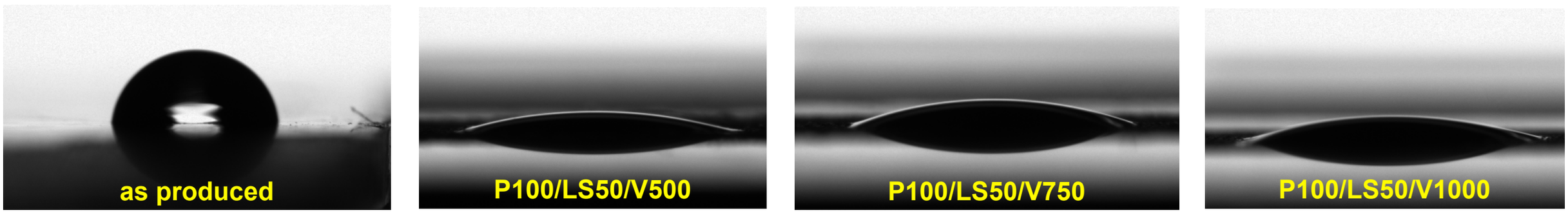

M. Alfano, F. Furgiuele, G. Lubineau, G. H. Paulino, Role of laser surface preparation on damage and decohesion of Al/epoxy joints. Submitted for publication.

Laser velocity increases →

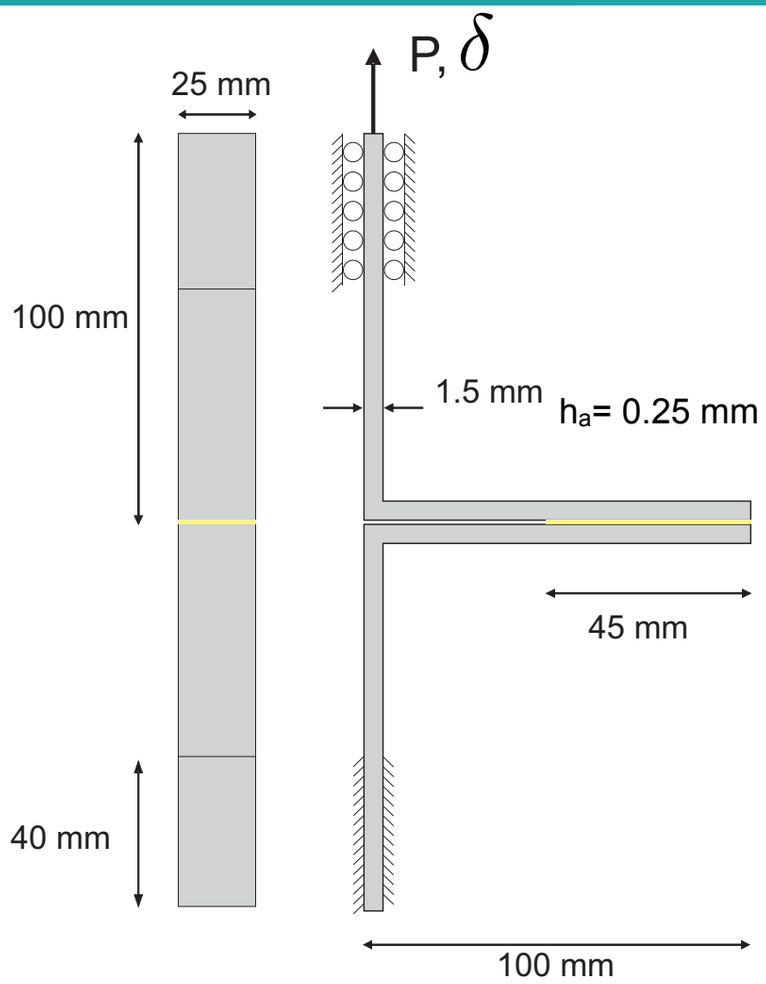
P, δ
25 mm
100 mm
1.5 mm
h_a= 0.25 mm
45 mm
40 mm
100 mm

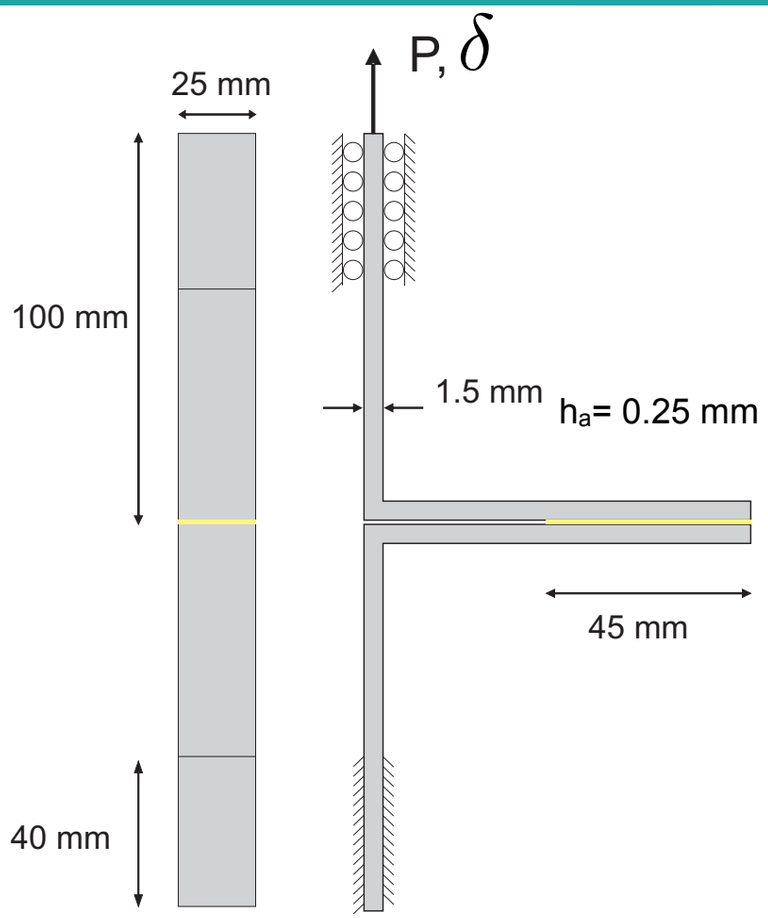
P, δ
25 mm
100 mm
1.5 mm
h_a= 0.25 mm
45 mm
40 mm
100 mm

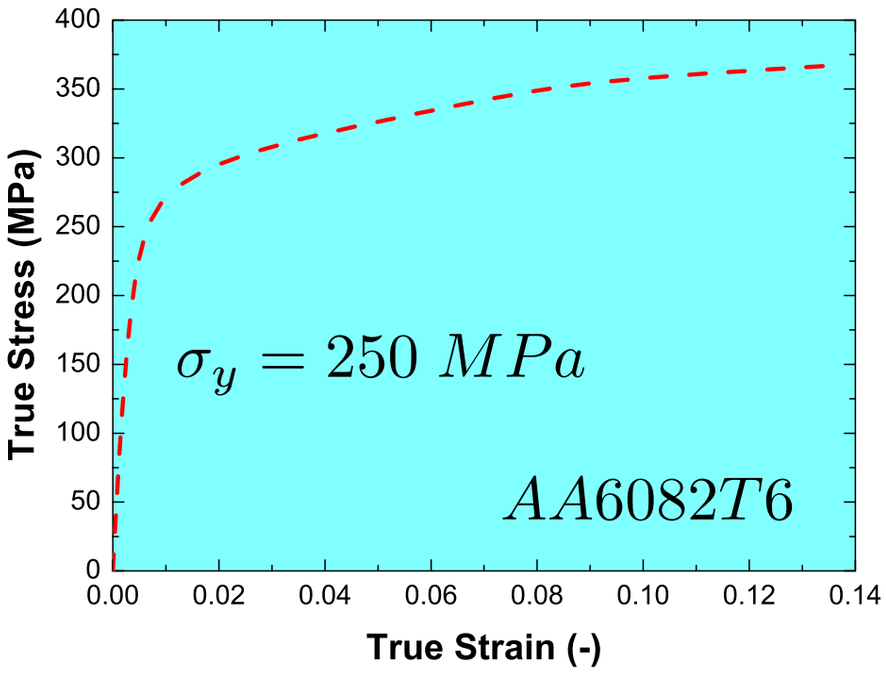
True Stress (MPa)
True Strain (-)
0
50
100
150
200
250
300
350
400
0.00
0.02
0.04
0.06
0.08
0.10
0.12
0.14
$\sigma_y = 250\ MPa$
$AA6082T6$

Mechanical testing of Al/epoxy T-peel joints

Sample preparation and testing

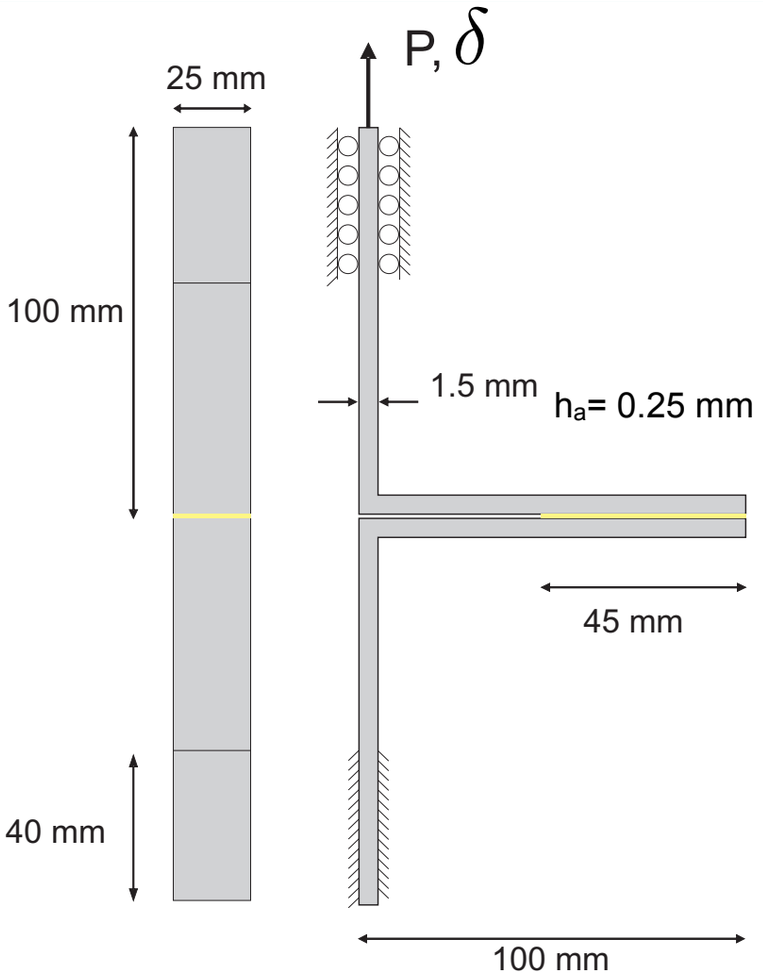

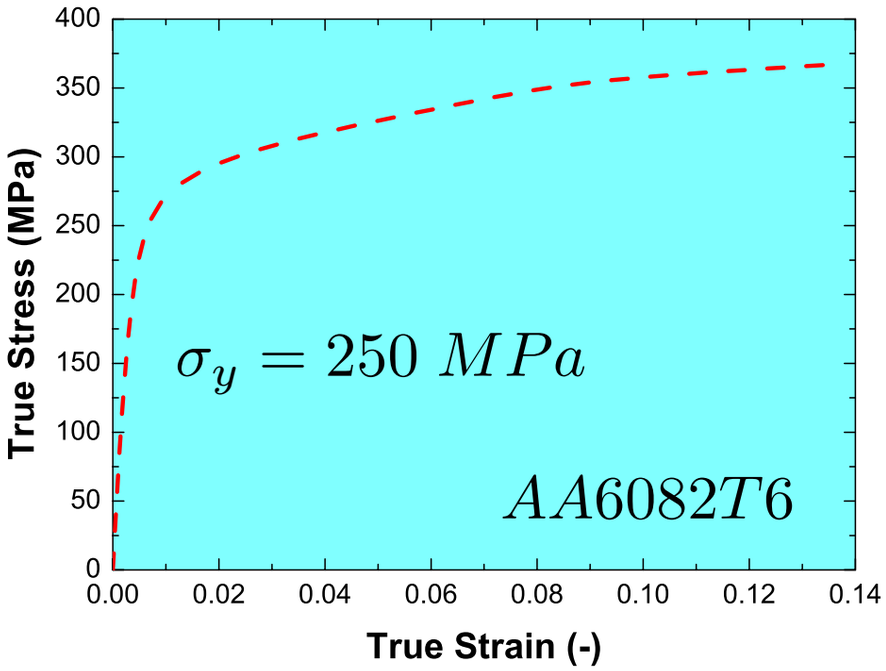

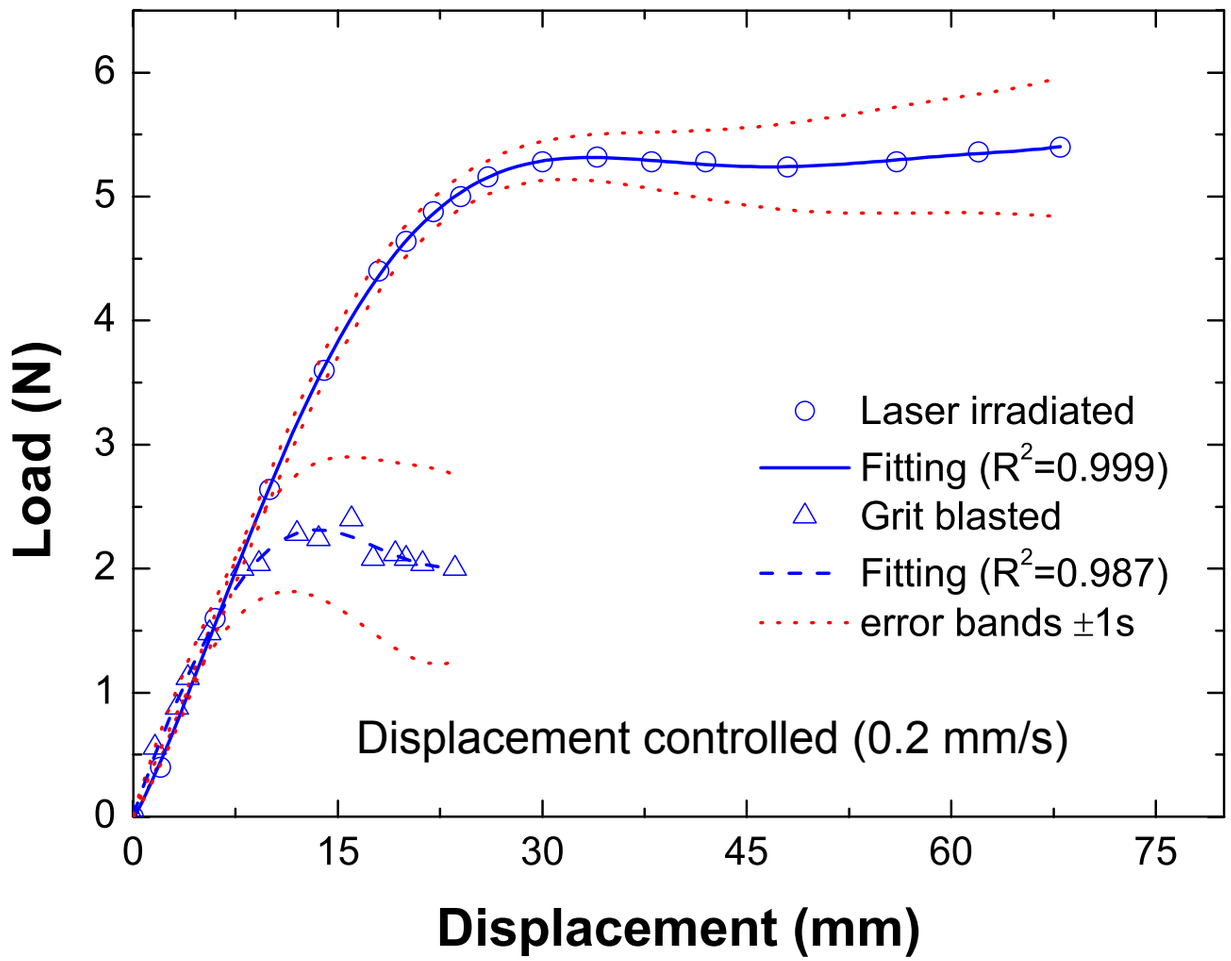

Mechanical testing of Al/epoxy T-peel joints

Sample preparation and testing

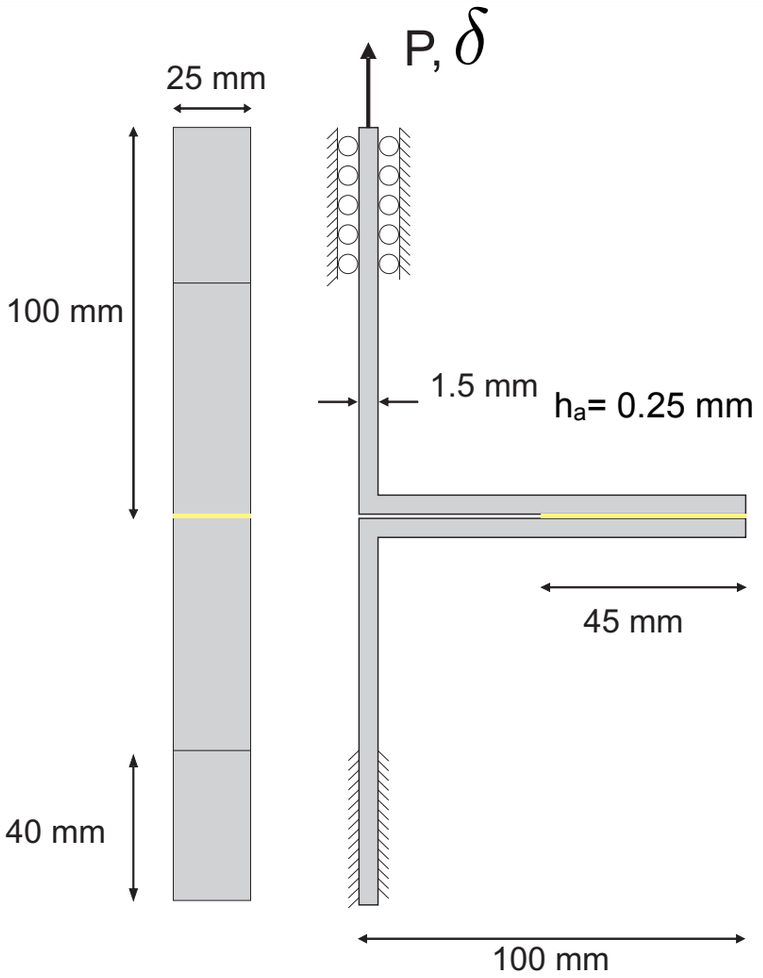

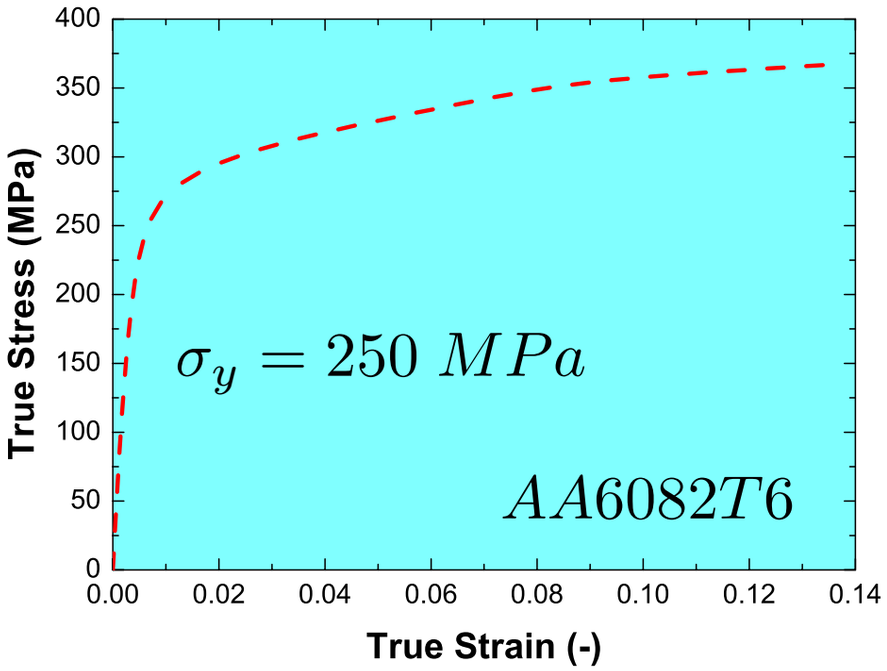

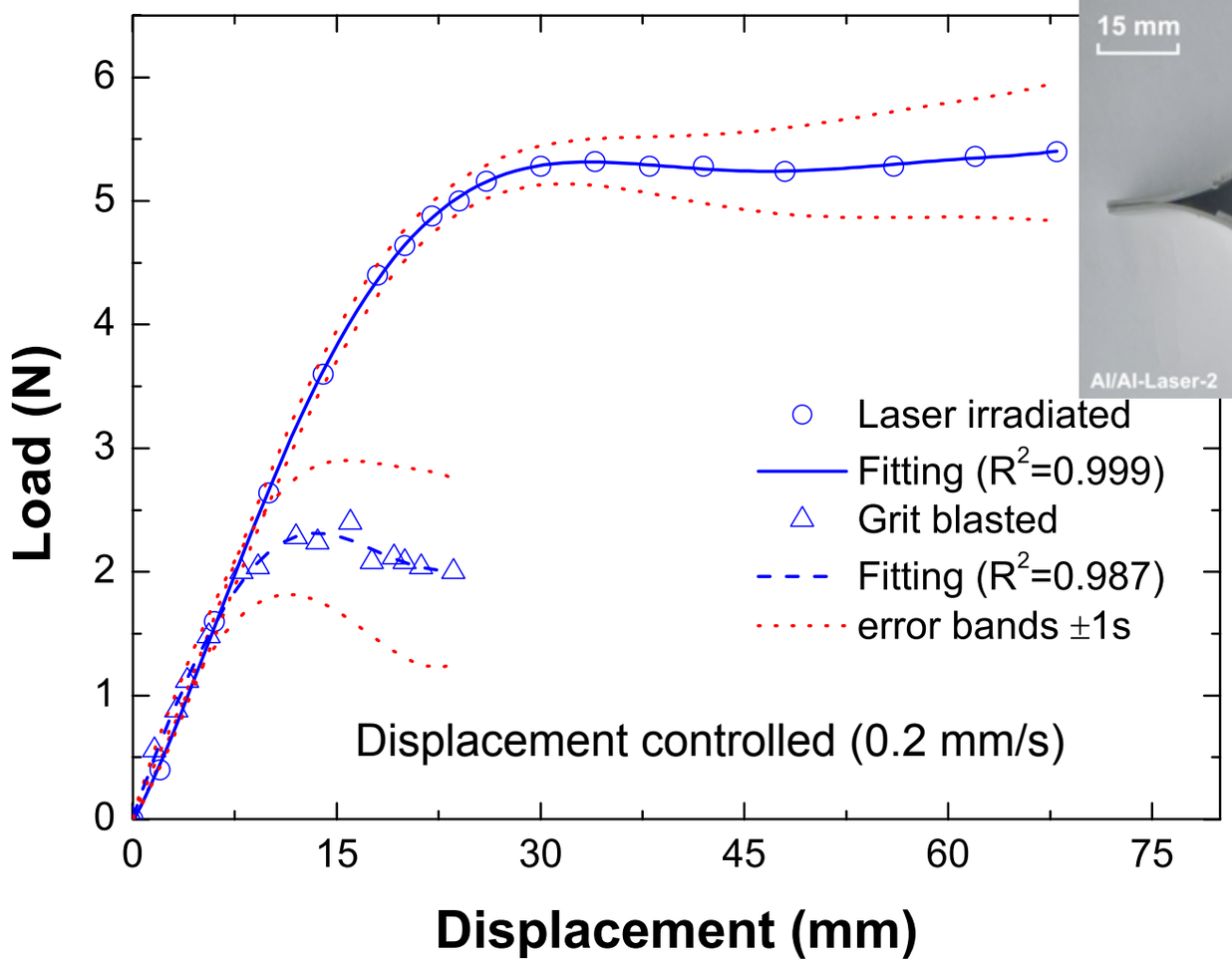

- Increased maximum load and elongation at failure
- Lower scatter
- Extensive plastic deformations for LT samples.
- Elastic deformation only for GB samples
- Cohesive vs adhesive failure (SEM required)

Grit blasted samples

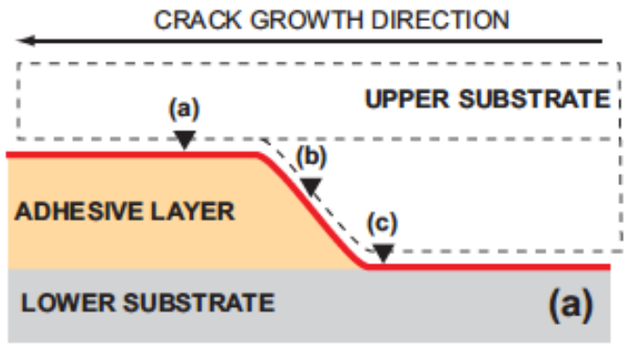

Grit blasted samples

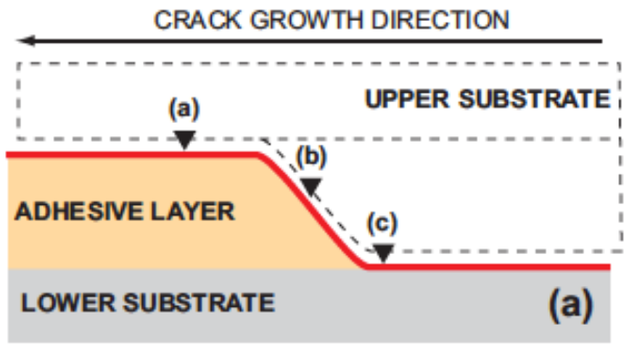

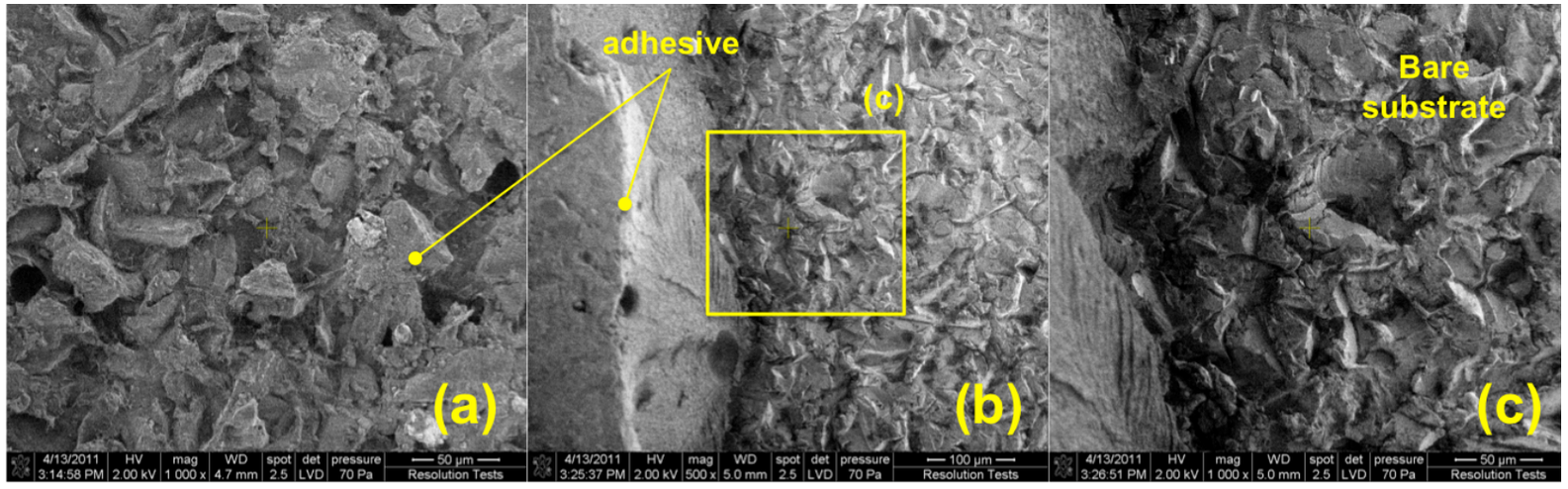

- Adhesive failure at the adhesive\substrate interface
- Transition from upper to lower substrate and *vice versa*

Mechanical testing of Al/epoxy T-peel joints

SEM analyses of fracture surfaces

Grit blasted samples

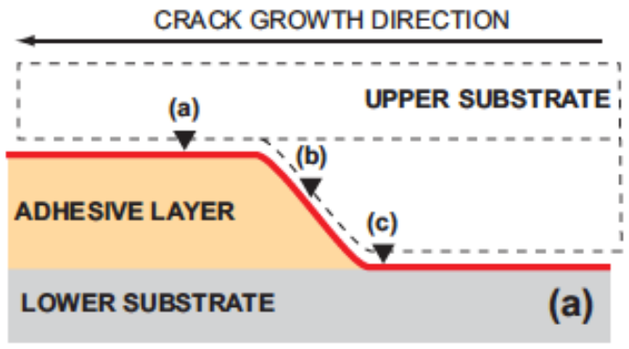

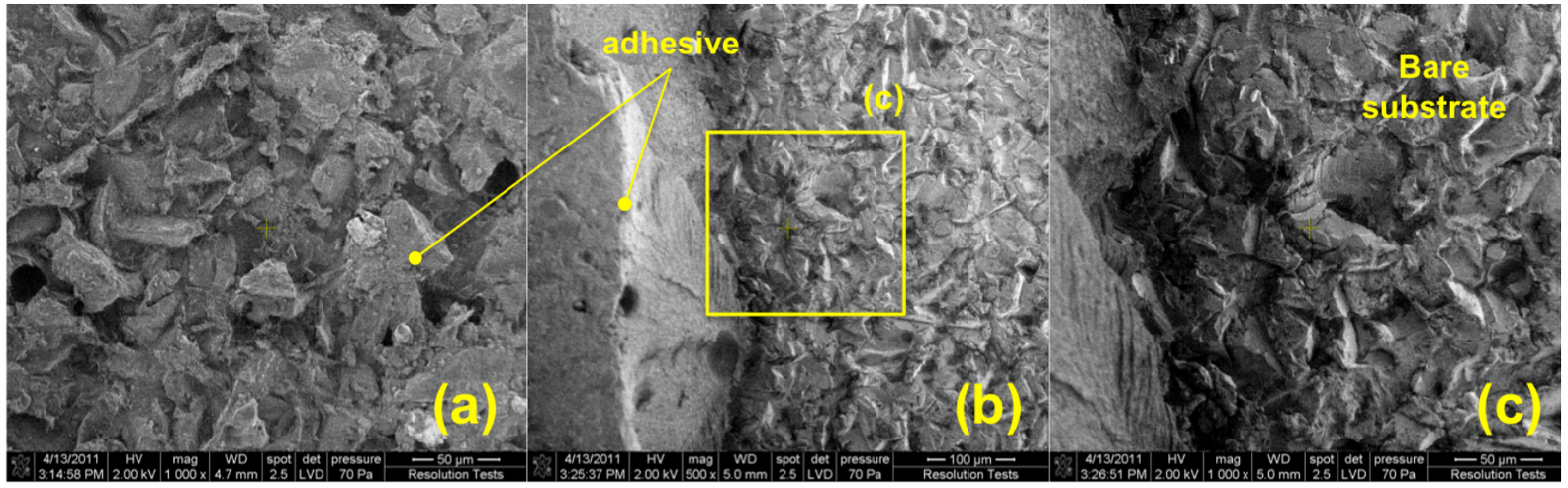

- Adhesive failure at the adhesive\substrate interface
- Transition from upper to lower substrate and *vice versa*

Laser irradiated samples

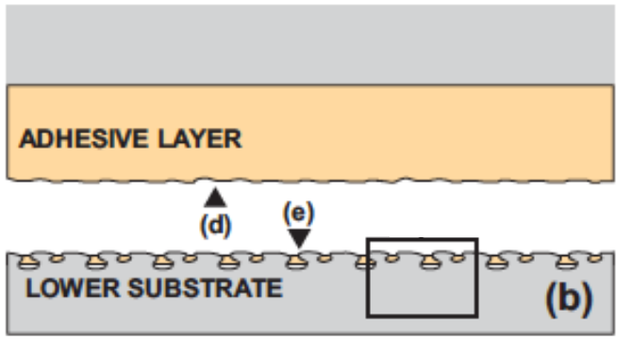

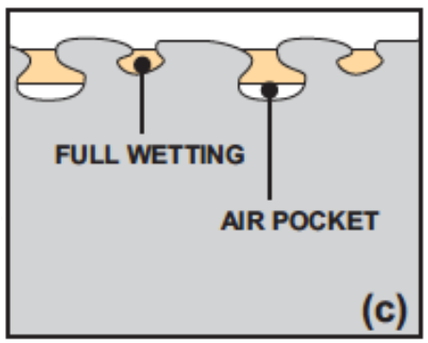

Grit blasted samples

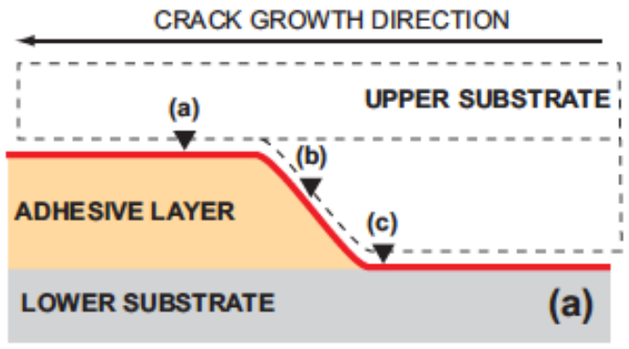

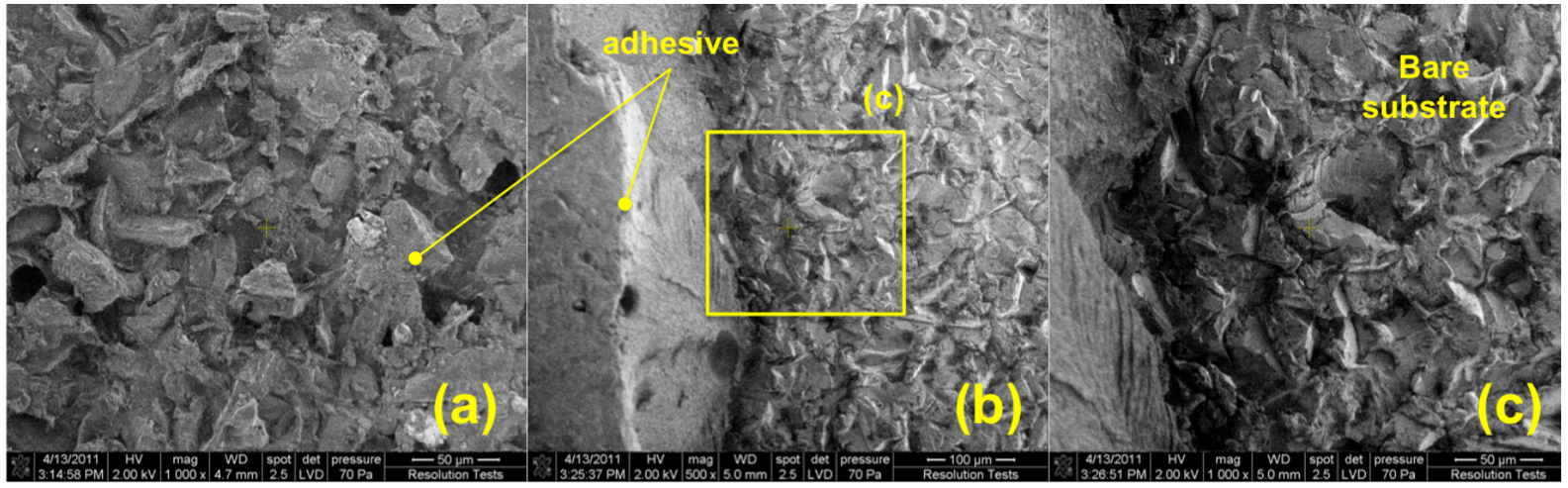

- Adhesive failure at the adhesive\substrate interface
- Transition from upper to lower substrate and *vice versa*

Laser irradiated samples

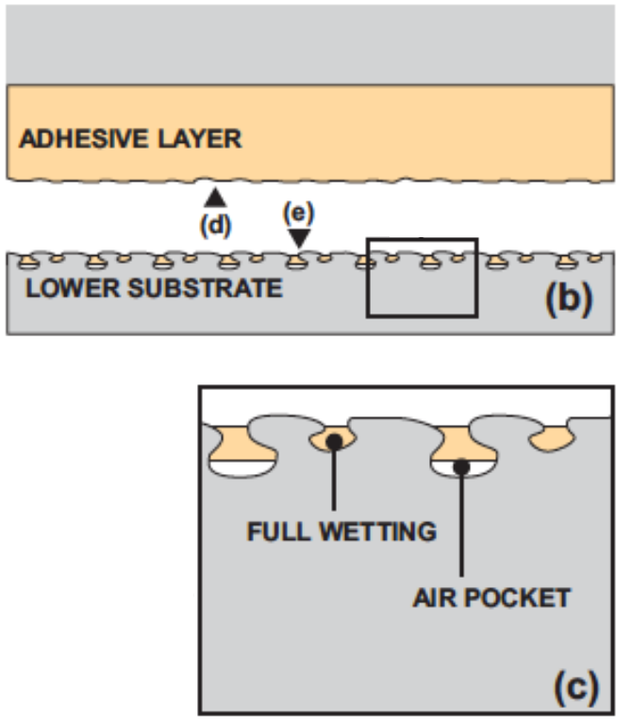

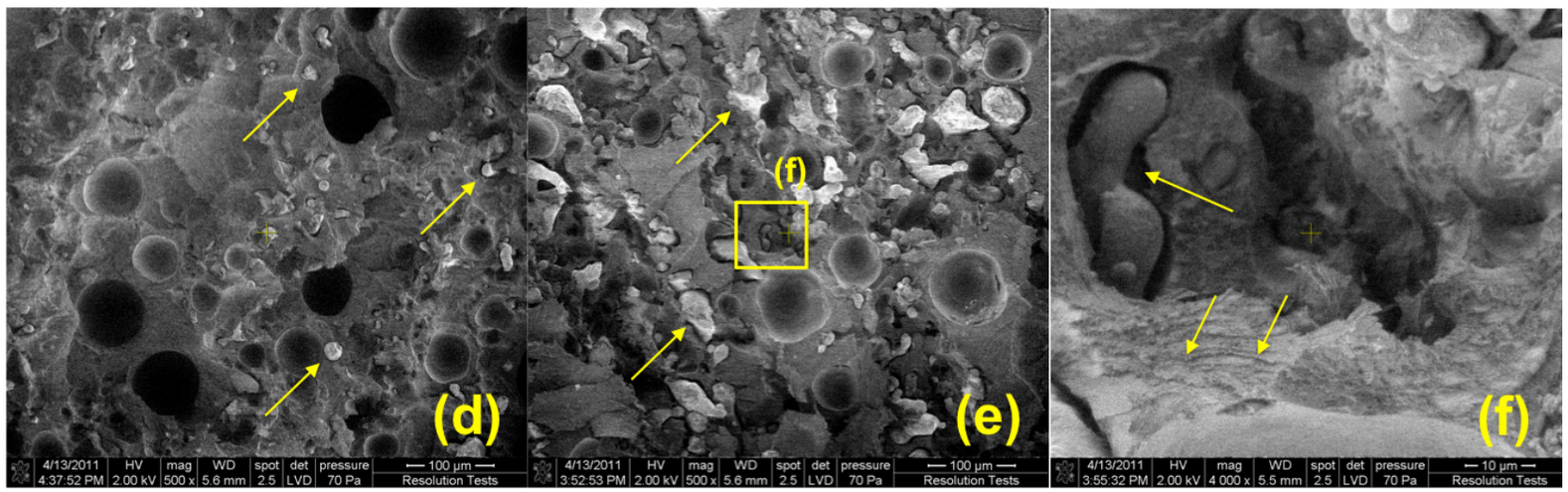

- Cohesive failure in the adhesive layer
- Adhesive interlocked with surface features of treated surfaces
- Imperfect wetting (the adhesive “gels” before complete penetration)

Grit blasted samples

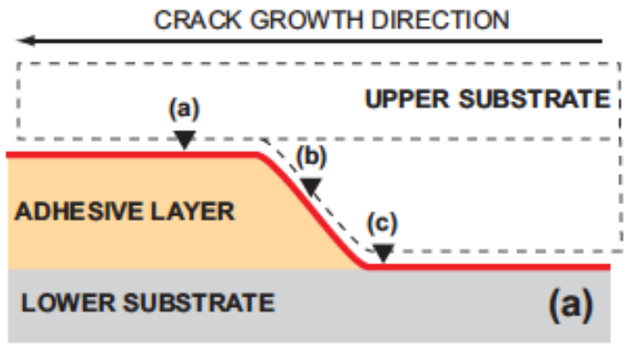

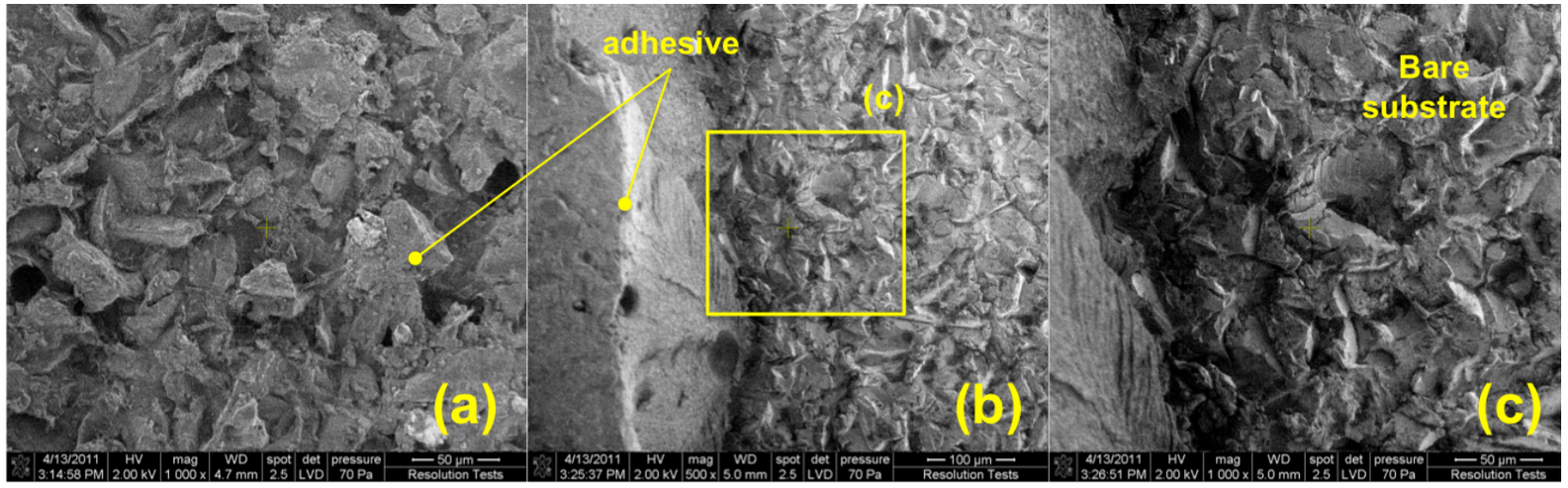

- Adhesive failure at the adhesive\substrate interface
- Transition from upper to lower substrate and *vice versa*

Laser irradiated samples

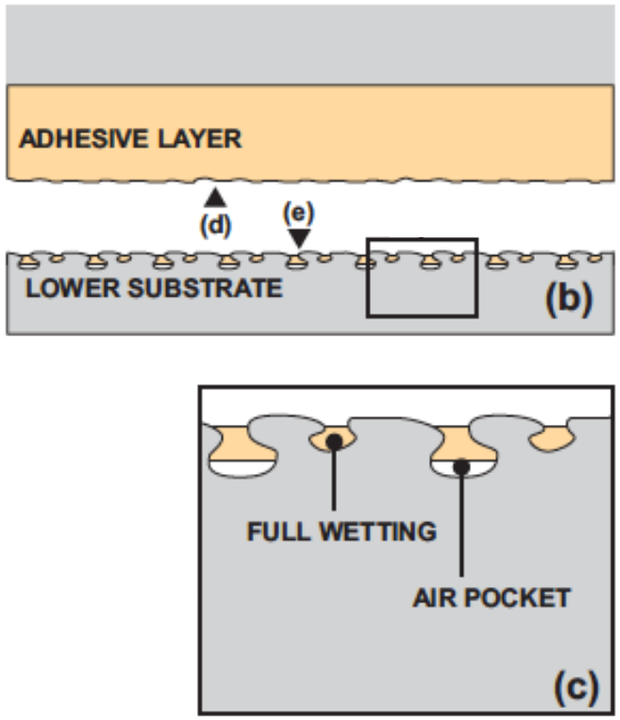

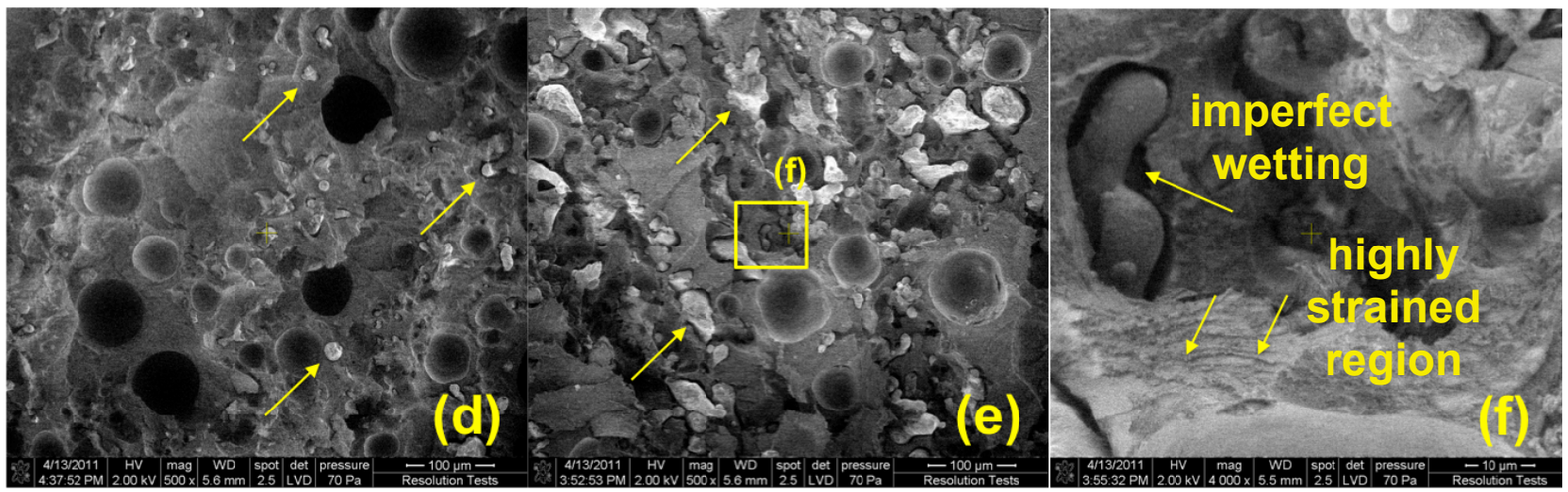

- Cohesive failure in the adhesive layer
- Adhesive interlocked with surface features of treated surfaces
- Imperfect wetting (the adhesive “gels” before complete penetration)

$$\Psi(\Delta_n, \Delta_t) = \min(\phi_n, \phi_t) + \left[\Gamma_n\left(1 - \frac{\Delta_n}{\delta_n}\right)^{\alpha}\left(\frac{m}{\alpha} + \frac{\Delta_n}{\delta_n}\right)^{m} + \langle \phi_n - \phi_t \rangle\right]$$
$$\times \left[\Gamma_t\left(1 - \frac{|\Delta_t|}{\delta_t}\right)^{\beta}\left(\frac{n}{\beta} + \frac{|\Delta_t|}{\delta_t}\right)^{n} + \langle \phi_t - \phi_n \rangle\right].$$

K. Park, G. H. Paulino, J. Roesler, A unified potential-based cohesive model of mixed-mode fracture. JMPS 57, 2009, 891-908.

Determination of bond toughness

Potential based cohesive model

$$\Psi(\Delta_n, \Delta_t) = \min(\phi_n, \phi_t) + \left[\Gamma_n\left(1 - \frac{\Delta_n}{\delta_n}\right)^{\alpha}\left(\frac{m}{\alpha} + \frac{\Delta_n}{\delta_n}\right)^{m} + \langle \phi_n - \phi_t \rangle\right] \times \left[\Gamma_t\left(1 - \frac{|\Delta_t|}{\delta_t}\right)^{\beta}\left(\frac{n}{\beta} + \frac{|\Delta_t|}{\delta_t}\right)^{n} + \langle \phi_t - \phi_n \rangle\right].$$

δ_n, δ_t	characteristic length scale parameters
$\bar{\delta}_n$, $\bar{\delta}_t$	normal and tangential conjugate final crack opening widths
λ_n, λ_t	initial slope indicators
σ_{max}, τ_{max}	normal and tangential cohesive strengths
ϕ_n, ϕ_t	modes I and II fracture energies
Ψ	potential function for cohesive fracture
α, β	shape parameters in the PPR model

K. Park, G. H. Paulino, J. Roesler, A unified potential-based cohesive model of mixed-mode fracture. JMPS 57, 2009, 891-908.

Determination of bond toughness

Potential based cohesive model

$$\Psi(\Delta_n, \Delta_t) = \min(\phi_n, \phi_t) + \left[\Gamma_n\left(1 - \frac{\Delta_n}{\delta_n}\right)^{\alpha}\left(\frac{m}{\alpha} + \frac{\Delta_n}{\delta_n}\right)^{m} + \langle \phi_n - \phi_t \rangle\right] \times \left[\Gamma_t\left(1 - \frac{|\Delta_t|}{\delta_t}\right)^{\beta}\left(\frac{n}{\beta} + \frac{|\Delta_t|}{\delta_t}\right)^{n} + \langle \phi_t - \phi_n \rangle\right].$$

δ_n, δ_t	characteristic length scale parameters
$\bar{\delta}_n$, $\bar{\delta}_t$	normal and tangential conjugate final crack opening widths
λ_n, λ_t	initial slope indicators
σ_{max}, τ_{max}	normal and tangential cohesive strengths
ϕ_n, ϕ_t	modes I and II fracture energies
Ψ	potential function for cohesive fracture
α, β	shape parameters in the PPR model

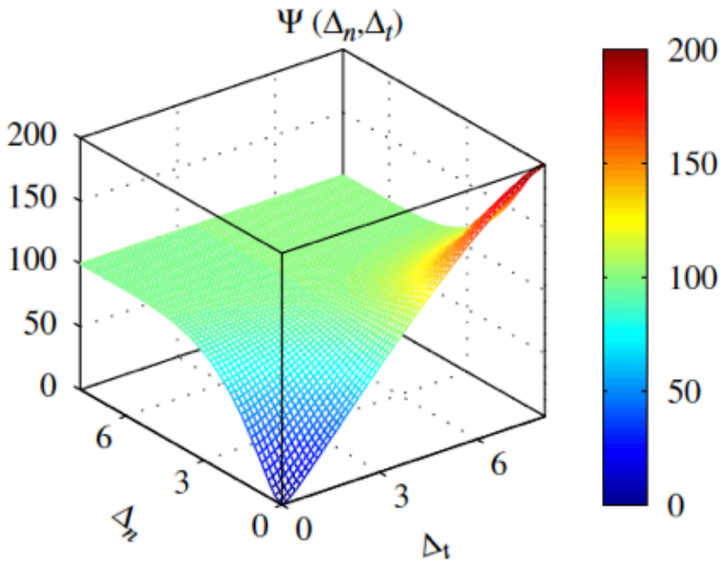

Axis	Units
Ψ	N/m
T_n, T_t	MPa
Δ_n, Δ_t	μm

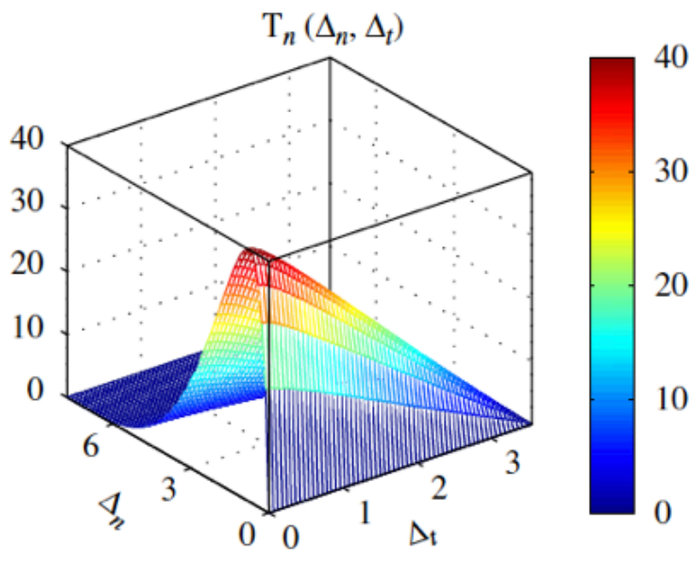

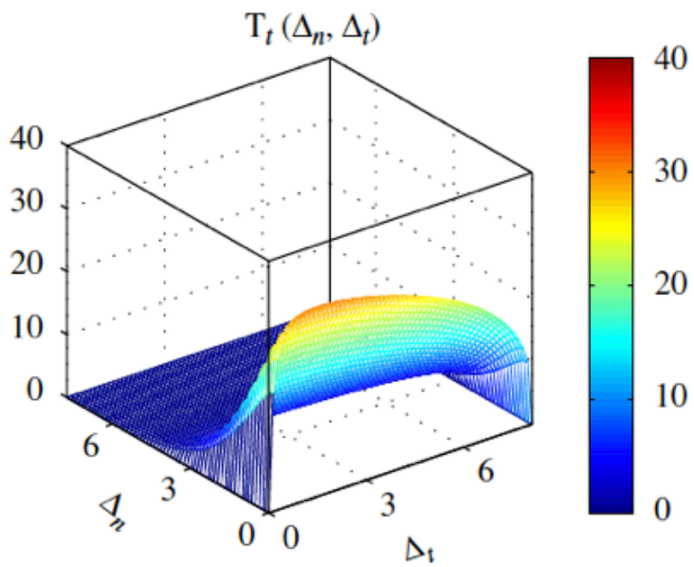

$$\phi_n = 100,\ \phi_t = 200\ [N/mm]$$
$$\sigma_{max} = 40,\ \tau_{max} = 30\ [MPa]$$
$$\alpha = 5,\ \beta = 1.3$$
$$\lambda_n = 0.1,\ \lambda_t = 0.2$$

K. Park, G. H. Paulino, J. Roesler, A unified potential-based cohesive model of mixed-mode fracture. JMPS 57, 2009, 891-908.

$$\Psi(\Delta_n) = \phi_n + \Gamma_n \left(1 - \frac{\Delta_n}{\delta_n}\right)^{\alpha} \left(\frac{m}{\alpha} + \frac{\Delta_n}{\delta_n}\right)^{m}$$

$$\Psi(\Delta_n) = \phi_n + \Gamma_n \left(1 - \frac{\Delta_n}{\delta_n}\right)^{\alpha} \left(\frac{m}{\alpha} + \frac{\Delta_n}{\delta_n}\right)^{m}$$

$$T(\Delta_n) = \frac{\partial \Psi}{\partial \Delta_n} =$$

$$= \frac{\Gamma_n}{\delta_n} \left[m \left(1 - \frac{\Delta_n}{\delta_n}\right)^{\alpha} \left(\frac{m}{\alpha} + \frac{\Delta_n}{\delta_n}\right)^{m-1} - \alpha \left(1 - \frac{\Delta_n}{\delta_n}\right)^{\alpha-1} \left(\frac{m}{\alpha} + \frac{\Delta_n}{\delta_n}\right)^{m} \right]$$

$$\Gamma_n = -\phi_n \left(\frac{\alpha}{m}\right)^{m}$$

$$m = \frac{\alpha(\alpha - 1)\lambda_n^2}{1 - \alpha\lambda_n^2}$$

$$\delta_n = \frac{\phi_n}{\sigma_{max}} \alpha\lambda_n (1 - \lambda_n)^{\alpha-1} \left(\frac{\alpha}{m} + 1\right) \cdot \left(\frac{\alpha}{m}\lambda_n + 1\right)^{m-1}$$

$$\mathbf{X} = \{\phi_n, \sigma_{max}, \lambda_n, \alpha\}$$

energy constant;

non-dimensional exponent;

final crack opening width;

unknown properties to be identified

$$\Psi(\Delta_n) = \phi_n + \Gamma_n \left(1 - \frac{\Delta_n}{\delta_n}\right)^{\alpha} \left(\frac{m}{\alpha} + \frac{\Delta_n}{\delta_n}\right)^{m}$$

$$T(\Delta_n) = \frac{\partial \Psi}{\partial \Delta_n} =$$

$$= \frac{\Gamma_n}{\delta_n} \left[m \left(1 - \frac{\Delta_n}{\delta_n}\right)^{\alpha} \left(\frac{m}{\alpha} + \frac{\Delta_n}{\delta_n}\right)^{m-1} - \alpha \left(1 - \frac{\Delta_n}{\delta_n}\right)^{\alpha-1} \left(\frac{m}{\alpha} + \frac{\Delta_n}{\delta_n}\right)^{m} \right]$$

$$\Gamma_n = -\phi_n \left(\frac{\alpha}{m}\right)^{m}$$

$$m = \frac{\alpha(\alpha - 1)\lambda_n^2}{1 - \alpha\lambda_n^2}$$

$$\delta_n = \frac{\phi_n}{\sigma_{max}} \alpha\lambda_n (1 - \lambda_n)^{\alpha-1} \left(\frac{\alpha}{m} + 1\right) \cdot \left(\frac{\alpha}{m}\lambda_n + 1\right)^{m-1}$$

$$\mathbf{X} = \{\phi_n, \sigma_{max}, \lambda_n, \alpha\}$$

energy constant;

non-dimensional exponent;

final crack opening width;

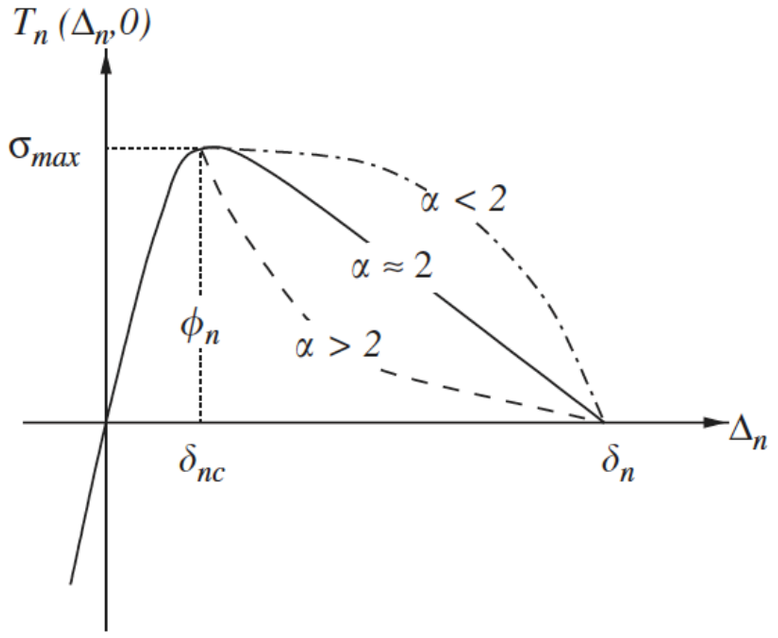

unknown properties to be identified

Determination of bond toughness

Sensitivity analysis to α and λ_n

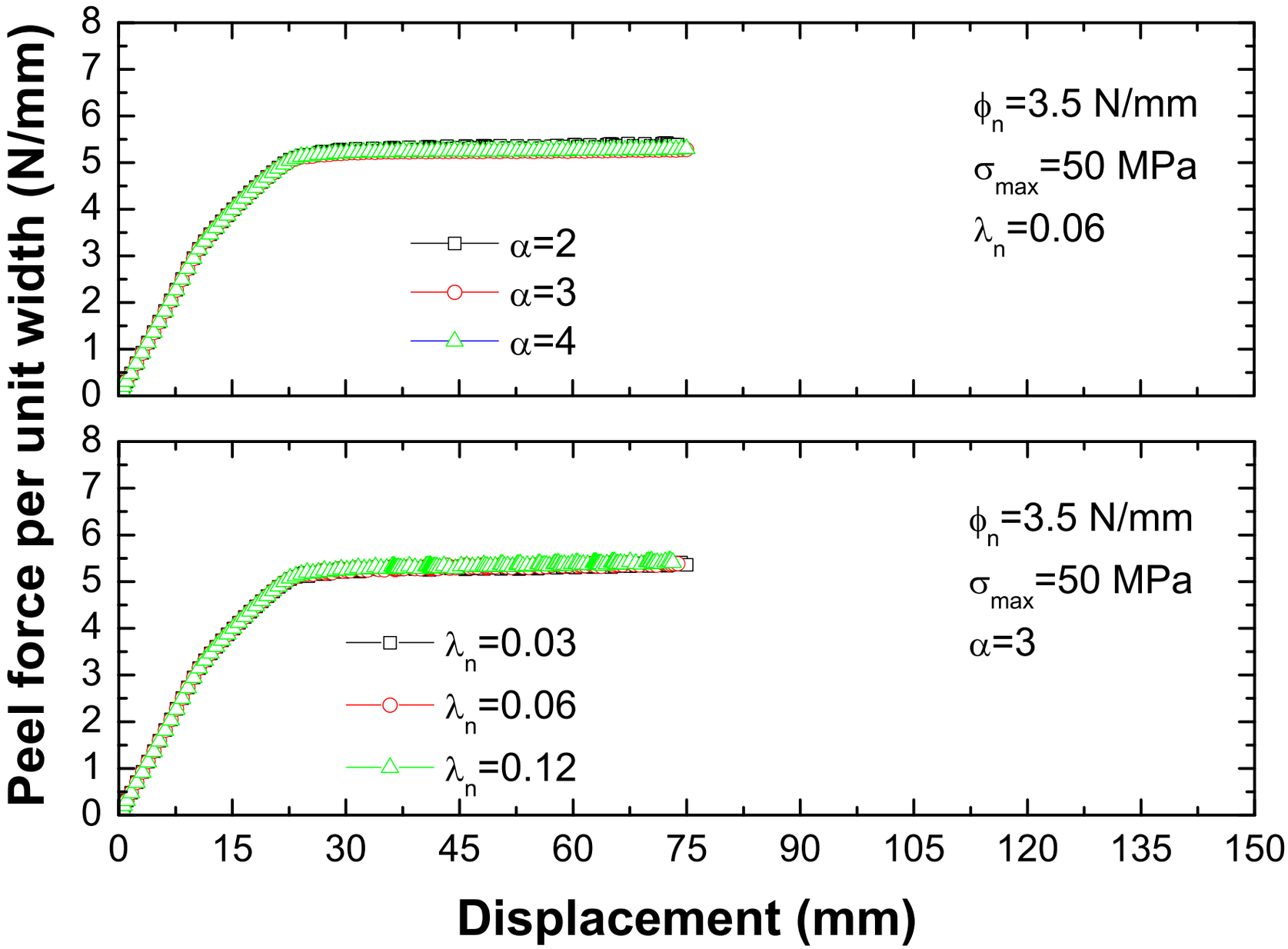

Thouless et al, Numerical simulations of adhesively-bonded beams failing with extensive plastic deformation. JMPS 77, 1999, 1337-1353.

Determination of bond toughness

Sensitivity analysis to α and λ_n

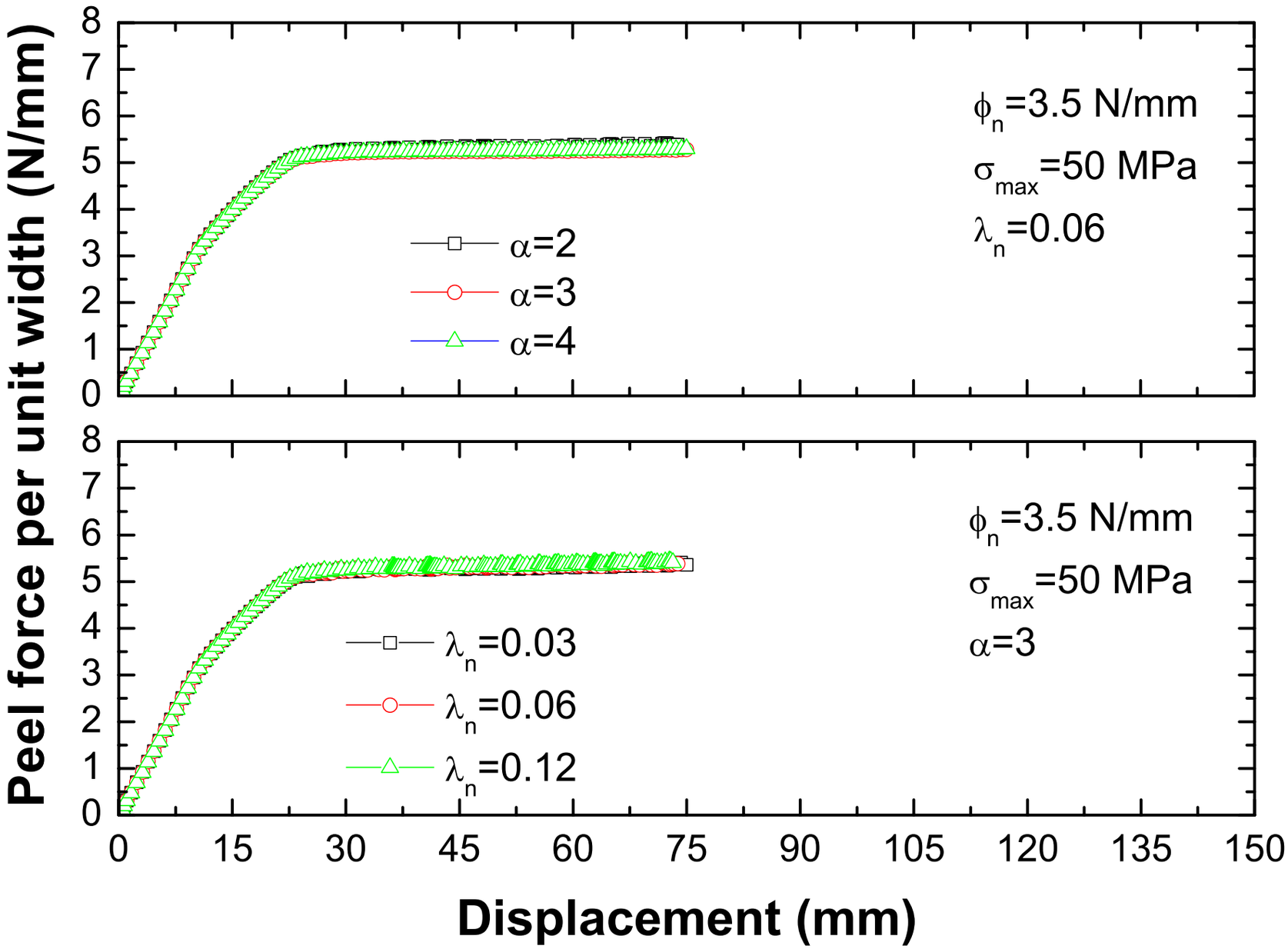

• In the subsequent numerical simulations, the shape parameter and the slope indicator have been set to 3 and 0.06, respectively.

Thouless et al, Numerical simulations of adhesively-bonded beams failing with extensive plastic deformation. JMPS 77, 1999, 1337-1353.

Standard dimensional analysis dictates the non-dimensional load to depend on the following non-dimensional groups:

$$\frac{\bar{P}}{\sigma_y\, h} = f\left(\frac{\delta}{h},\ \frac{\phi_n}{\sigma_y\, h},\ \frac{\sigma_y}{\sigma_{max}},\ \frac{\sigma_y}{E},\ n\right)$$

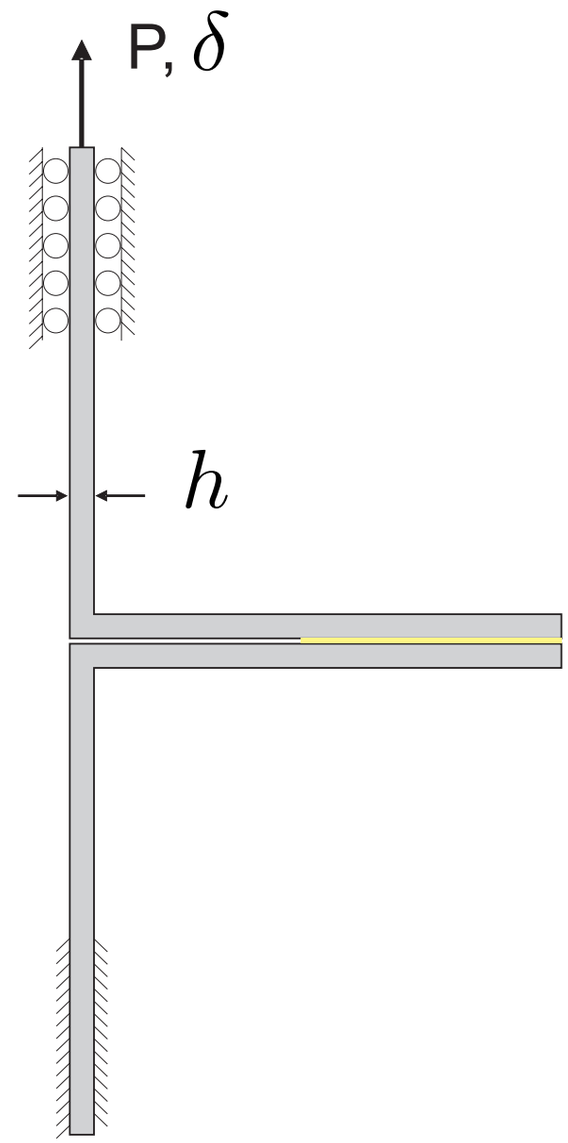

Standard dimensional analysis dictates the non-dimensional load to depend on the following non-dimensional groups:

$$\frac{\bar{P}}{\sigma_y\, h} = f\left(\frac{\delta}{h},\ \frac{\phi_n}{\sigma_y\, h},\ \frac{\sigma_y}{\sigma_{max}},\ \frac{\sigma_y}{E},\ n\right)$$

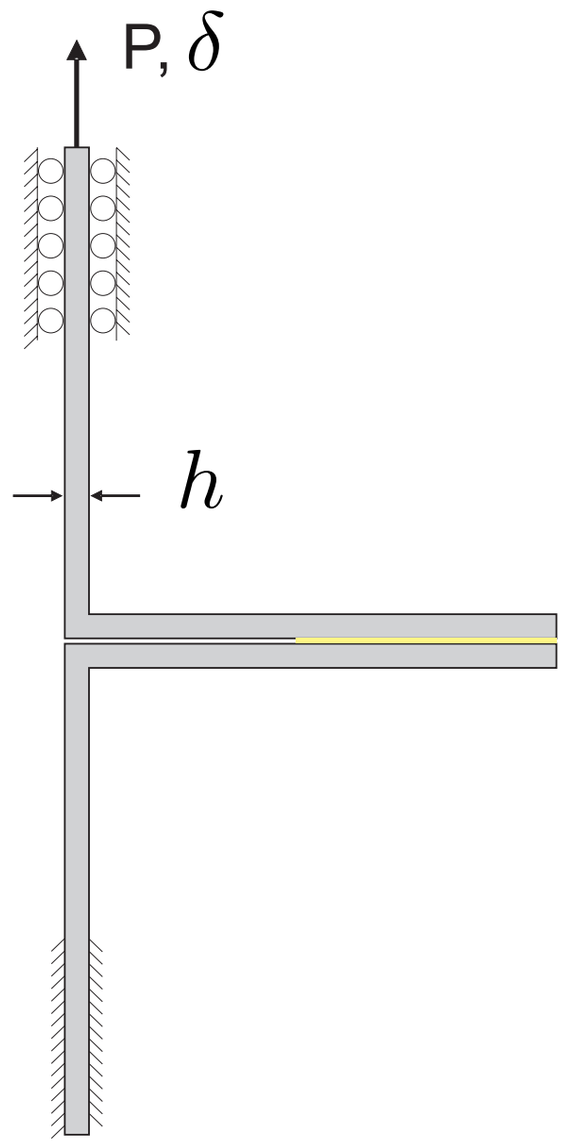

Standard dimensional analysis dictates the non-dimensional load to depend on the following non-dimensional groups:

$$\frac{\bar{P}}{\sigma_y\, h} = f\left(\frac{\delta}{h},\ \frac{\phi_n}{\sigma_y\, h},\ \frac{\sigma_y}{\sigma_{max}},\ \frac{\sigma_y}{E},\ n\right)$$

opening displacement;

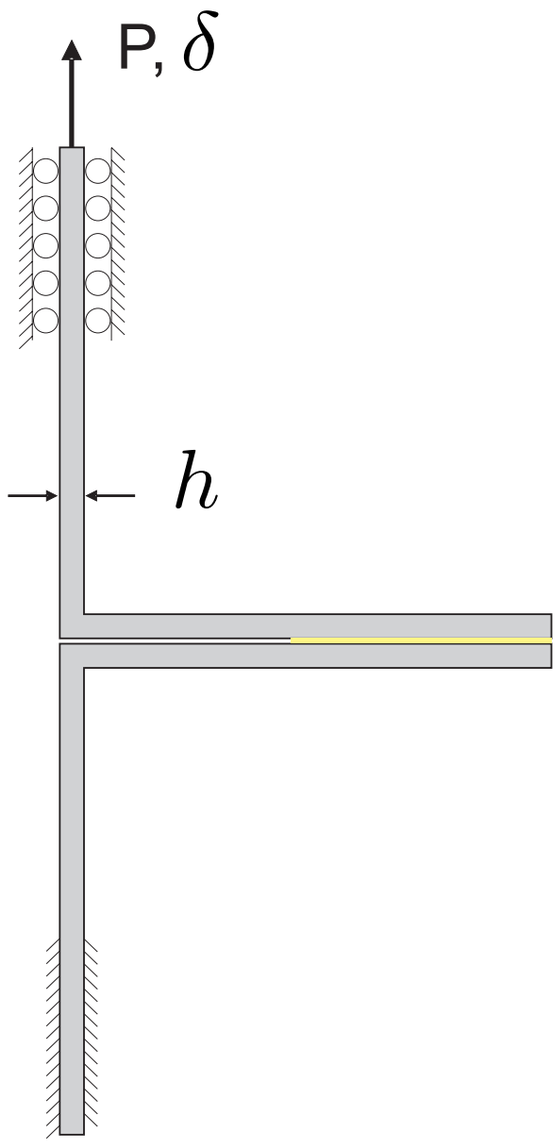

Standard dimensional analysis dictates the non-dimensional load to depend on the following non-dimensional groups:

$$\frac{\bar{P}}{\sigma_y\, h} = f\left(\frac{\delta}{h}, \frac{\phi_n}{\sigma_y\, h}, \frac{\sigma_y}{\sigma_{max}}, \frac{\sigma_y}{E}, n\right)$$

opening displacement;

non-dimensional fracture energy;

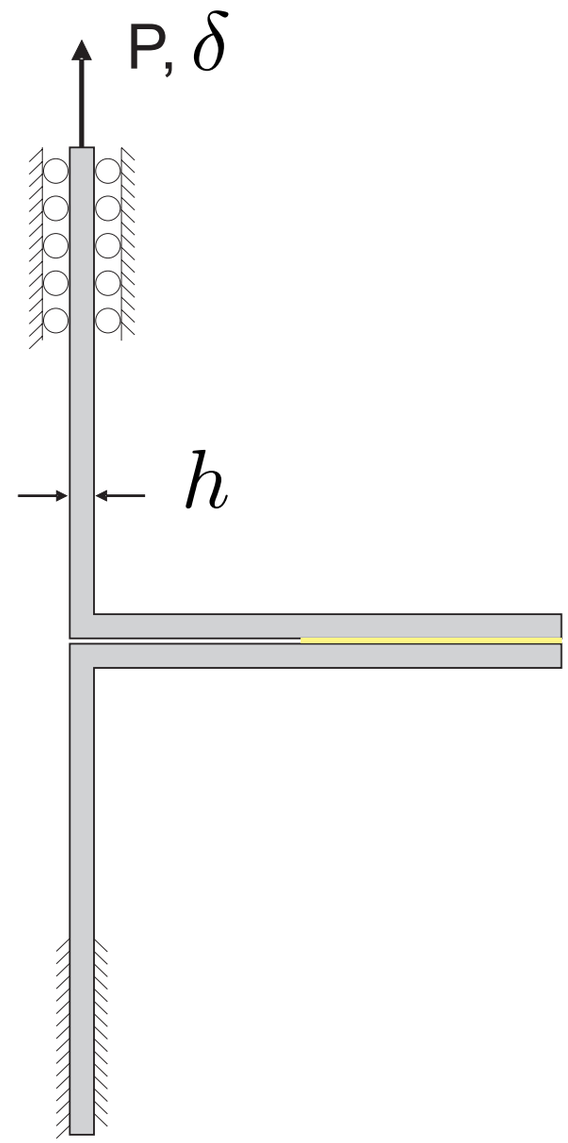

Standard dimensional analysis dictates the non-dimensional load to depend on the following non-dimensional groups:

$$\frac{\bar{P}}{\sigma_y\, h} = f\left(\frac{\delta}{h}, \frac{\phi_n}{\sigma_y\, h}, \frac{\sigma_y}{\sigma_{max}}, \frac{\sigma_y}{E}, n\right)$$

opening displacement;

non-dimensional fracture energy;

non-dimensional cohesive strength;

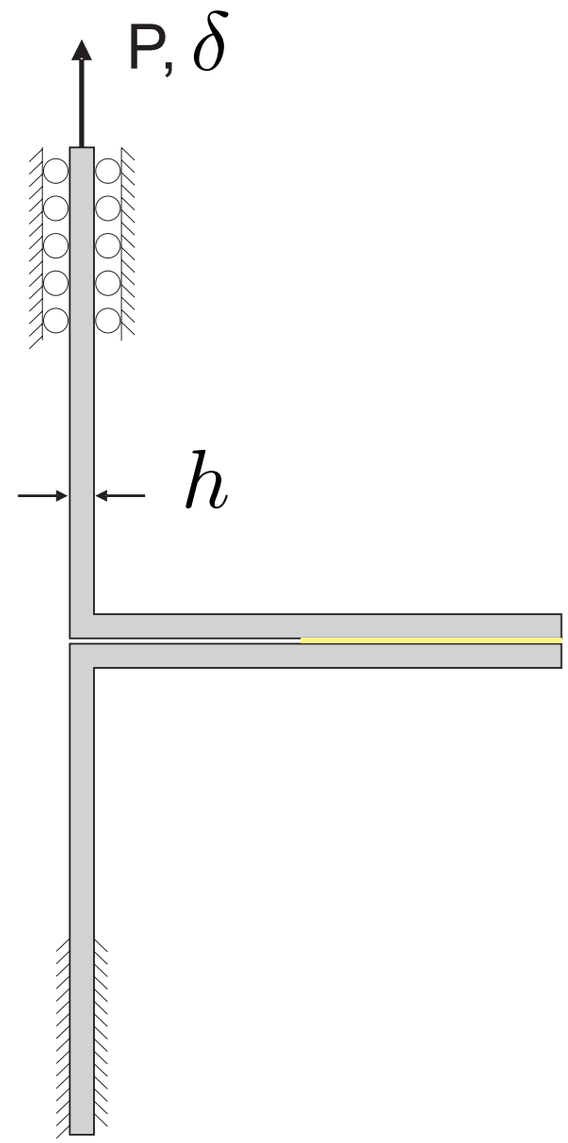

Standard dimensional analysis dictates the non-dimensional load to depend on the following non-dimensional groups:

$$\frac{\bar{P}}{\sigma_y\, h} = f\left(\frac{\delta}{h}, \frac{\phi_n}{\sigma_y\, h}, \frac{\sigma_y}{\sigma_{max}}, \frac{\sigma_y}{E}, n\right)$$

opening displacement;

non-dimensional fracture energy;

non-dimensional cohesive strength;

elasto-plastic properties of the adherents;

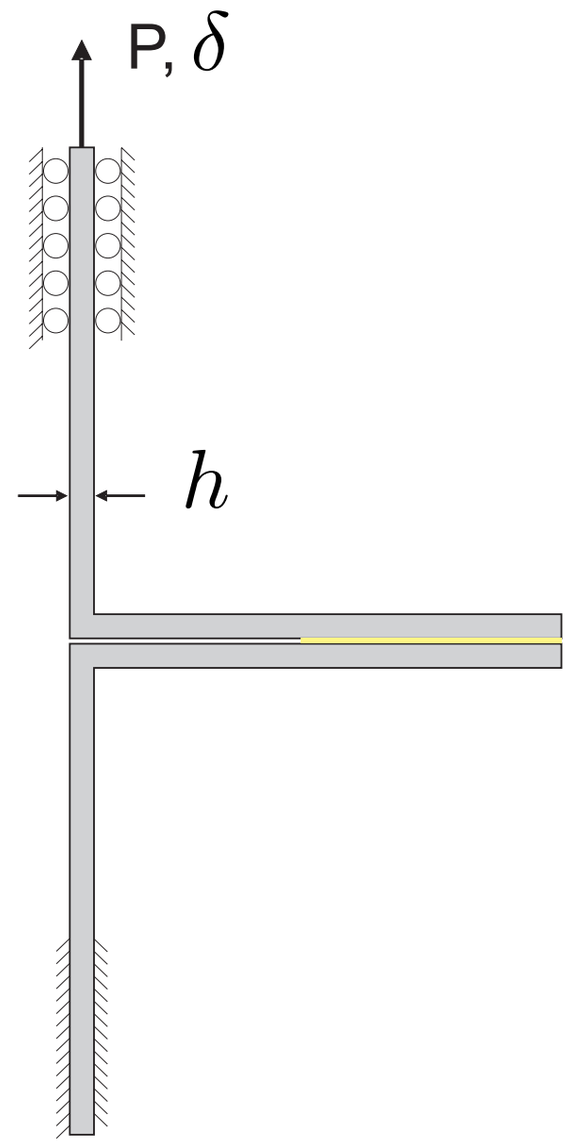

Determination of bond toughness

Sensitivity analysis to Φ_n and σ_{max}

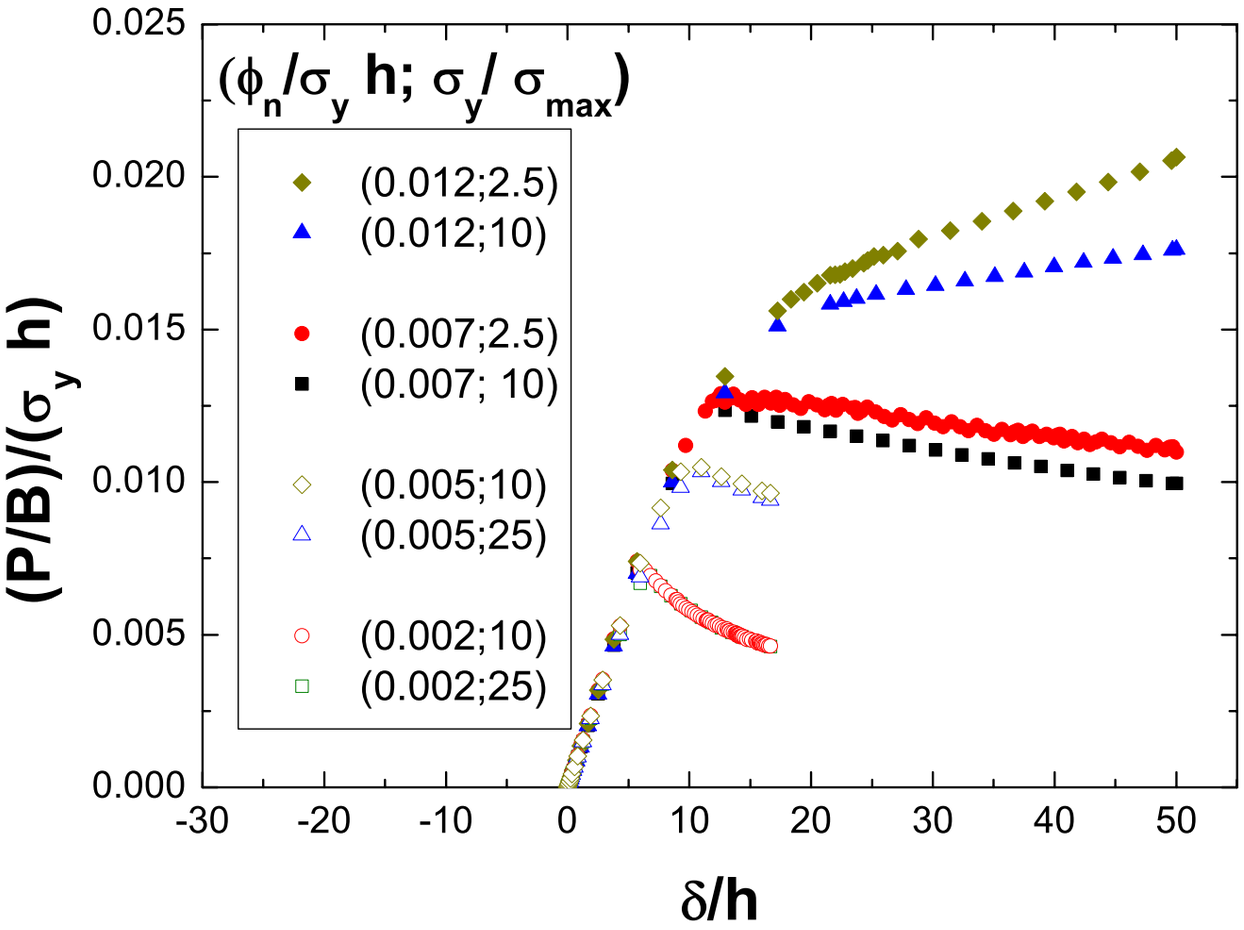

Determination of bond toughness

Sensitivity analysis to Φ_n and σ_{max}

range of exp. results for grit blasted (GB) samples

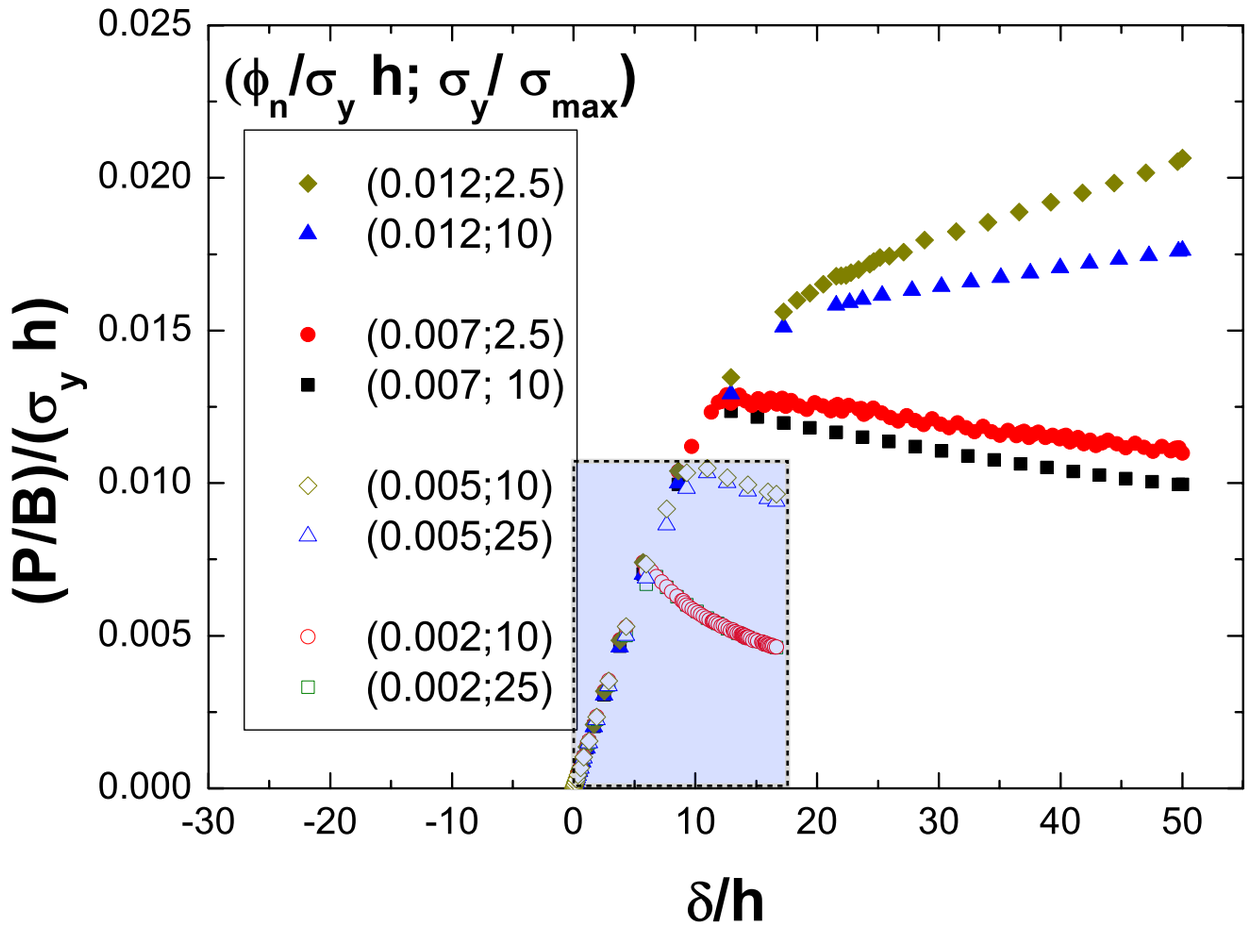

Determination of bond toughness

Sensitivity analysis to Φ_n and σ_{max}

range of exp. results for grit blasted (GB) samples

range of exp. results for laser treated (L) samples

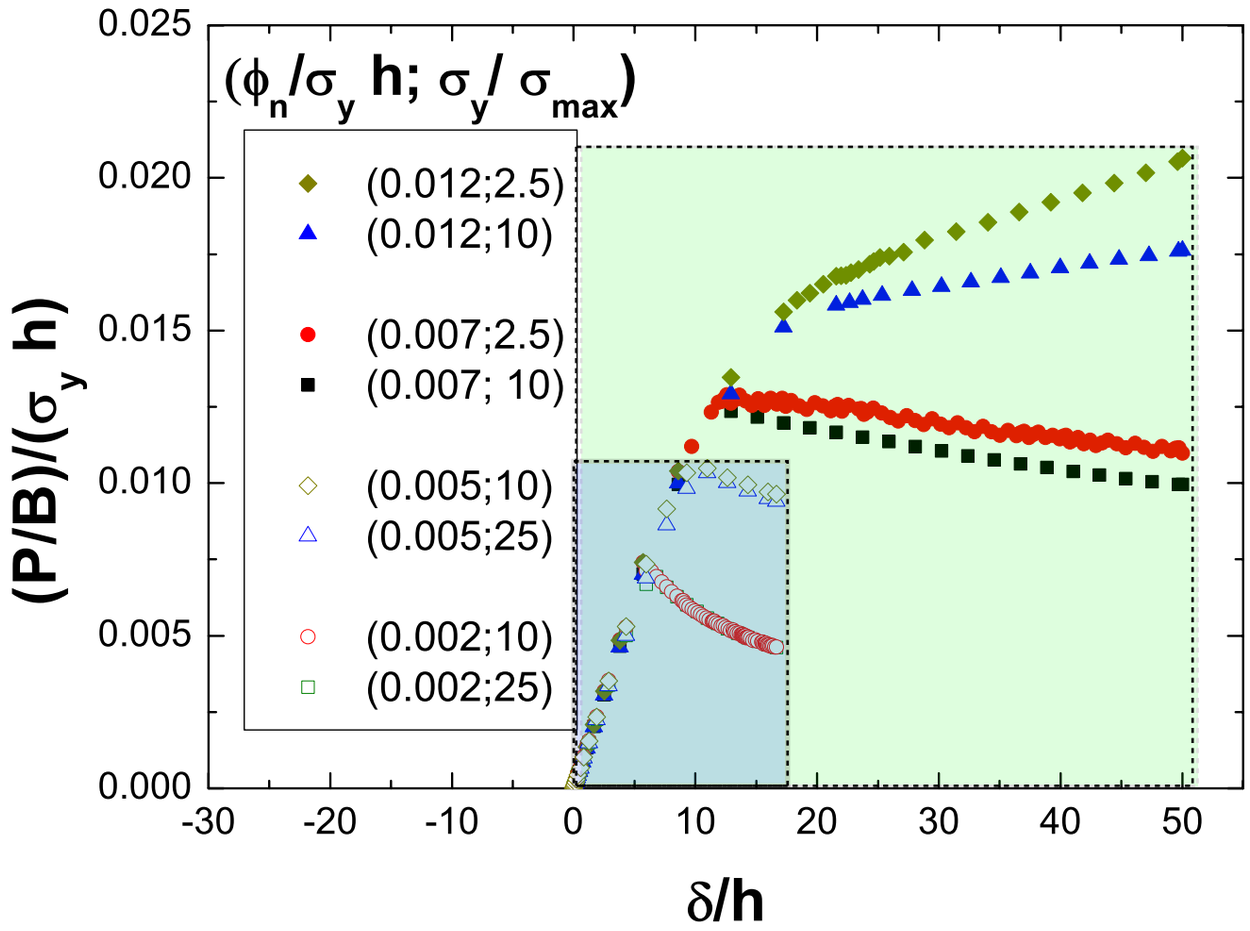

Determination of bond toughness

Sensitivity analysis to Φ_n and σ_{max}

range of exp. results for grit blasted (GB) samples

range of exp. results for laser treated (L) samples

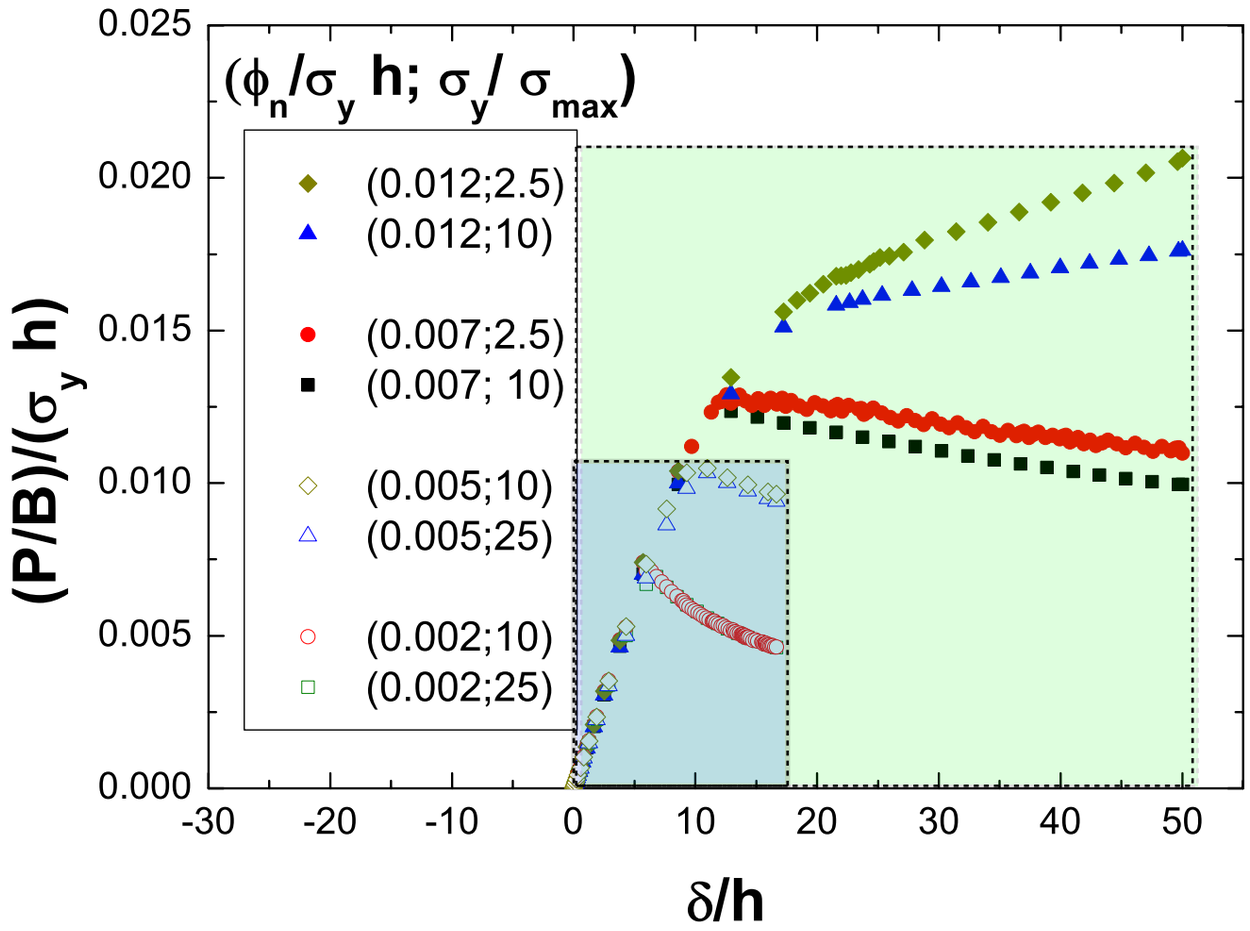

- The area under the curve increases as the fracture energy increases,
- GB samples: the post peak slope depends on fracture energy,
- LT samples, it depends on both cohesive strength and fracture energy.

Determination of bond toughness

Sensitivity analysis to Φ_n and σ_{max}

range of exp. results for grit blasted (GB) samples

range of exp. results for laser treated (L) samples

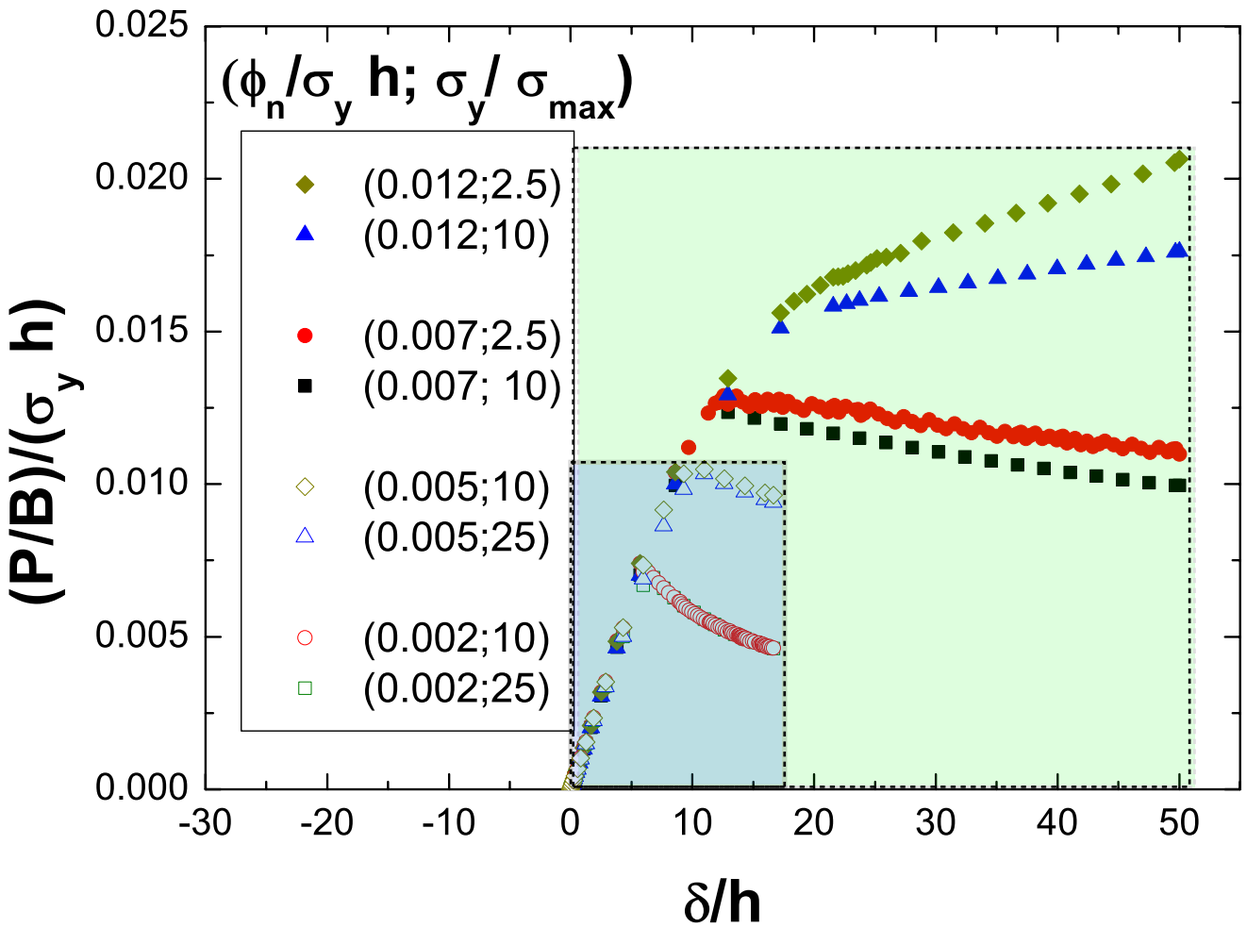

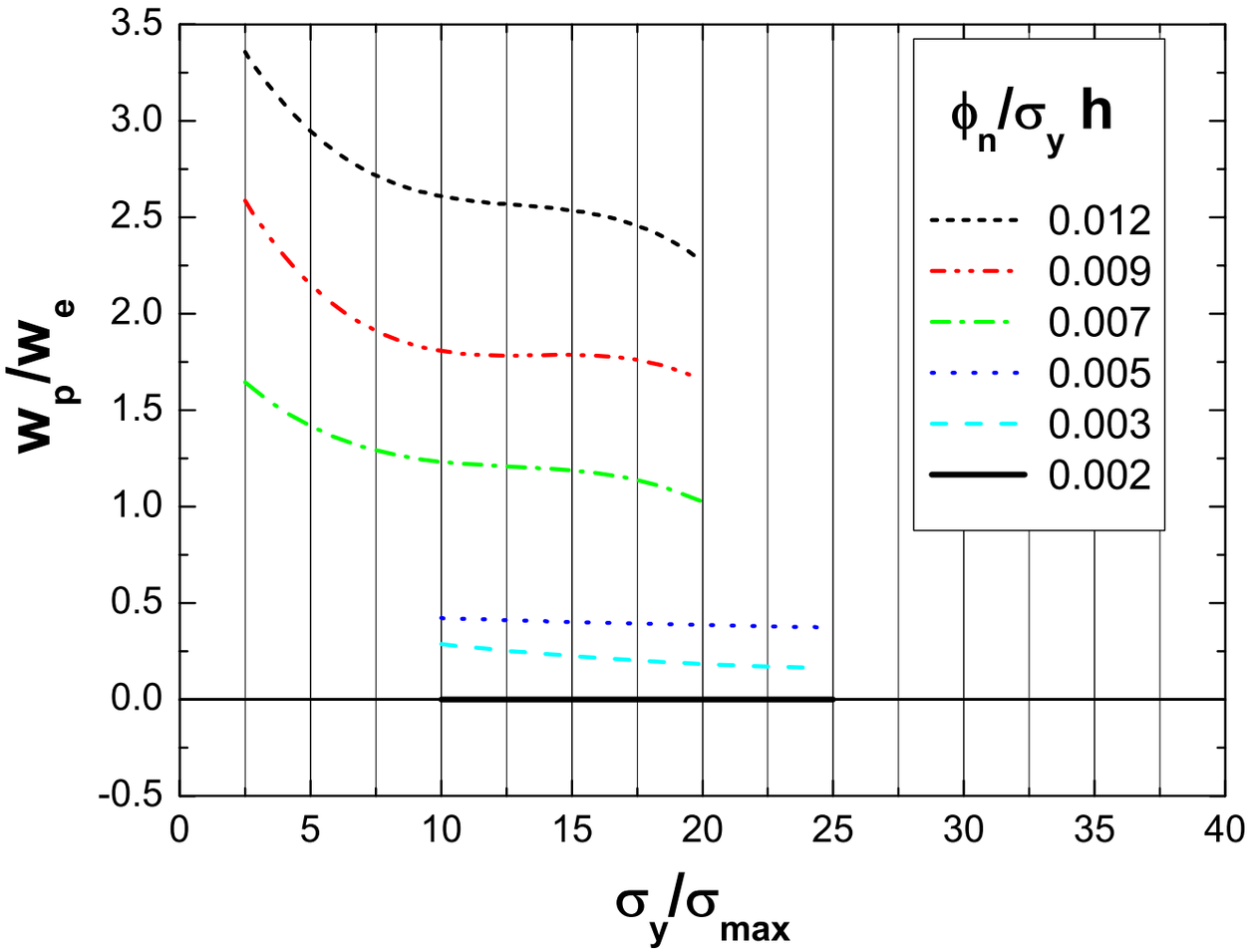

- The area under the curve increases as the fracture energy increases,
- GB samples: the post peak slope depends on fracture energy,
- LT samples, it depends on both cohesive strength and fracture energy.

Determination of bond toughness

Sensitivity analysis to Φ_n and σ_{max}

range of exp. results for grit blasted (GB) samples

range of exp. results for laser treated (L) samples

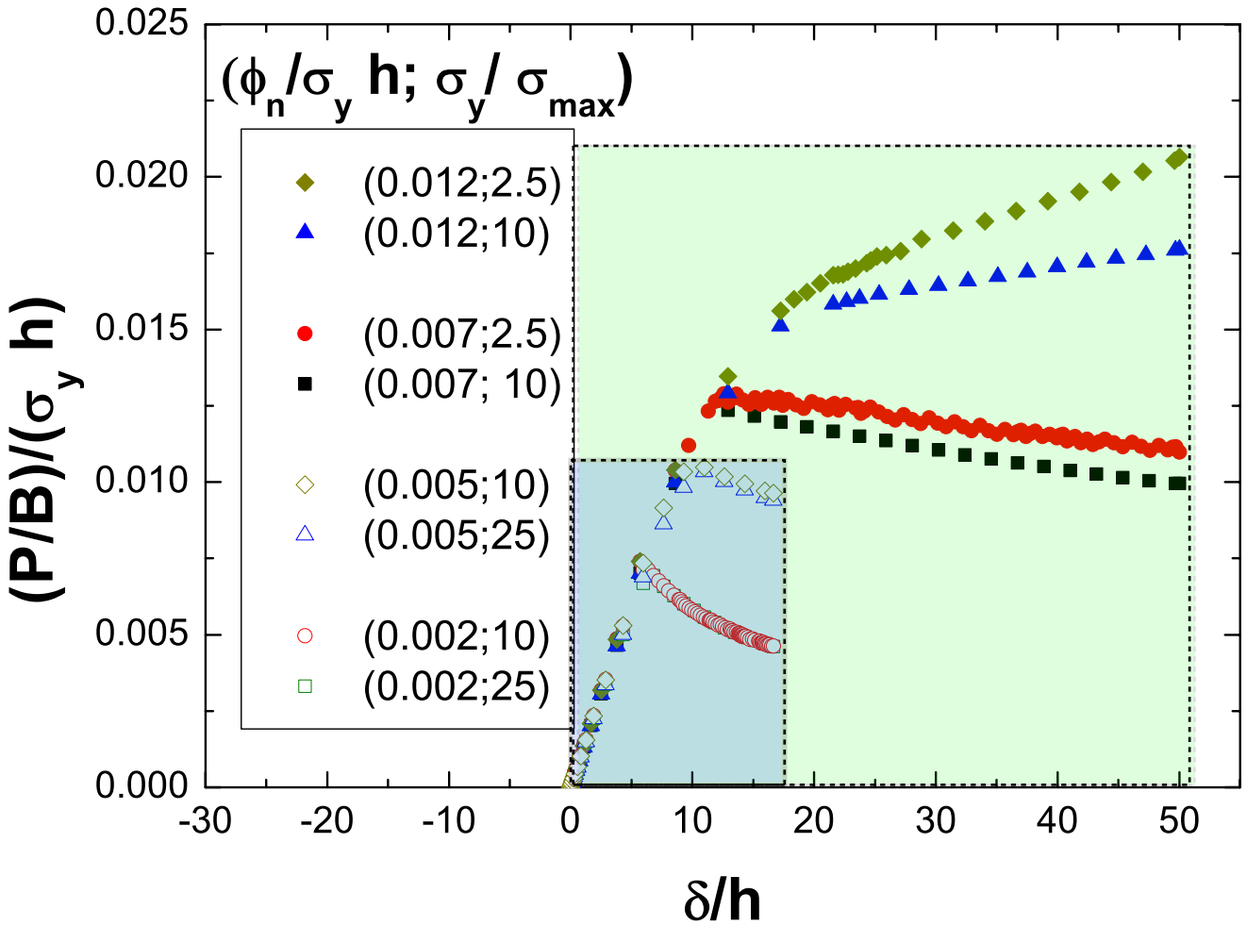

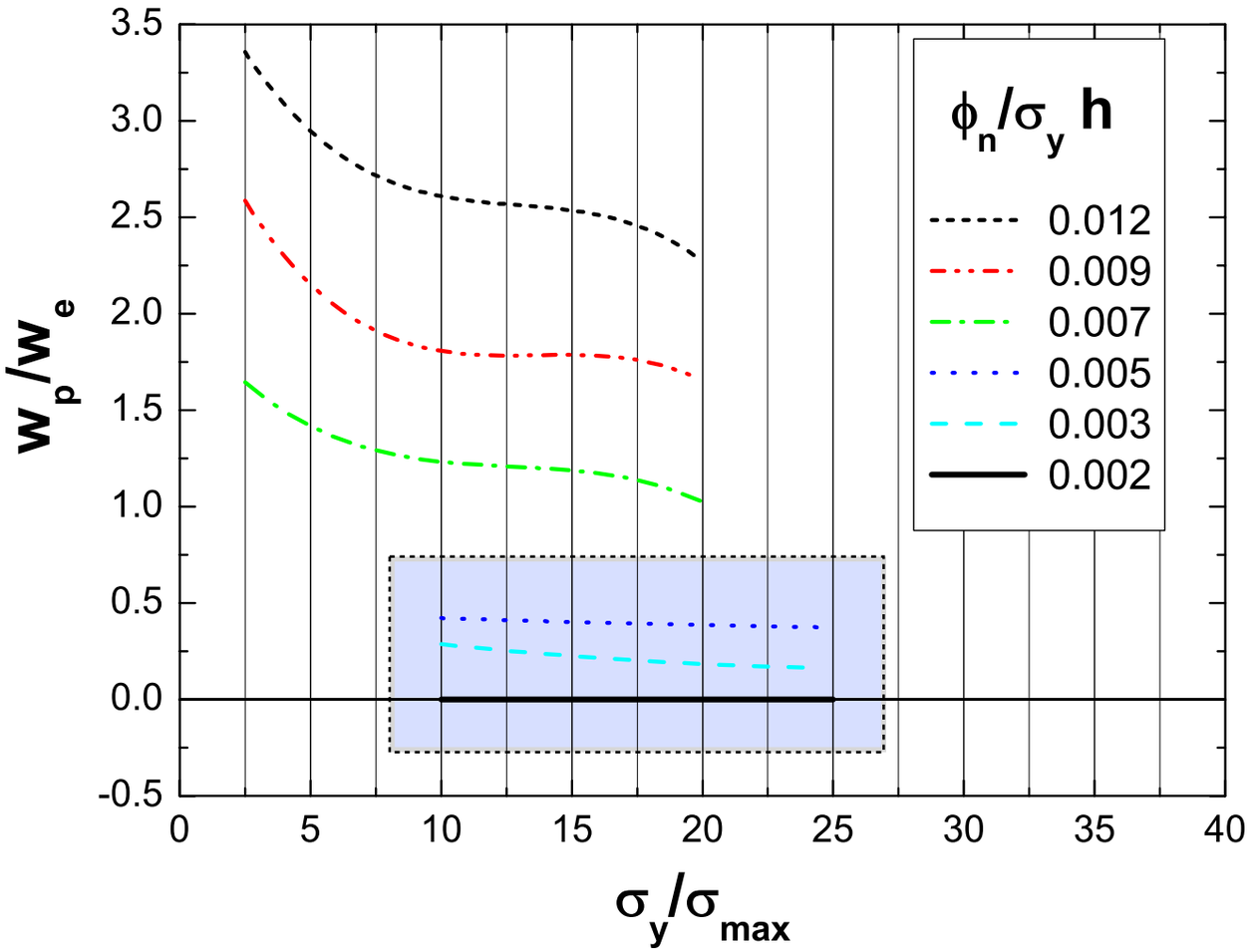

- The area under the curve increases as the fracture energy increases,
- GB samples: the post peak slope depends on fracture energy,
- LT samples, it depends on both cohesive strength and fracture energy.

Determination of bond toughness

Sensitivity analysis to Φ_n and σ_{max}

range of exp. results for grit blasted (GB) samples

range of exp. results for laser treated (L) samples

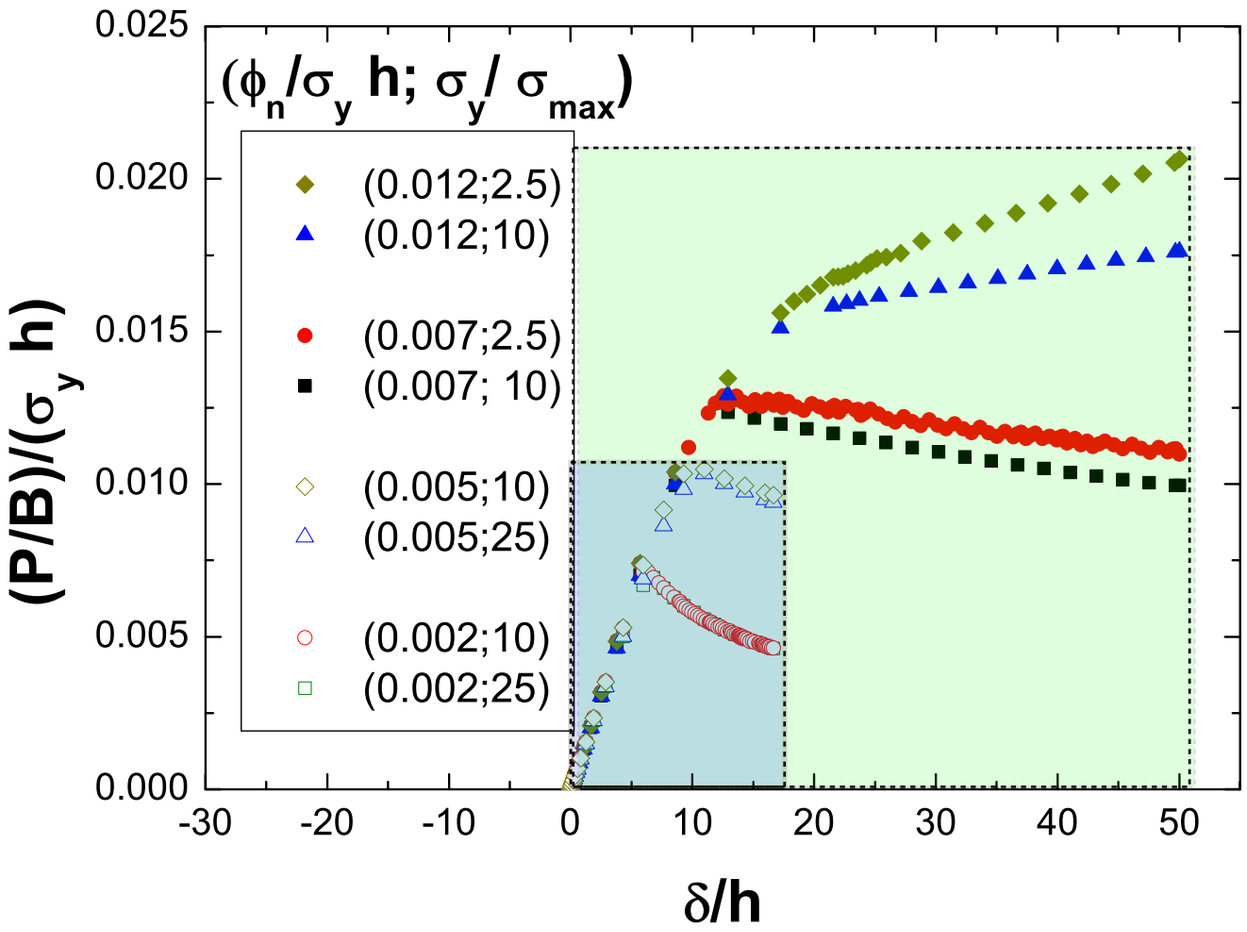

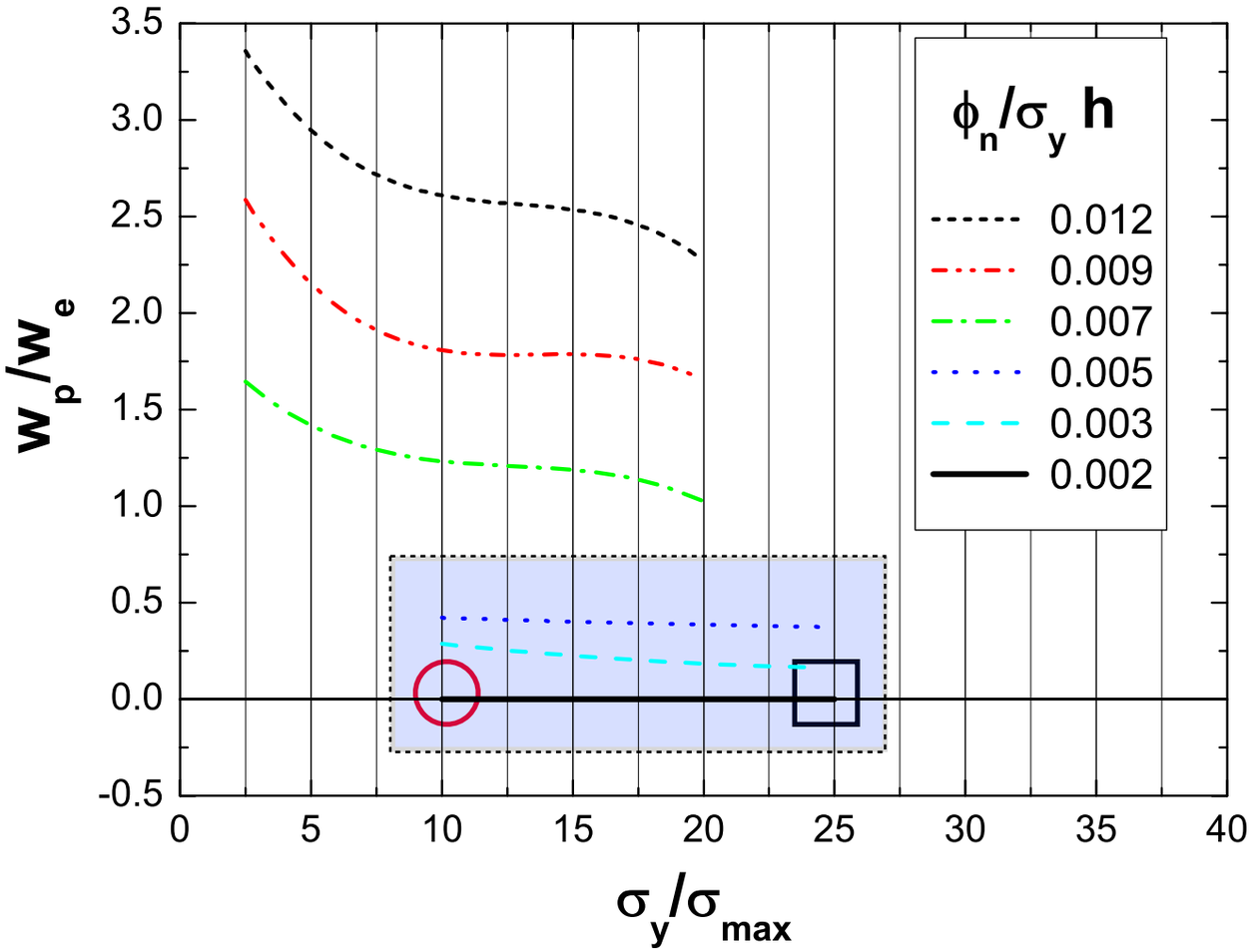

- The area under the curve increases as the fracture energy increases,
- GB samples: the post peak slope depends on fracture energy,
- LT samples, it depends on both cohesive strength and fracture energy.

Determination of bond toughness

Sensitivity analysis to Φ_n and σ_{max}

range of exp. results for grit blasted (GB) samples

range of exp. results for laser treated (L) samples

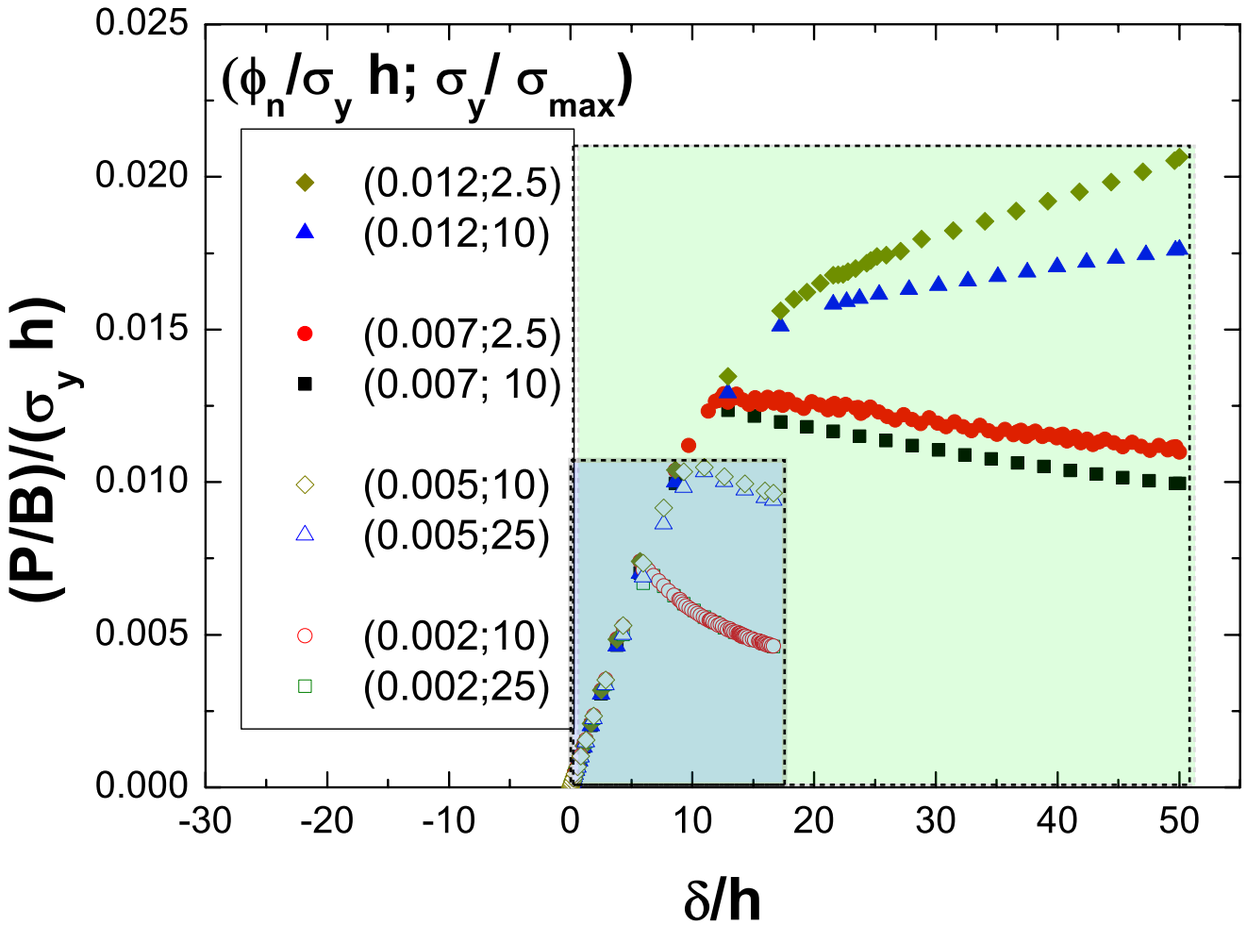

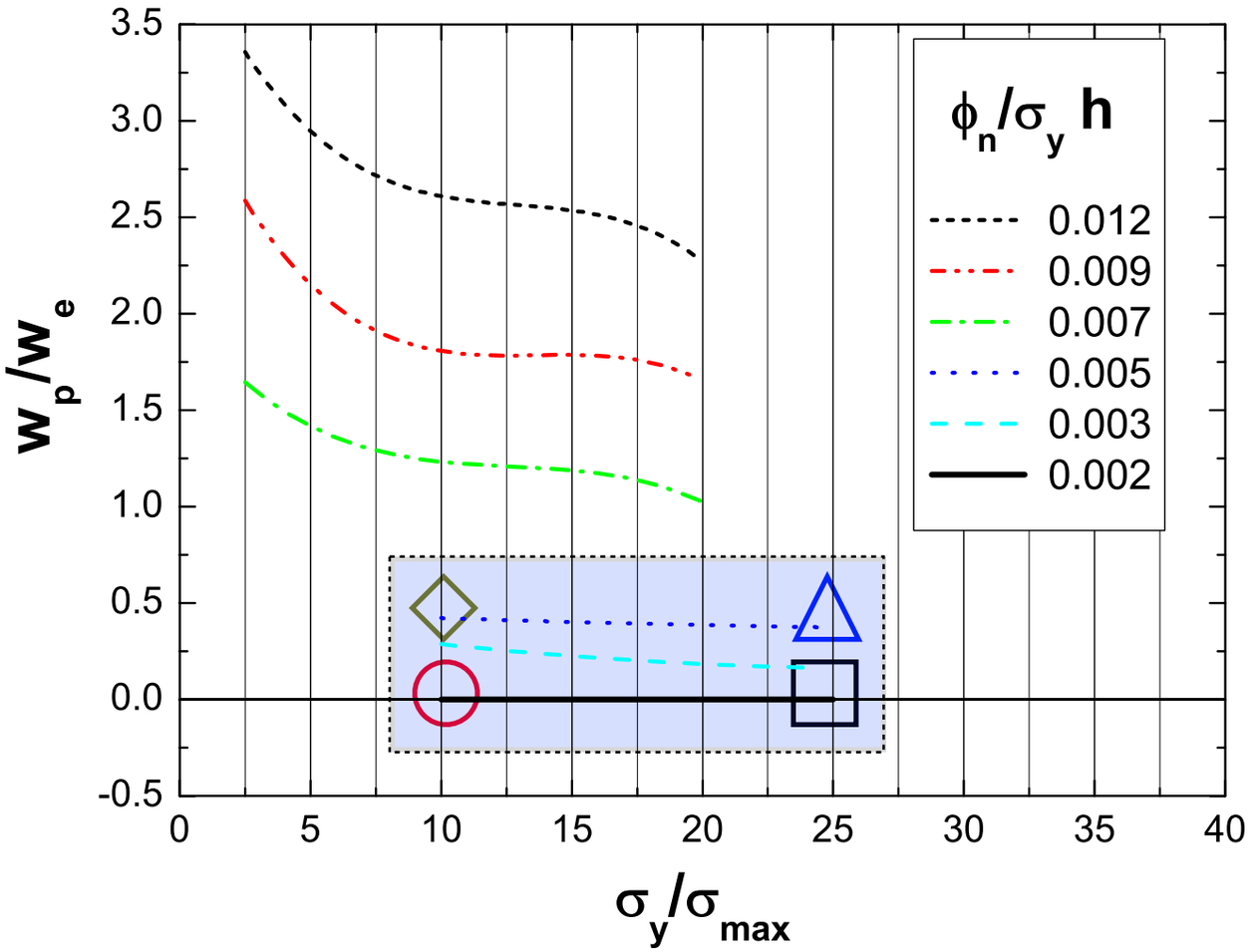

- The area under the curve increases as the fracture energy increases,
- GB samples: the post peak slope depends on fracture energy,
- LT samples, it depends on both cohesive strength and fracture energy.

Determination of bond toughness

Sensitivity analysis to Φ_n and σ_{max}

range of exp. results for grit blasted (GB) samples

range of exp. results for laser treated (L) samples

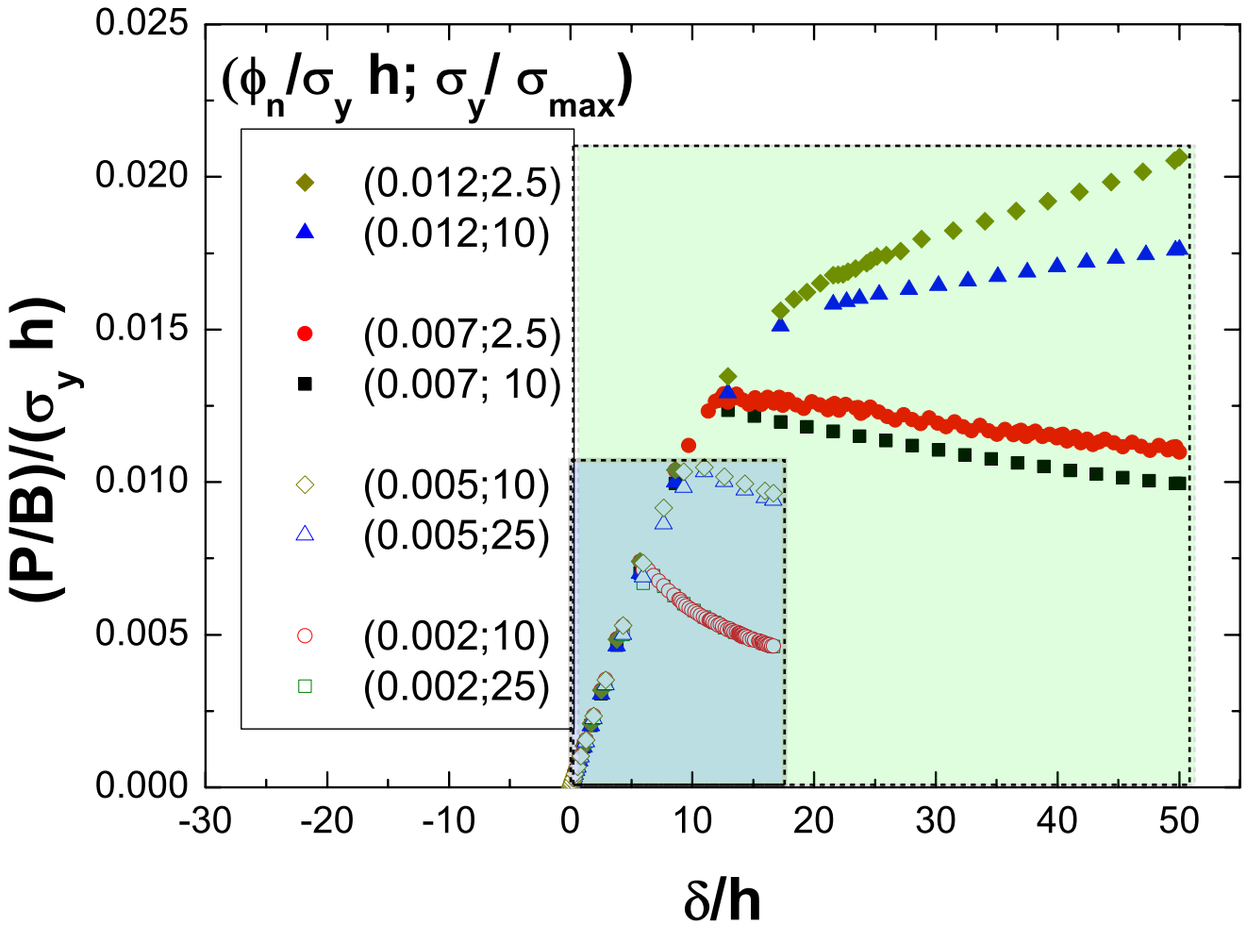

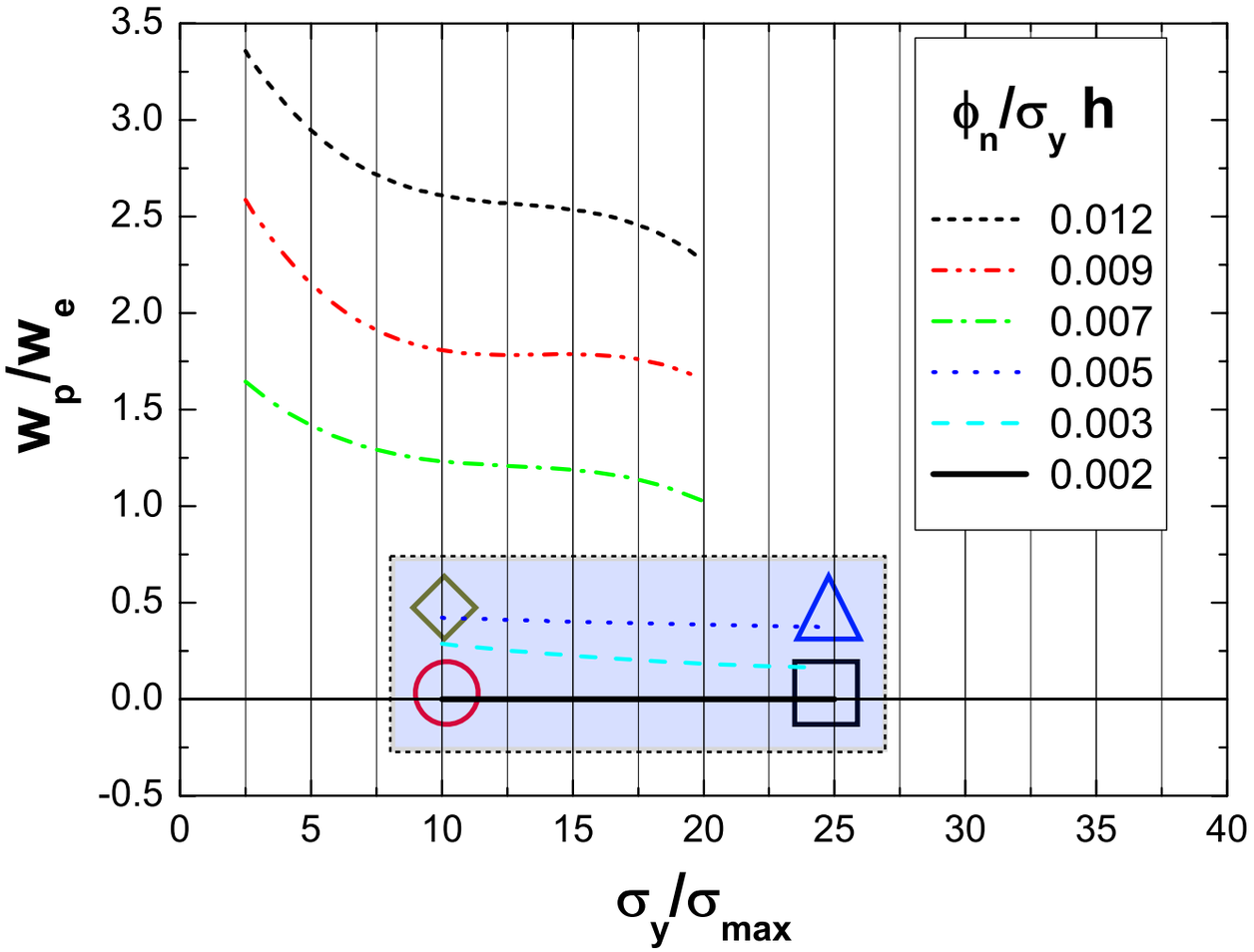

- The area under the curve increases as the fracture energy increases,
- GB samples: the post peak slope depends on fracture energy,
- LT samples, it depends on both cohesive strength and fracture energy.

- GB samples: plastic dissipation increases as the energy increases. No effect of coh. strength in the investigated range,

Determination of bond toughness

Sensitivity analysis to Φ_n and σ_{max}

range of exp. results for grit blasted (GB) samples

range of exp. results for laser treated (L) samples

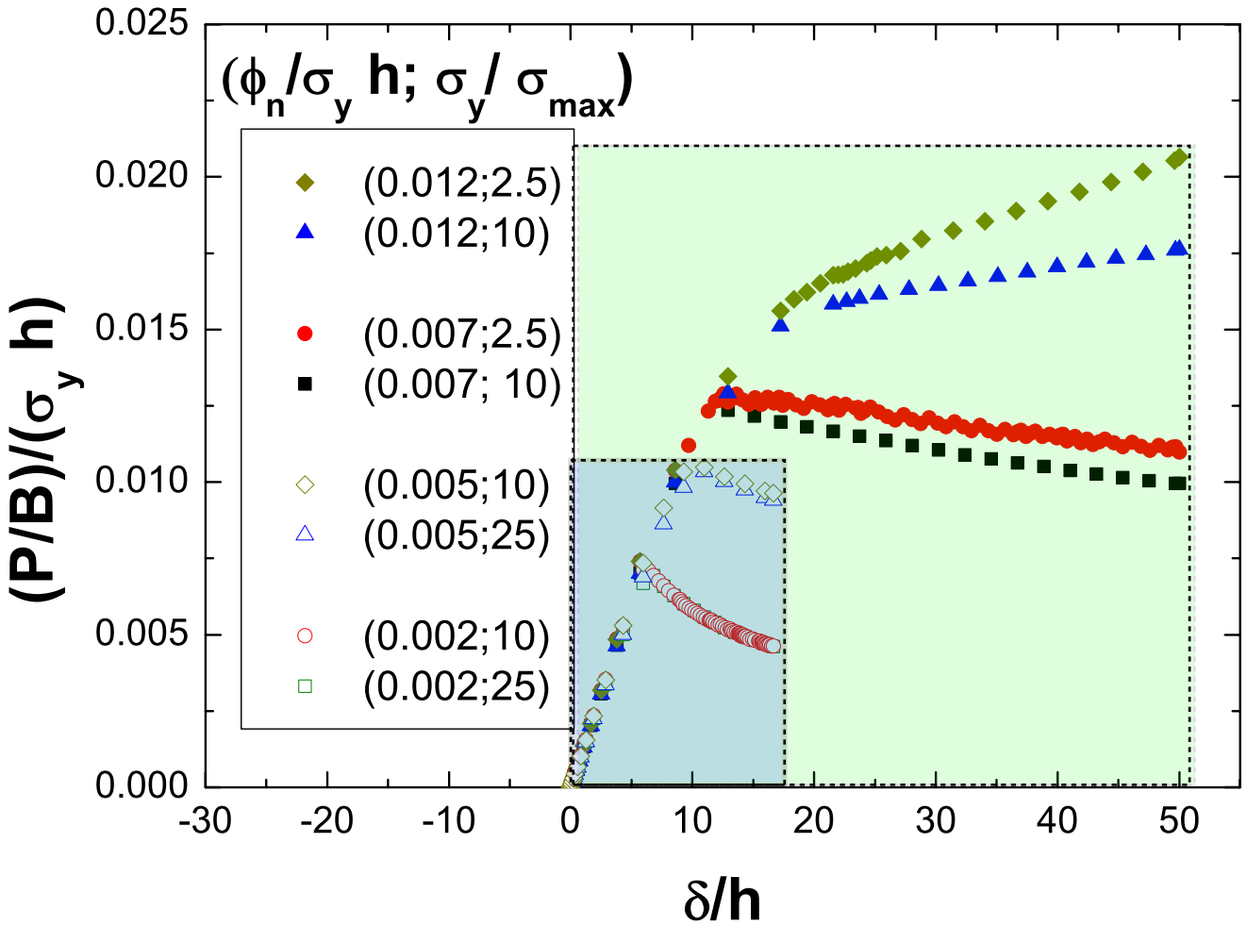

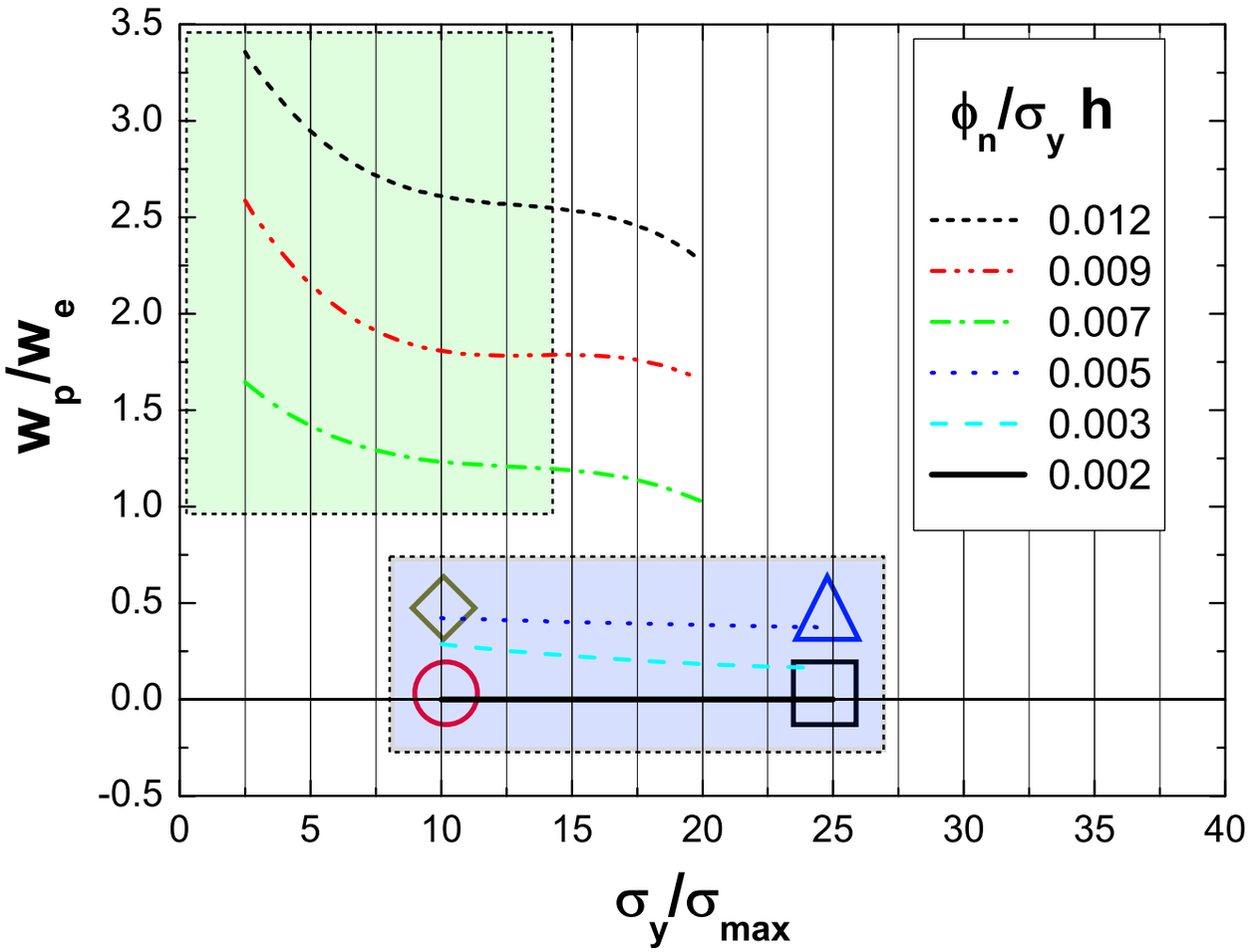

- The area under the curve increases as the fracture energy increases,
- GB samples: the post peak slope depends on fracture energy,
- LT samples, it depends on both cohesive strength and fracture energy.

- GB samples: plastic dissipation increases as the energy increases. No effect of coh. strength in the investigated range,

Determination of bond toughness

Sensitivity analysis to Φ_n and σ_{max}

range of exp. results for grit blasted (GB) samples

range of exp. results for laser treated (L) samples

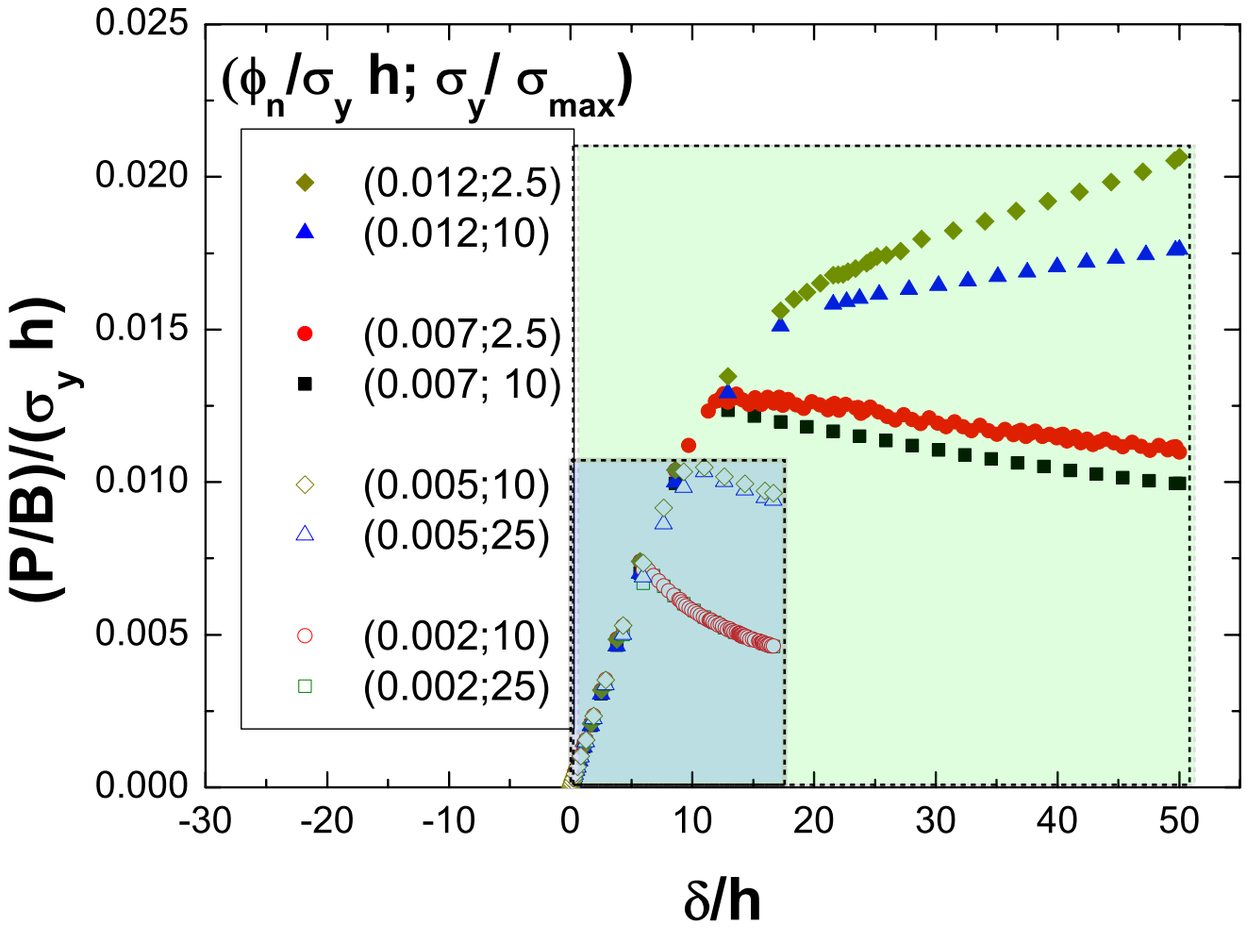

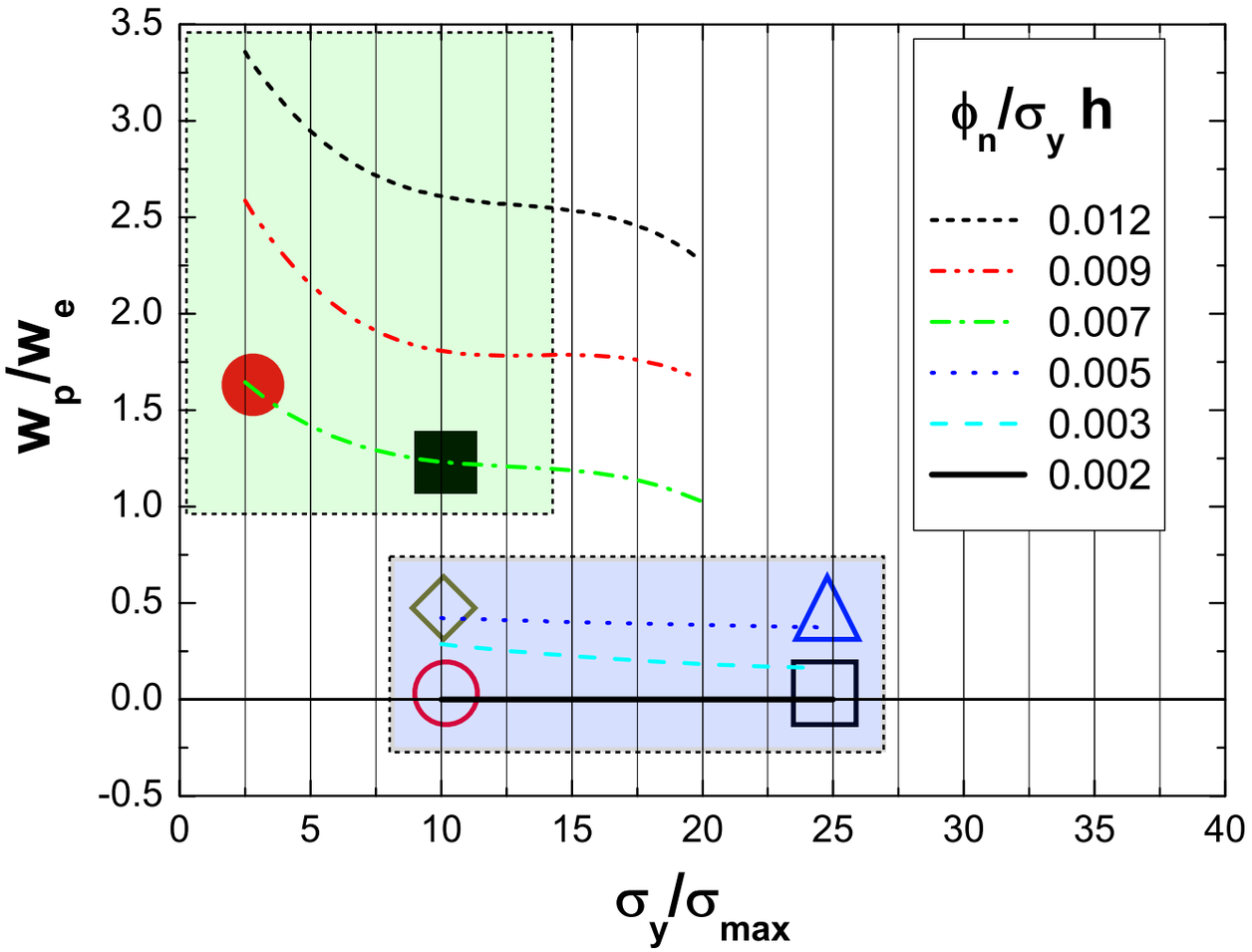

- The area under the curve increases as the fracture energy increases,
- GB samples: the post peak slope depends on fracture energy,
- LT samples, it depends on both cohesive strength and fracture energy.

- GB samples: plastic dissipation increases as the energy increases. No effect of coh. strength in the investigated range,

Determination of bond toughness

Sensitivity analysis to Φ_n and σ_{max}

range of exp. results for grit blasted (GB) samples

range of exp. results for laser treated (L) samples

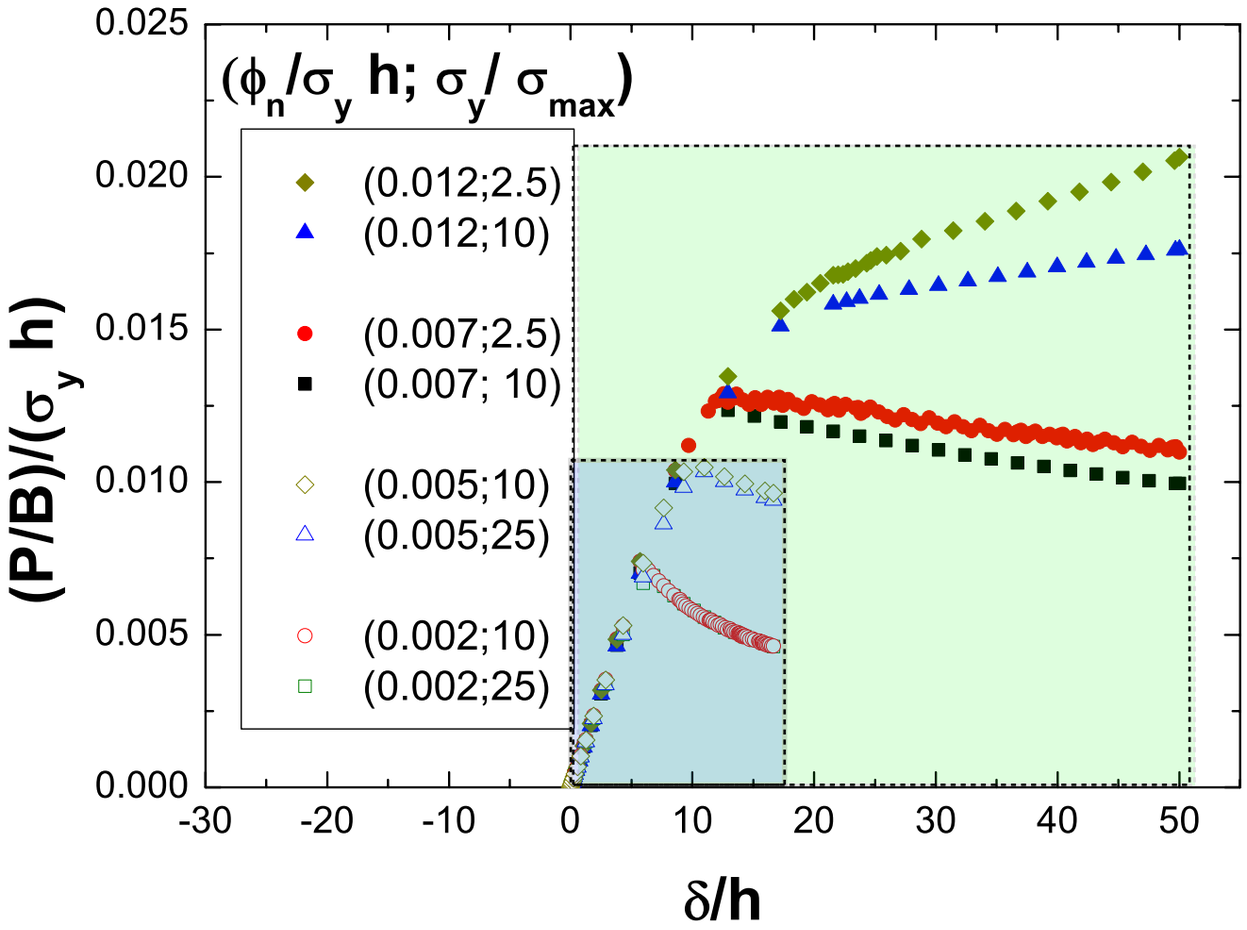

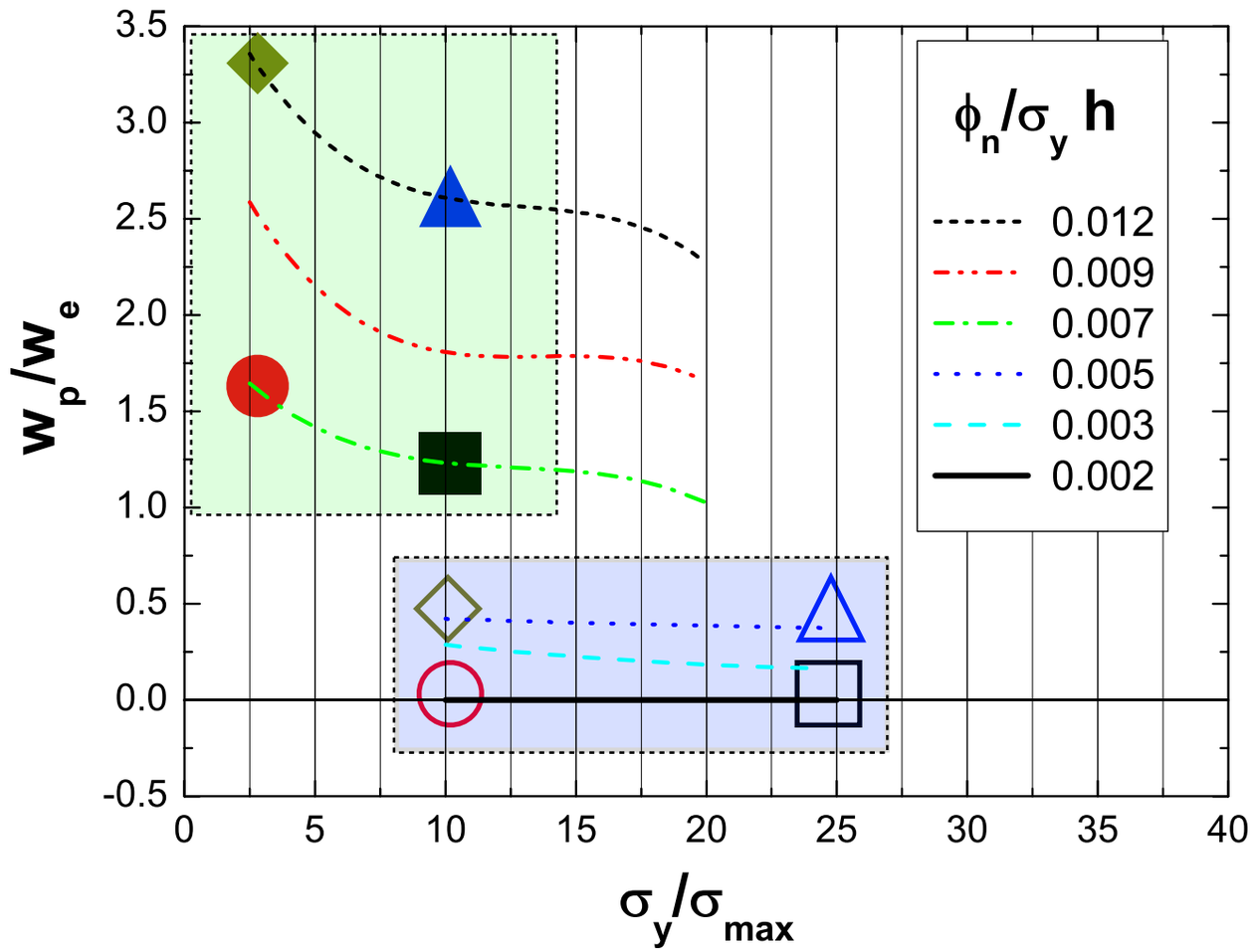

- The area under the curve increases as the fracture energy increases,
- GB samples: the post peak slope depends on fracture energy,
- LT samples, it depends on both cohesive strength and fracture energy.

- GB samples: plastic dissipation increases as the energy increases. No effect of coh. strength in the investigated range,

Determination of bond toughness

Sensitivity analysis to Φ_n and σ_{max}

range of exp. results for grit blasted (GB) samples

range of exp. results for laser treated (L) samples

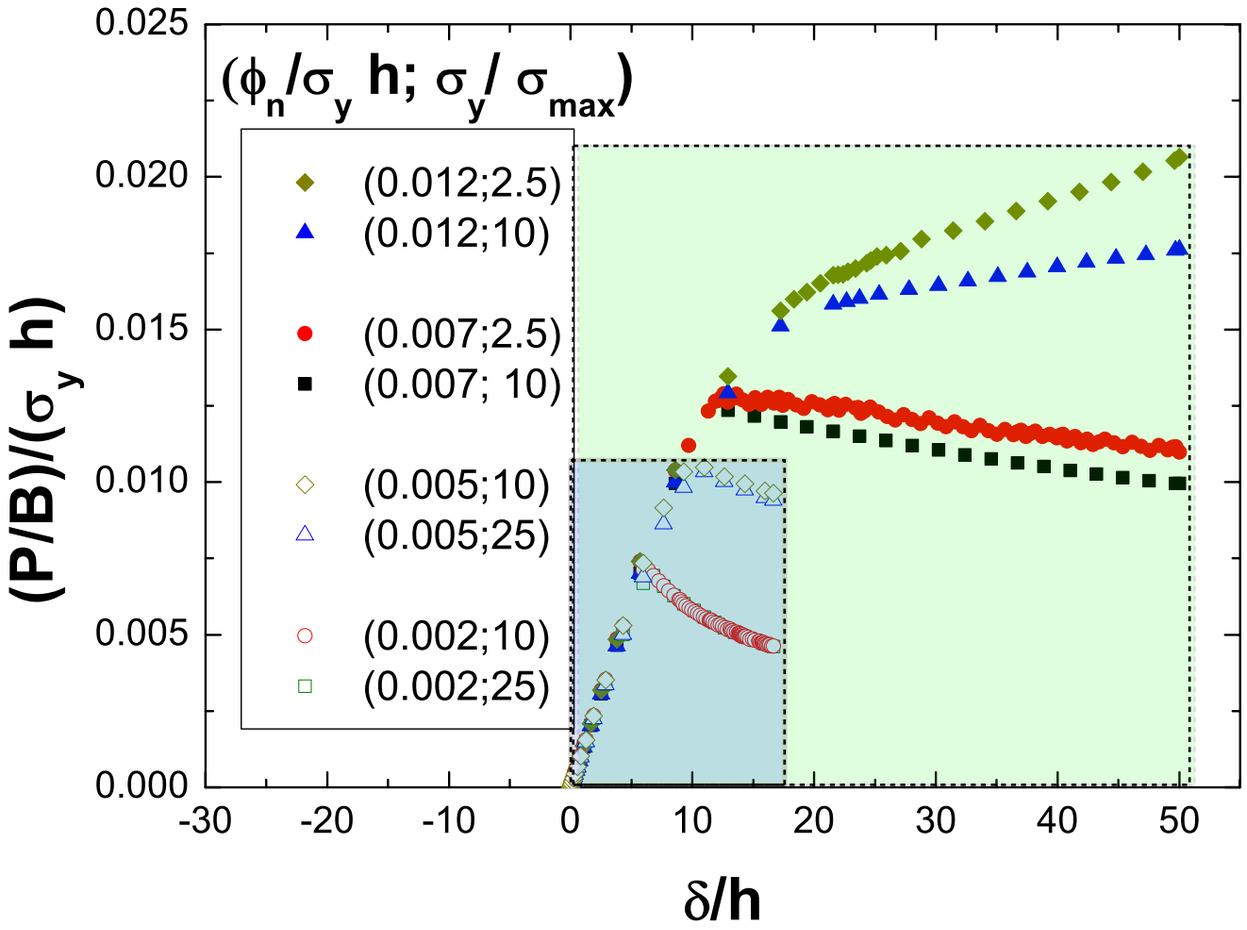

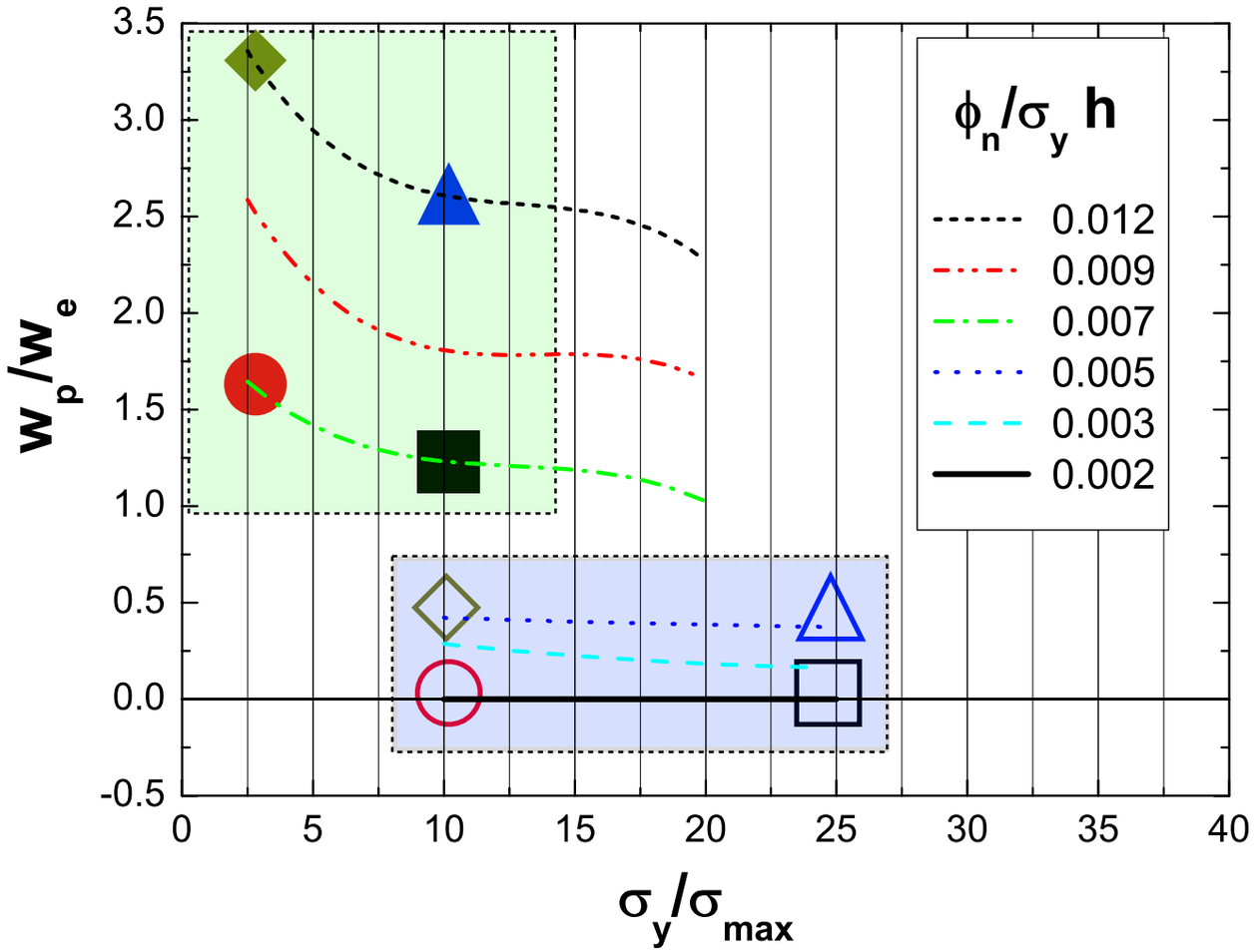

- The area under the curve increases as the fracture energy increases,
- GB samples: the post peak slope depends on fracture energy,
- LT samples, it depends on both cohesive strength and fracture energy.

- GB samples: plastic dissipation increases as the energy increases. No effect of coh. strength in the investigated range,
- LT samples: plastic dissipation increases as cohesive strength and fract. energy increases. Sensitivity is higher to fracture energy

Determination of bond toughness

Response map

$$\Phi = \| U(\delta)_{EXP} - U(\delta)_{FE} \|_2$$

$$U(\delta) = \int_{\delta_{i-1}}^{\delta_i} P(\delta) d\delta = (\delta_i - \delta_{i-1}) \times \frac{P(\delta_i) + P(\delta_{i-1})}{2}$$

Determination of bond toughness

Response map

$$\Phi = \| U(\delta)_{EXP} - U(\delta)_{FE} \|_2$$

$$U(\delta) = \int_{\delta_{i-1}}^{\delta_i} P(\delta) d\delta = (\delta_i - \delta_{i-1}) \times \frac{P(\delta_i) + P(\delta_{i-1})}{2}$$

LT samples

$$\phi_n = 2.5 \div 4.5 \; N/mm$$

$$\sigma_{max} = 5 \div 100 \; MPa$$

Determination of bond toughness

Response map

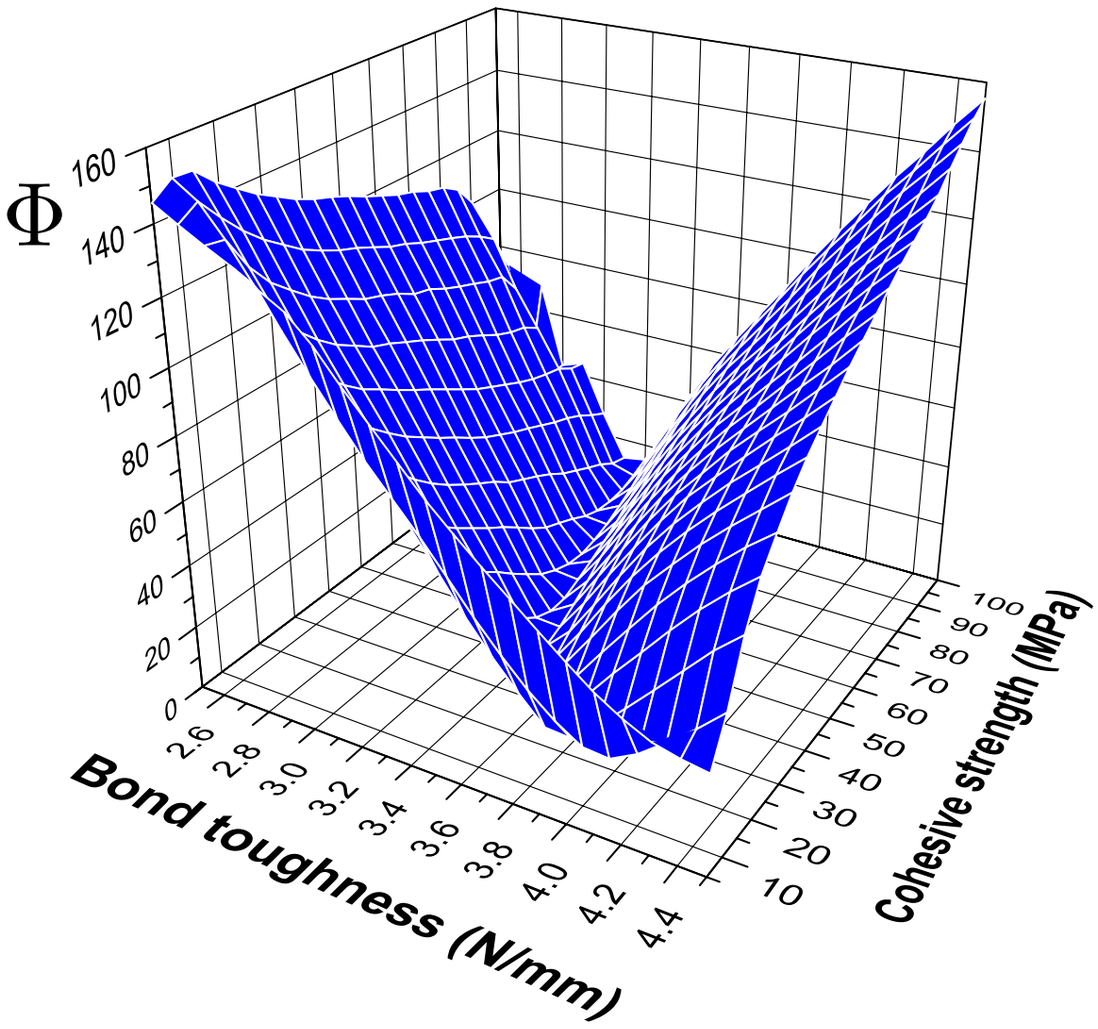

$$\Phi = \| U(\delta)_{EXP} - U(\delta)_{FE} \|_2$$

$$U(\delta) = \int_{\delta_{i-1}}^{\delta_i} P(\delta) d\delta = (\delta_i - \delta_{i-1}) \times \frac{P(\delta_i) + P(\delta_{i-1})}{2}$$

LT samples

$$\phi_n = 2.5 \div 4.5 \; N/mm$$

$$\sigma_{max} = 5 \div 100 \; MPa$$

Determination of bond toughness

Response map

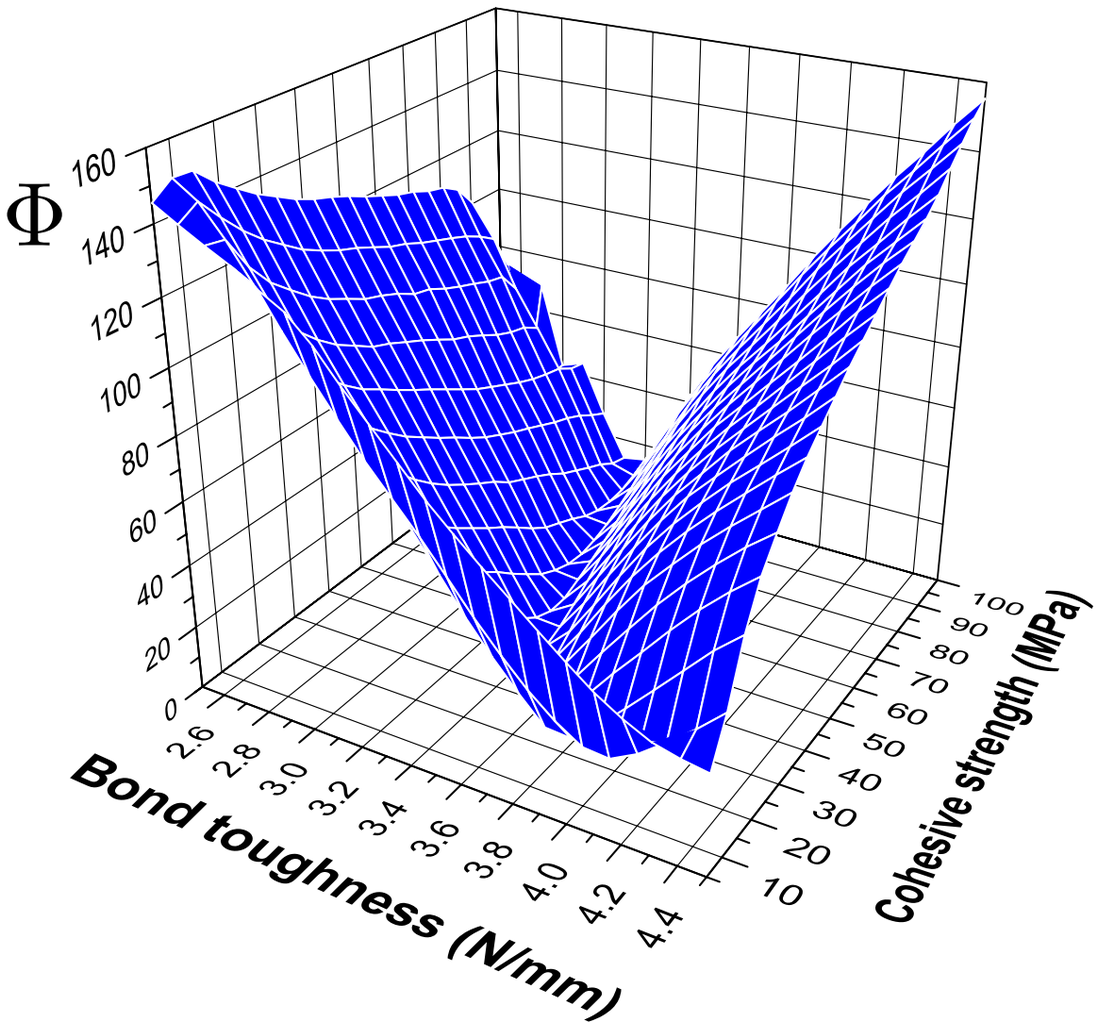

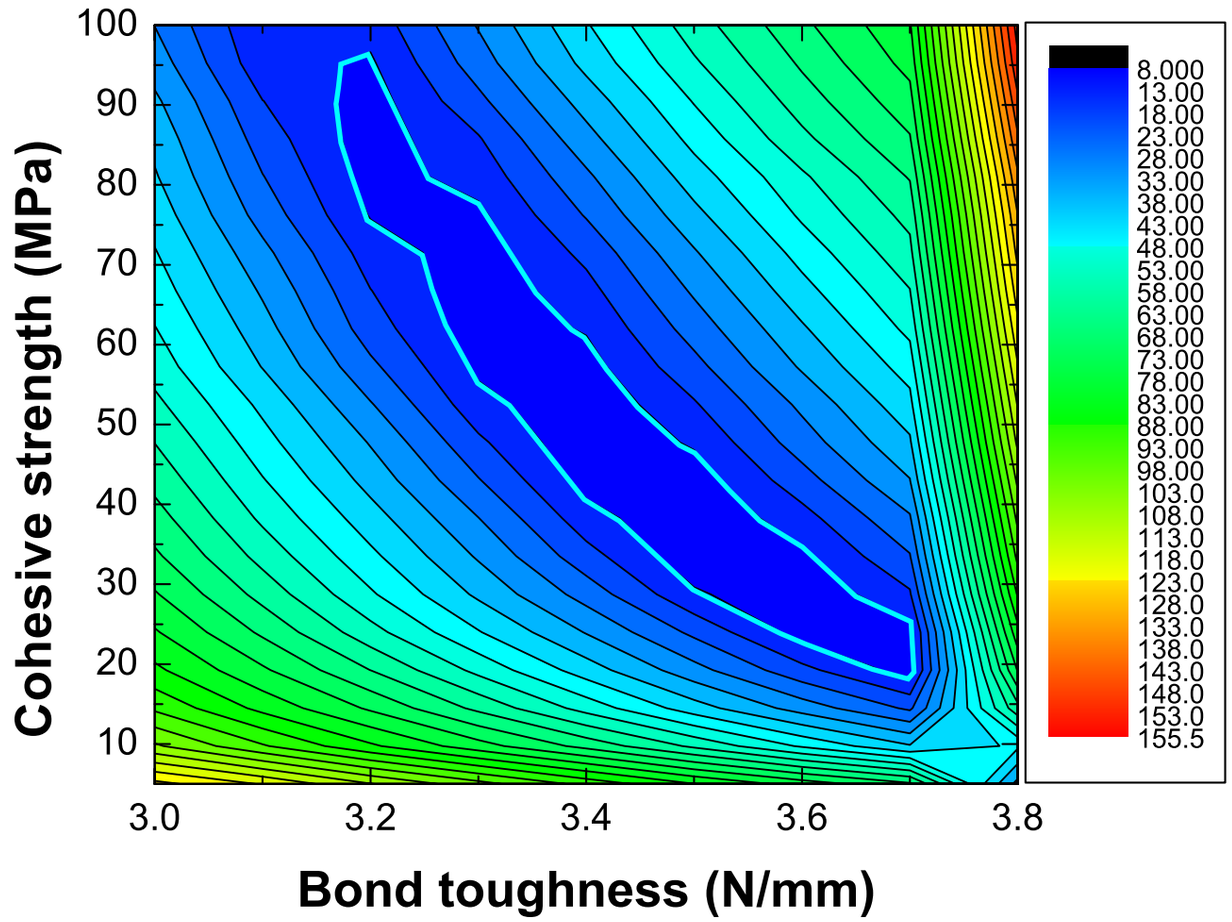

$$\Phi = \| U(\delta)_{EXP} - U(\delta)_{FE} \|_2$$

$$U(\delta) = \int_{\delta_{i-1}}^{\delta_i} P(\delta) d\delta = (\delta_i - \delta_{i-1}) \times \frac{P(\delta_i) + P(\delta_{i-1})}{2}$$

LT samples

$$\phi_n = 2.5 \div 4.5 \; N/mm$$

$$\sigma_{max} = 5 \div 100 \; MPa$$

Determination of bond toughness

Response map

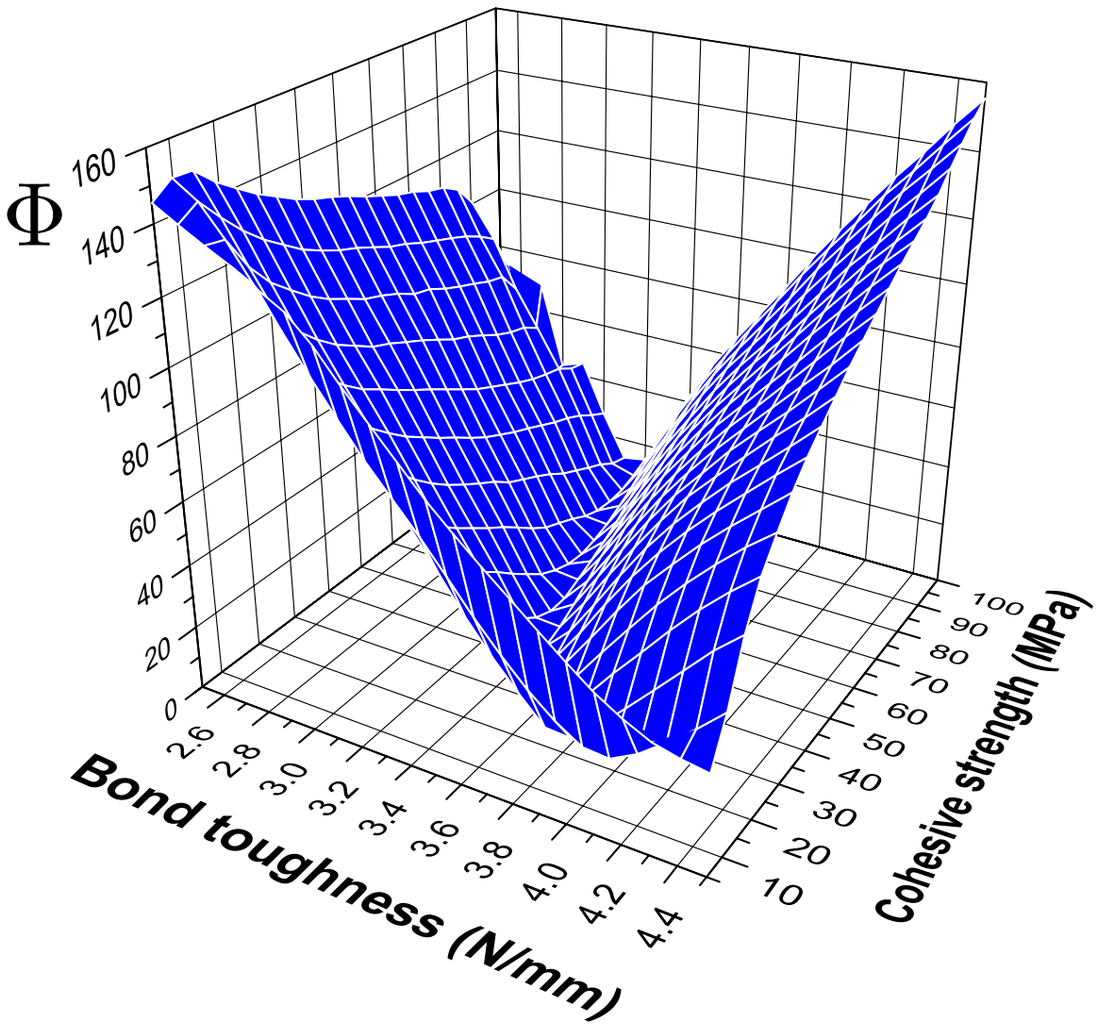

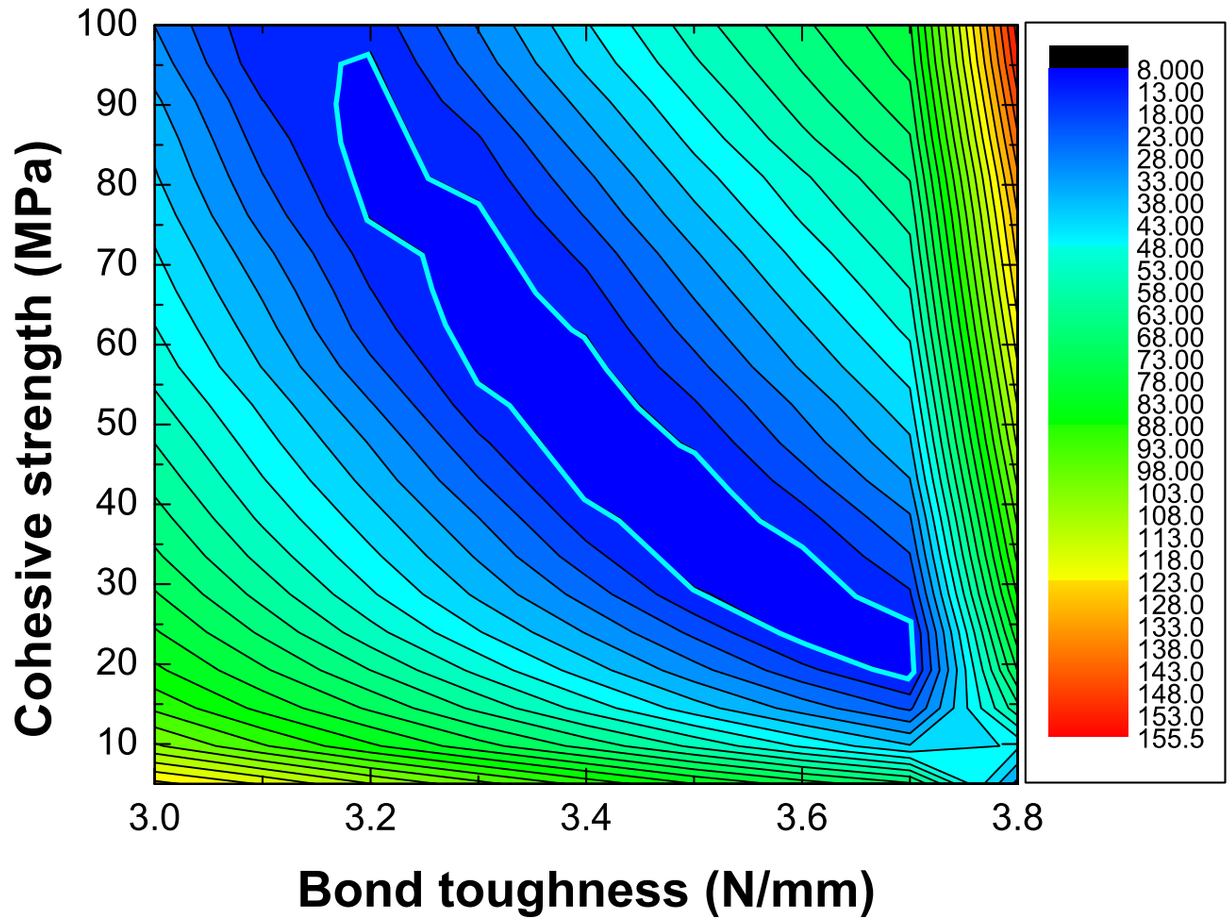

$$\Phi = \| U(\delta)_{EXP} - U(\delta)_{FE} \|_2$$

$$U(\delta) = \int_{\delta_{i-1}}^{\delta_i} P(\delta)d\delta = (\delta_i - \delta_{i-1}) \times \frac{P(\delta_i) + P(\delta_{i-1})}{2}$$

LT samples

$$\phi_n = 2.5 \div 4.5 \; N/mm$$

$$\sigma_{max} = 5 \div 100 \; MPa$$

- There is not a unique combination (Φ_n;σ_{max}) which minimizes the difference between experimental and simulated load-displacement curves
- A reasonable narrow range of bond toughness can be identified

Determination of bond toughness

Response map

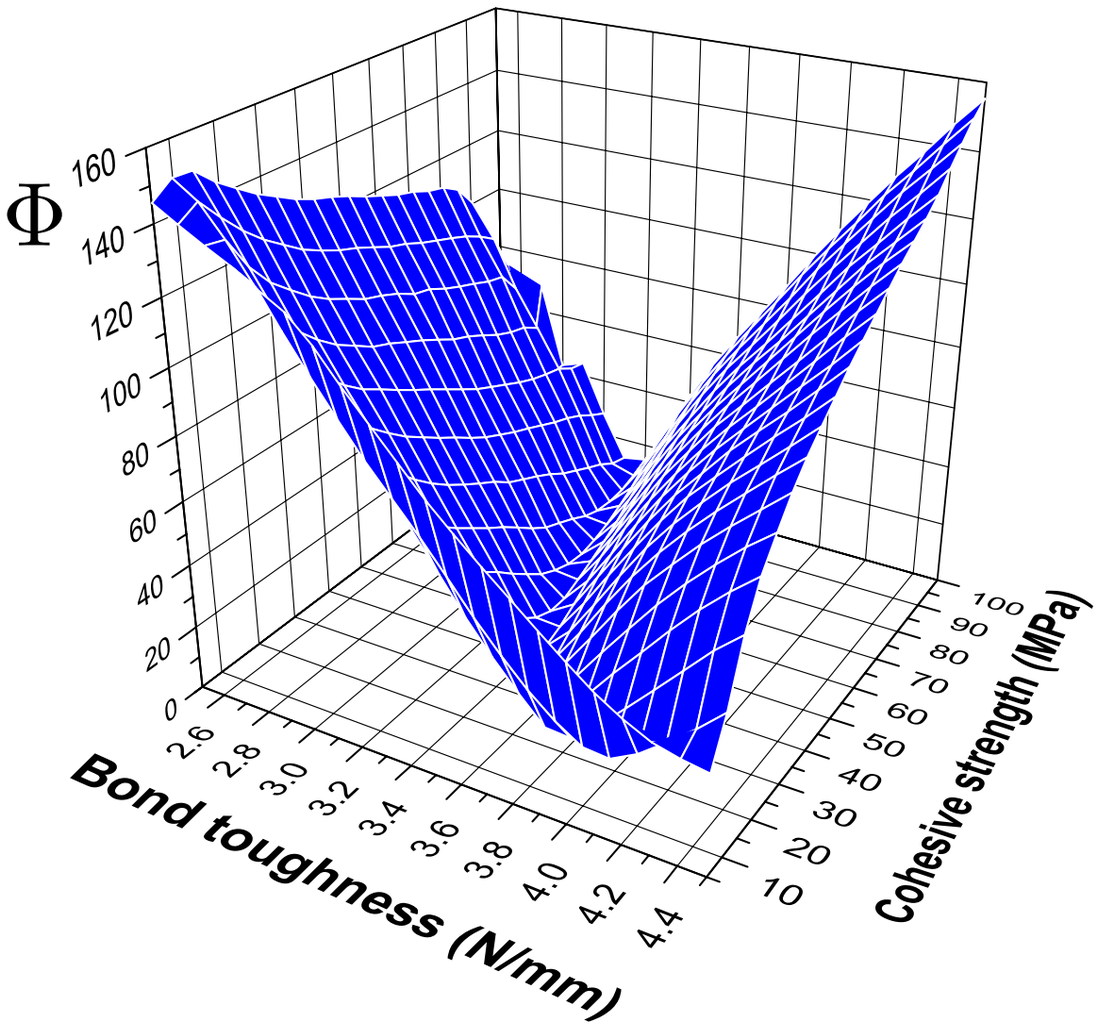

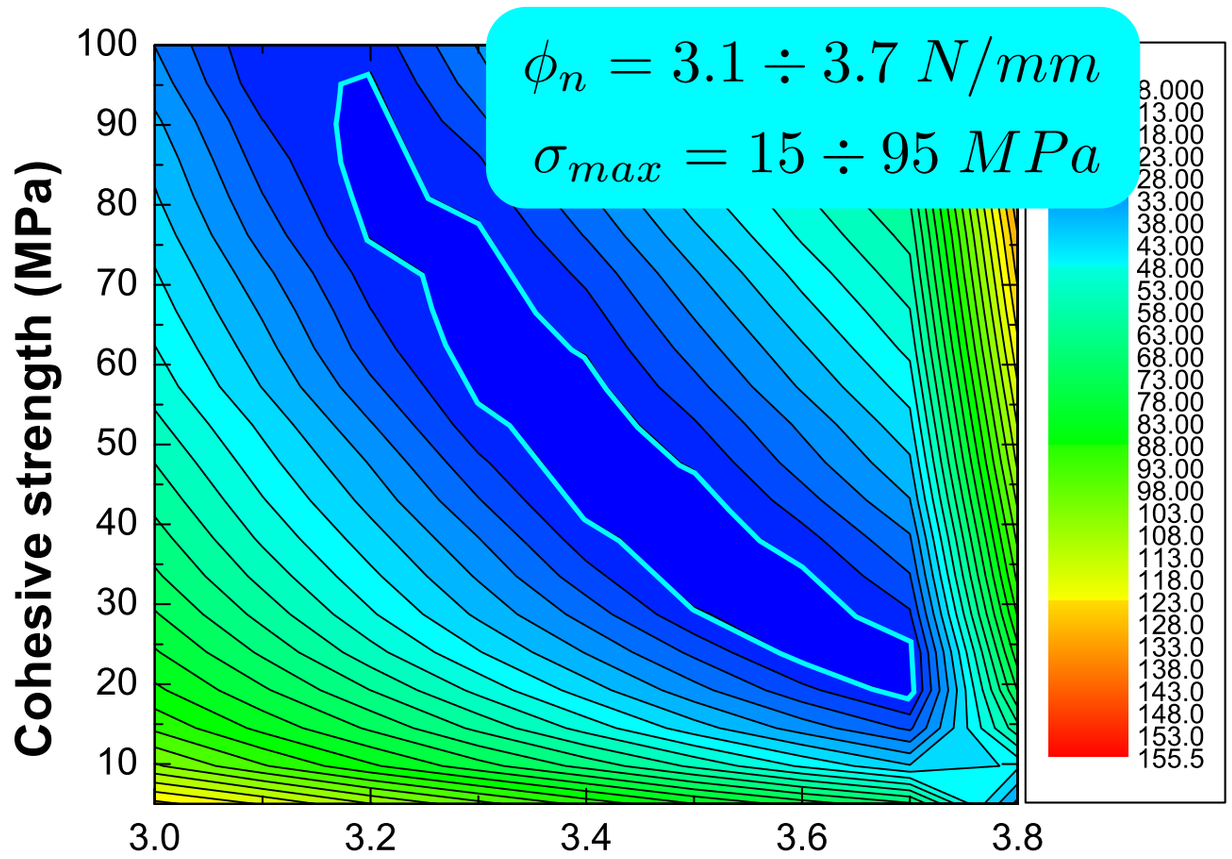

$$\Phi = \| U(\delta)_{EXP} - U(\delta)_{FE} \|_2$$

$$U(\delta) = \int_{\delta_{i-1}}^{\delta_i} P(\delta)d\delta = (\delta_i - \delta_{i-1}) \times \frac{P(\delta_i) + P(\delta_{i-1})}{2}$$

LT samples

$$\phi_n = 2.5 \div 4.5\ N/mm$$
$$\sigma_{max} = 5 \div 100\ MPa$$

- There is not a unique combination (Φ_n;σ_{max}) which minimizes the difference between experimental and simulated load-displacement curves
- A reasonable narrow range of bond toughness can be identified

Determination of bond toughness

Experimental data for laser treated samples

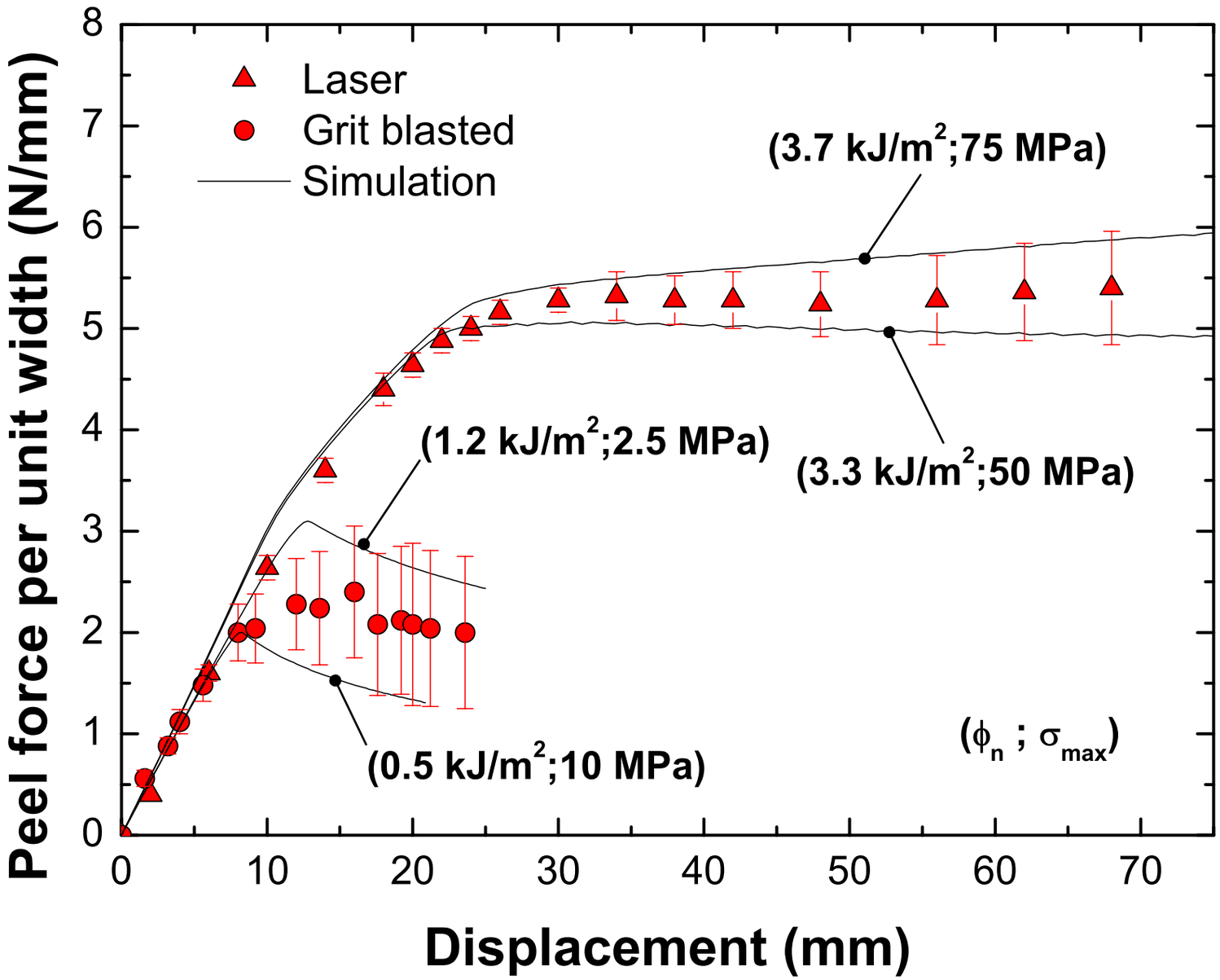

Determination of bond toughness

Experimental data for laser treated samples

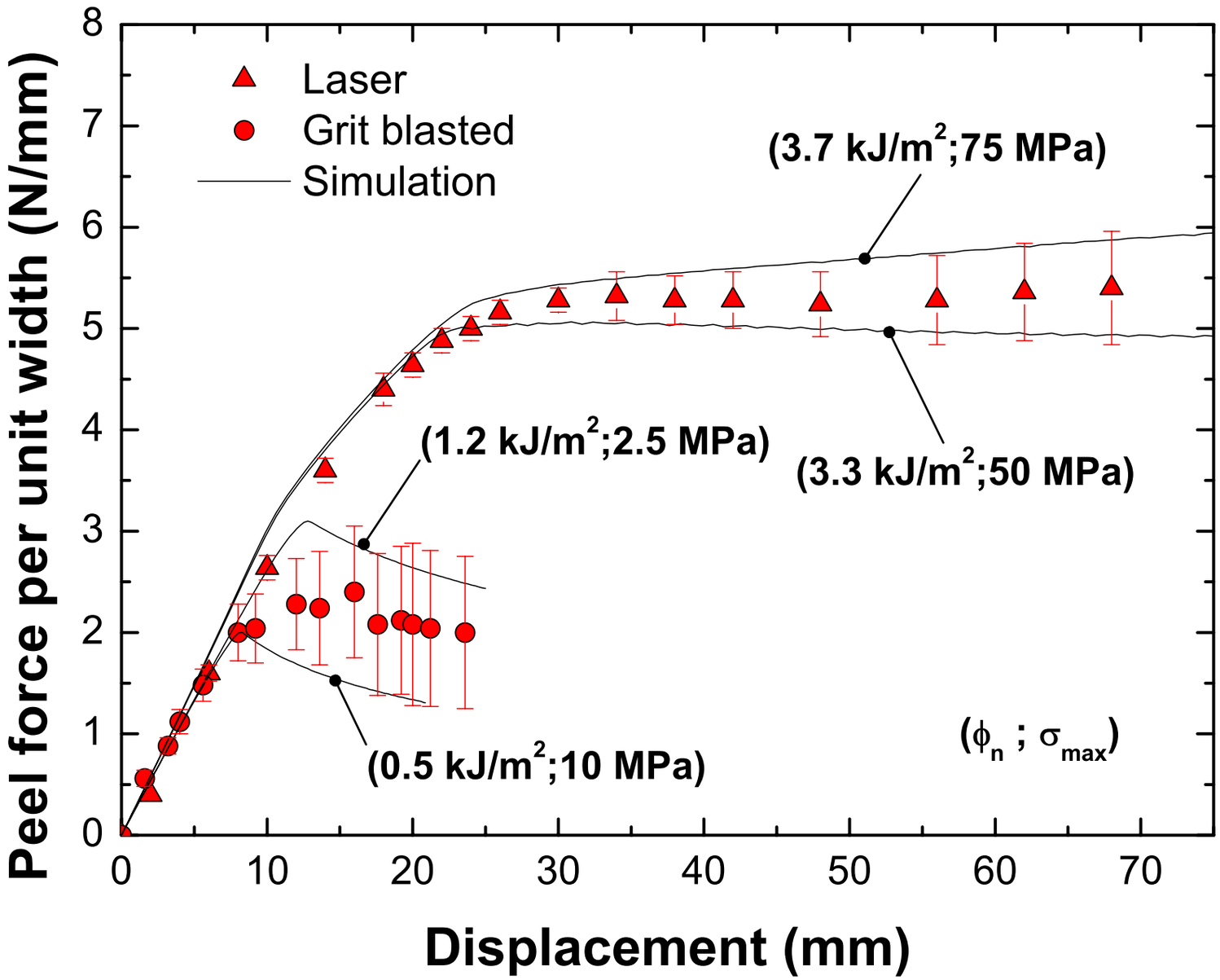

- The average bond toughness for laser treated samples is almost four times the one determined for grit blasted samples

Conclusions and future work

Conclusions

- The bond toughness of adhesive joints with laser treated substrates has been investigated,
- laser surface preparation of sample substrates provides improved wetting,
- in turn the bond toughness of the joint is up to four times higher than that of samples treated with standard grit blasting

Follow-up work

- Effect of surface patterning on the bond toughness of adhesive joints.
- Performance of the surface treatment in aggressive conditions.
- Identification of cohesive properties combining inverse techniques and full field kinematic data (already under development).